DEPARTAMENTO DE COMUNICACIONES

UNIVERSITAT POLITÈCNICA DE VALÈNCIA

DOCTORADO EN TELECOMUNICACIONES

BRILLOUIN-BASED FULL POLARIZATION CONTROL OF LIGHT AND APPLICATIONS

MEng. Gustavo Zoireff

Prof. Borja Vidal
Director - Universitat Politècnica de València
Prof. Laureano A. Bulus Rossini
Co-Director - Instituto Balseiro
Prof. Pablo A. Costanzo Caso
Co-Director - Instituto Balseiro

April 2024

Centro de Tecnología Nanofotónica
Universitat Politècnica de València
València, España

A mi esposa, Yanet, y a mi hija, Gabriela.

List of abbreviations

AM	Amplitude Modulation
ASE	Amplified Spontaneous Emission
AWG	Arbitrary Waveform Generator
BDG	Brillouin Dynamic Gratings
BLS	Brillouin Light Scattering
BOSA	Brillouin Optical Spectrum Analyzer
BOTDA	Brillouin Optical Time Domain Analysis
BP	Balanced Photodetector
DD-MZM	Dual-Drive Mach-Zehnder Modulator
DGD	Differential Group Delay
DGDD	Differential Group Delay Dispersion
DPSK	Differential Phase Shift Keying
EDFA	Erbium-Doped Fiber Amplifier
FBG	Fiber Bragg Grating
FLS	Fixed Light Source
FSBS	Forward Stimulated Brillouin Light Scattering
FWHM	Full Width at Half Maximum
FWM	Four-Wave Mixing
GVD	Group Velocity Dispersion
HNLF	Highly Nonlinear Fiber
IPSBS	Inter-Polarization Stimulated Brillouin Scattering
ISO	Isolator
LCoS	Liquid Crystals on Silica
MEMs	Micro-Electromechanical Systems
MITB	Minimum Transmission Bias
MZM	Mach-Zehnder Modulator
OC	Optical Circulator
ODL	Optical Delay Line
PA	Polarization Analyzer
PBS	Polarization Beam Splitter

PC	Polarization Controller
PD	Photodetector
PIC	Photonic Integrated Circuit
PM	Polarization-Maintaining
PMD	Polarization-Mode Dispersion
POL	Polarizer
RF	Radiofrequency
RHCP	Right-Handed Circular Polarization
RIN	Relative Intensity Noise
RMS	Root Mean Square
RRMSE	Relative Root Mean Squared Error
SBS	Stimulated Brillouin Scattering
SNR	Signal-to-Noise Ratio
SoP	State of Polarization
SSB	Single-Sideband
SSB+C	Single-Sideband with Carrier
TIA	Transimpendance Amplifier
TLS	Tunable Light Source
TTR	True Time Reversal
VNA	Vector Network Analyzer
VOA	Variable Optical Attenuator
WSS	Wavelength Selective Switch

Index of Contents

Index of Figures

Index of Tables

Abstract

Brillouin-based full polarization control of light and applications

Polarization is a fundamental property of light with many implications in daily life and in the most advanced technological developments. Consequently, controlling the polarization of light is a critical task in most optic and photonic systems. This process is often achieved using passive devices, such as waveplates, which induce a fixed amount of birefringence, or mechanical polarization controllers, whose main disadvantages are their inability to produce a specific type of birefringence (pure linear, circular, or elliptical) and bulky designs, that make them unsuitable for integration. As a result, research is focused on alternative polarization controllers, primarily based on linear and nonlinear optical phenomena. Among the various nonlinear light-matter interactions studied, backward-stimulated Brillouin scattering (SBS) emerges as a promising candidate for polarization control of light. Its response to an intense light wave (pump) is polarization-dependent, and it is the nonlinear process with the least optical activation power. Additionally, its frequency and bandwidth tuning flexibility have been consistently demonstrated by altering the wavelength and the frequency response of the pumping wave.

This PhD Thesis delves into the polarization-dependent properties of SBS, aiming to achieve full polarization control of light in terms of birefringence, frequency, and bandwidth. The theoretical basis developed here provides the knowledge to generate and control the type and magnitude of birefringence and differential group delay (DGD) and DGD dispersion (DGDD) in optical fibers. The practical implications of this research are significant, demonstrating through that these parameters can be dynamically adjusted with only slight variations in the system's SBS-induced gain.

Our research demonstrates that polarization can be controlled over a bandwidth wider than the natural Brillouin response and tailored to provide a specific retardance profile. This achievement is a significant finding, as it expands the capabilities of SBS-based polarization control beyond previously thought possible. The spectral broadening of the SBS-based polarization controller is achieved through engineering the Brillouin phase frequency response via feedback pump regulation, a novel approach that sets our research apart. We demonstrated retardance broadening from 51 MHz (natu-

ral SBS interaction) to 0.9 GHz, along with retardance spectrum flattening, providing concrete evidence of the effectiveness of our approach.

Finally, various devices employing the SBS-based polarization controller as a core subsystem are analyzed. This analysis leads to a new photonic technique for implementing stopband and passband microwave filters in a single device. The operating principle relies on rotating the state of polarization of the band of interest using the SBS-based polarization controller in combination with polarization-sensitive balanced photodetection. These concepts enable the implementation of a single-fiber stage microwave photonic filter that can be dynamically switched from a stopband to a passband response, providing flexibility to the system and enhancing its application potential. Tests conducted with a single stage of a dispersion-shifted fiber show that a very high rejection of 67 dB can be achieved in the stopband. Out-of-band attenuation in the passband configuration, at 30 dB, performs similarly to other SBS-based microwave photonic filters.

Keywords: NONLINEAR OPTICS, STIMULATED BRILLOUIN SCATTERING, POLARIZATION CONTROL, MICROWAVE PHOTONICS.

Resumen

Control total de la luz y aplicaciones basados en Brillouin

La polarización es una propiedad fundamental de la luz con muchas implicaciones tanto en la vida diaria y como en los desarrollos tecnológicos más avanzados. En consecuencia, controlar la polarización de la luz es una tarea crítica en la mayoría de los sistemas ópticos y fotónicos. Este proceso a menudo se logra utilizando dispositivos pasivos, como retardadores de onda, que inducen una cantidad fija de birrefringencia, o controladores de polarización mecánicos, cuyas principales desventajas son su incapacidad para inducir un determinado tipo de birrefringencia (pura lineal, circular o elíptica) y sus diseños voluminosos, que los hacen inadecuados para la integración. Entonces, la investigación se centra en controladores de polarización alternativos, basados principalmente en fenómenos ópticos lineales y no lineales. Entre las diversas interacciones no lineales luz-materia estudiadas, la dispersión de Brillouin estimulada hacia atrás (SBS) emerge como un candidato prometedor para el control de la polarización de la luz. Su respuesta a una onda de luz intensa (bombeo) es dependiente de la polarización, y es el proceso no lineal con menor potencia óptica de activación. Además, la flexibilidad para la sintonización de frecuencia y ancho de banda se ha demostrado consistentemente alterando la longitud de onda y la respuesta en frecuencia de la onda de bombeo.

Esta Tesis doctoral profundiza en las propiedades dependientes de la polarización del SBS, con el objetivo de lograr un control total de la polarización de la luz en términos de birrefringencia, frecuencia y ancho de banda. Los fundamentos teóricos desarrollados aquí proporcionan el conocimiento para generar y controlar el tipo y magnitud de la birrefringencia, el retardo de grupo diferencial(DGD) y la dispersión de DGD (DGDD) en fibras ópticas. Las consecuencias prácticas de esta investigación son significativas, demostrando a través de experimentos que estos parámetros se pueden ajustar dinámicamente con sólo ligeras variaciones en la ganancia inducida por SBS del sistema.

Nuestra investigación demuestra que la polarización puede controlarse en un ancho de banda más amplio que la respuesta natural de Brillouin y adaptarse para proporcionar un perfil de retardancia específico. Este logro es un hallazgo importante, ya que

amplía las capacidades del control de polarización basado en SBS más allá de lo que antes se creía posible. La ampliación espectral del controlador de polarización basado en SBS se logra mediante la ingeniería de la respuesta en frecuencia de la fase de Brillouin mediante la regulación del bombeo por retroalimentación, un enfoque novedoso que distingue nuestra investigación. Demostramos una ampliación de la retardancia de 51 MHz (interacción SBS natural) a 0,9 GHz, junto con un aplanamiento del espectro de retardo, lo que proporciona evidencia concreta de la efectividad de nuestro enfoque.

Finalmente, se analizan varios dispositivos que emplean el controlador de polarización basado en SBS como subsistema central. Este análisis condujo a desarrollar una nueva técnica fotónica para implementar filtros de microondas rechaza banda y pasa banda en una único dispositivo. El principio de funcionamiento se basa en rotar el estado de polarización de la banda de interés utilizando el controlador de polarización basado en SBS en combinación con una fotodetección balanceada sensible a la polarización. Estos conceptos permitieron la implementación de un filtro de microondas fotónico en una única etapa de fibra que permite alternar dinámicamente entre respuestas rechaza banda y pasa banda, dotando de flexibilidad al sistema e incrementando su potencial de aplicación. Las pruebas realizadas con una sola etapa de una fibra con dispersión desplazada muestran que se puede lograr un rechazo muy alto de 67 dB en la banda suprimida. La atenuación fuera de banda en la configuración pasa banda, de 30 dB, tiene un desempeño similar a otros filtros de microondas fotónicos basados en SBS.

Palabras clave: ÓPTICA NO LINEAL, DISPERSIÓN DE BRILLOUIN ESTIMULADO, CONTROL DE LA POLARIZACIÓN, FOTÓNICA EN SISTEMAS DE MICROONDAS.

Resum

Control total de la llum i aplicacions basats en Brillouin

La polarització és una propietat fonamental de la llum amb moltes implicacions tant en la vida diària i com en els desenvolupaments tecnològics més avançats. En conseqüència, controlar la polarització de la llum és una tasca crítica en la majoria dels sistemes òptics i fotònics. Este procés sovint s'aconseguix utilitzant dispositius passius, com a retardadors d'ona, que induïxen una quantitat fixa de birefringència, o controladors de polarització mecànics, els principals desavantatges de la qual són la seua incapacitat per a induir un determinat tipus de birefringència (pura lineal, circular o el·líptica) i els seus dissenys voluminosos, que els fan inadequats per a la integració. Llavors, la investigació se centra en controladors de polarització alternatius, basats principalment en fenòmens òptics lineals i no lineals. Entre les diverses interaccions no lineals llum-matèria estudiades, la dispersió de Brillouin estimulada cap arrere (SBS) emergix com un candidat prometedor per al control de la polarització de la llum. La seua resposta a una ona de llum intensa (bombament) és dependent de la polarització, i és el procés no lineal amb menor potència òptica d'activació. A més, la flexibilitat per a la sintonització de freqüència i amplada de banda s'ha demostrat consistentment alterant la longitud d'ona i la resposta en freqüència de l'ona de bombament.

Esta Tesi doctoral aprofundix en les propietats dependents de la polarització del SBS, amb l'objectiu d'aconseguir un control total de la polarització de la llum en termes de birefringència, freqüència i amplada de banda. Els fonaments teòrics desenvolupats ací proporcionen el coneixement per a generar i controlar el tipus i magnitud de la birefringència, el retard de grup diferencial(DGD) i la dispersió de DGD (DGDD) en fibres òptiques. Les conseqüències pràctiques d'esta investigació són significatives, demostrant a través d'experiments que estos paràmetres es poden ajustar dinàmicament amb només lleugeres variacions en el guany induït per SBS del sistema.

La nostra investigació demostra que la polarització pot controlar-se en una amplada de banda més àmplia que la resposta natural de Brillouin i adaptar-se per a proporcionar un perfil de retardancia específic. Este assoliment és una troballa important, ja que amplia les capacitats del control de polarització basat en SBS més enllà del que abans es creia possible. L'ampliació espectral del controlador de polarització basat en

SBS s'aconseguix mitjançant l'enginyeria de la resposta en freqüència de la fase de Brillouin mitjançant la regulació del bombament per retroalimentació, un enfocament nou que distingix la nostra investigació. Vam demostrar una ampliació de la retardancia de 51 MHz (interacció SBS natural) a 0,9 GHz, juntament amb un aplanament de l'espectre de retard, la qual cosa proporciona evidència concreta de l'efectivitat del nostre enfocament.

Finalment, s'analitzen diversos dispositius que empren el controlador de polarització basat en SBS com a subsistema central. Esta anàlisi va conduir a desenvolupar una nova tècnica fotònica per a implementar filtres de microones rebutja banda i passa banda en una único dispositiu. El principi de funcionament es basa a girar l'estat de polarització de la banda d'interés utilitzant el controlador de polarització basat en SBS en combinació amb una fotodetecció balancejada sensible a la polarització. Estos conceptes van permetre la implementació d'un filtre de microones fotònic en una única etapa de fibra que permet alternar dinàmicament entre respostes rebutja banda i passa banda, dotant de flexibilitat al sistema i incrementant el seu potencial d'aplicació. Les proves realitzades amb una sola etapa d'una fibra amb dispersió desplaçada mostren que es pot aconseguir un rebuig molt alt de 67 dB en la banda suprimida. L'atenuació fora de banda en la configuració passa banda, de 30 dB, té un acompliment similar a altres filtres de microones fotònics basats en SBS.

Paraules clau: ÒPTICA NO LINEAL, DISPERSIÓ DE BRILLOUIN ESTIMULAT, CONTROL DE LA POLARITZACIÓ, FOTÒNICA EN SISTEMES DE MICROONES.

Chapter 1

Introduction

> *"True progress is that which places technology in everyone's hands."*
>
> — Henry Ford.

One fundamental property of any transverse wave is polarization. Its importance can only be measured by the impact of the applications derived from it, especially in the field of optics, where, with the boom of photonics, research remains solid and steady. Polarization offers an additional degree of freedom that is leveraged in different fields. Modern optical networks based on coherent optical links strongly rely on polarization mode multiplexation to increase the data rate over the same physical channel [1]. In industrial quality control and material characterization, polarized light finds utility in inspection, aiding in the detection of stress and defects and allowing the characterization of samples through techniques such as ellipsometry [2]. Additionally, polarization-sensitive imaging techniques contribute to advancements in biomedical diagnostics, offering improved contrast and resolution [3]. In microwave photonics, polarization also plays a vital role in different areas, for example, in optical beamforming [4].

Polarization is a phenomenon exclusively associated with transverse waves, such as light, either propagated in free space or a guided medium. Transverse waves can be represented by two orthogonal electrical fields, according to [5]

$$\vec{E}(z,t) = (e_x\hat{x} + e_y\hat{y}) \exp\left[j(kz - \omega t)\right], \tag{1.1}$$

with $k = 2\pi n/\lambda_0$ the wavenumber, n the refractive index of the medium, λ_0 the wavelength in the vacuum, and ω the angular frequency. The state of polarization (SoP) denotes the relation in amplitude and phase between its spatially orthogonal components. An example of a linear -45° polarization state is depicted in Fig. 1.1, where e_x and e_y components are 180° phase shifted and have the same amplitude.

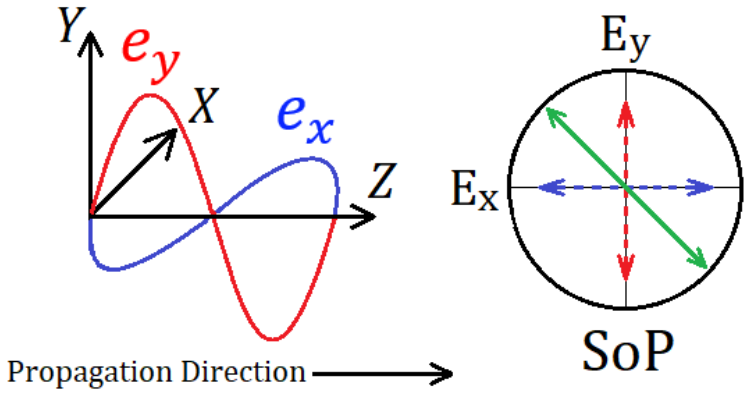

Figure 1.1: Spatially orthogonal components of an electrical field and its polarization state.

Some materials induce a different refractive index for each polarization axis. These optically anisotropic materials are said to be birefringent. This anisotropy induces a dependence of the material's refractive index on the polarization state and the light propagation direction. Birefringence manifests prominently in crystalline structures, liquid crystals, and specific polymers. Initially, it was demonstrated through the double refraction of light, where a single incident ray splits into two orthogonal polarized rays, each traveling at a distinct speed. This property finds practical applications in devices such as waveplates and polarizers, where controlled manipulation of polarized light is essential.

The mathematical description of the linear propagation of a light beam in a material is usually done in terms of matrix algebra, where the input and output signals are represented by vectors (Stokes polarization parameters), and the elements that alter the state of polarization are matrices that can be modeled using the Jones or Mueller formalism. Quarter/half/full-wave plates, linear polarizers, or any other birefringent material will have an associated Jones or Muller matrix, significantly simplifying the calculus and analysis of many linear optical systems. The main difference between Jones and Mueller's approaches is that the latter can deal with depolarized optical waves, providing a broader method for studying the evolution of polarization states of an input light beam as it propagates through a linear medium or optical device. However, this does not put Jones matrices in the back; in fact, both are complementary [6]. A complete analysis of polarization is given by a graphical representation of the states of polarization via the Poincaré sphere [5][6], that is shown in Fig. 1.2. The most representative states of polarization of light are presented here: linear horizontal and vertical, as well as right and left-handed SoPs. Any arbitrary SoP can be found on the Poincaré sphere, such as other linear states located in the equator line of the sphere, and elliptical SoP, which can be interpreted as transition SoP between linear and circular states of polarization. The Stokes vector of an optical signal can be obtained straightforwardly from the Poincaré sphere by extracting the Cartesian coordinates

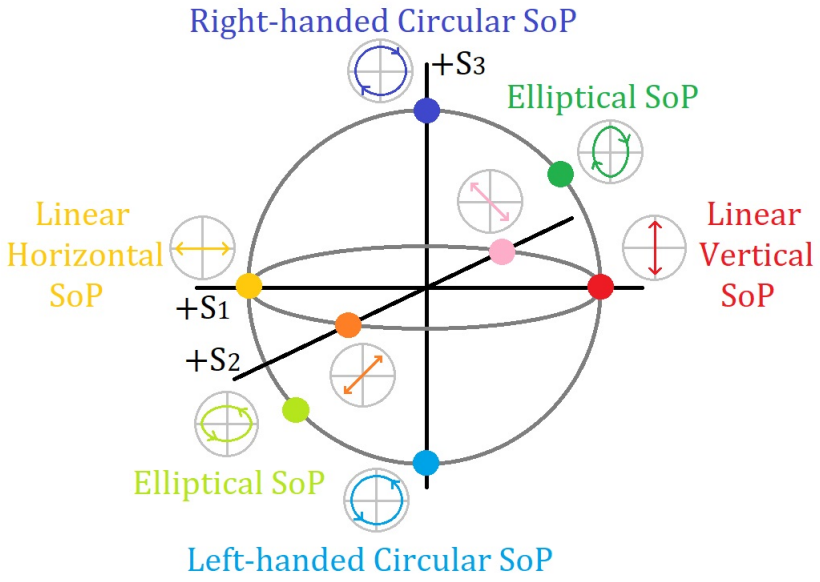

Figure 1.2: The Poincaré sphere with the most representative state of polarization (SoP) of light.

(denoted as S_1, S_2 and S_3) of the SoP plotted on it. The fourth element of the Stokes vector, S_4, is the power of the optical signal. Thus, the Poincaré sphere becomes a powerful graphical tool necessary to understand the polarization phenomenon deeply.

1.1. Polarization Controllers

A device that modifies the polarization state of a light beam in a controlled manner is called a polarization controller. In general, they are composed of retarders, which are birefringent components that have different refractive indexes along their polarization axes (also known as slow and fast axes). This difference in the refractive indexes leads to polarization-dependent phase shifts. Birefringence can be classified into linear, circular, and elliptical. Each one produces different changes in the polarization state of a light beam, following very distinct trajectories on the Poincaré sphere, as shown in 1.3. The associated Jones and Mueller matrices for each case have different characteristics, too (this will be further analyzed in Chapter 2). Some crystals, such as calcite, quartz, or synthetic retarders, induce linear birefringence [6]. For example, quartz is employed to build wave plates, i.e., retarders with a determined phase shift, typically quarter-wave $\lambda/4$ or half-wave $\lambda/2$ transformers.

Many research fields require a certain arbitrary SoP for an optical signal, usually achieved through polarization controllers. Examples of this include nonlinear optics [7][8], microwave photonics [9][10], quantum encryption [11] or holography [12] and imaging [13]. A typical example of this is the inclusion of a polarization controller at the input of an optical modulator to align the state of polarization of the incoming light

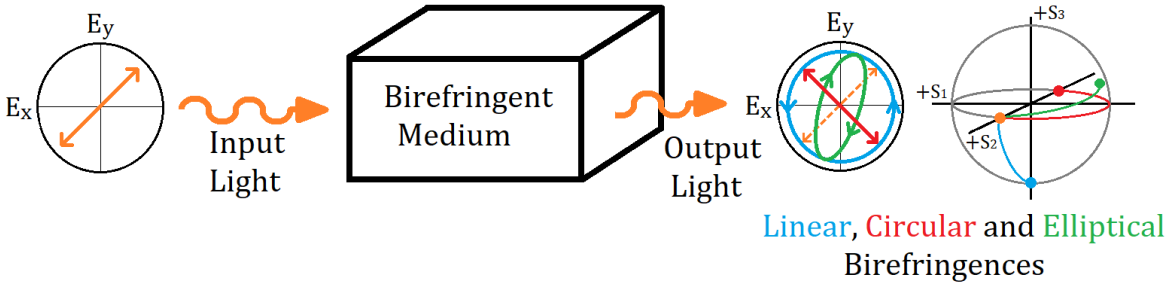

Figure 1.3: An incoming light beam is affected by three different types of material birefringence: linear, circular, and elliptical.

beam to the polarization axis of the modulator's crystalline structure so that the modulation index is maximized [14]. Current optical fiber technology commercially offers only two types of polarization controllers: the manual polarization controller, whose working principle is the twisting of an optical fiber, and the electronic-re-configurable version. These mechanically driven polarization controllers are broadband and cannot independently control a set of channels. As the change in the state of polarization of the optical signal is done in the total bandwidth of the optical fiber, specific applications demand the inclusion of extra subsystems that contain filters, polarization beam splitters, or polarizers to restrict its operational bandwidth. Due to how they are constructed (twisting an optical fiber), another disadvantage in this type of polarization controller is the difficulty of continuously following a determined path of birefringence (e.g., pure linear, pure circular, or pure elliptical).

1.2. Linear and Nonlinear Phenomena for Polarization Control of Light

Instead of mechanically driven polarization controllers, an alternative path to pursue full-polarization control is to modify the properties of an electromagnetic wave using unique attributes that some materials can offer. Natural anisotropic materials and metamaterials introduce changes in the refractive index that allow them to control the state of polarization of a light beam. Thus, a constant amount of birefringence for a given propagating direction is induced, which can be linear, circular, or, in general, elliptical [15]. Bulky components based on dielectrics and liquid crystals actively control the polarization state and/or introduce a phase delay in light [16]. Artificially structured metamaterials [17][18] have been designed to offer polarization control with additional degrees of freedom in the design of optical systems. Nanophotonic research intends to shrink the size of polarization controllers to the nanoscale by proposing new nanophotonic structures [19].

On the other hand, nonlinear interaction between light and matter has always been

in the spotlight to perform multiple types of optical signal processing, especially for the control of the state of polarization of light. The concept behind it consists of applying an electrical field to modify the refractive index of the material in a way that polarization-dependent phase shifts are induced in a light beam. A successful dynamic change of the polarization state of an optical signal using the Pockels effect in a LiNbO3 crystal has been proposed in [20]. Still, they presented practical limitations due to the high drive voltage (0.7 kV/mm) required to induce a π radians shift on the optical wave. The latest research in polarization controllers relies on the Kerr effect in high-finesse Fabry–Pérot fiber cavities [21], where it is shown only polarization conversion of a linearly polarized wave to right/left circularly polarized waves. Here, the Kerr effect is induced in the cavity by the input optical signal by increasing its optical power, provoking a change in its polarization state when it surpasses a determined threshold power level.

The fundamentals for polarization control based on a pump-probe scheme have been proposed and demonstrated via four different nonlinear phenomena: four-wave mixing [22], polarization and mode coupling (in multimode fibers) [23], stimulated Raman scattering [24] and stimulated Brillouin scattering (SBS) [25]. Among these candidates, SBS emerges as the most appealing option to perform polarization control because it is the nonlinear effect that requires less power to be activated and presents frequency ranges of application that can be easily handled by using current photonic technology [8]. The following two sections describe the stimulated Brillouin scattering process and the current state-of-the-art in polarization control using SBS.

1.3. Stimulated Brillouin Scattering

SBS is an inelastic scattering nonlinear phenomenon in which incident light (pump wave) photons are scattered within an optical fiber due to its interaction against thermally induced density fluctuations characterized by macroscopic vibrations of the material (i.e., sound waves). The scattered wave (named the Stokes wave) travels in the opposite direction of the pump wave. It reinforces the scattering process between the pump and sound waves via the mechanism of electrostriction, that is, a material deformation by applying an electric field. Subsequently, more photons that stimulate the electrostriction process are backscattered, establishing a positive feedback loop. As a consequence of the inelastic scattering, where the Stokes photons have less energy than the pump photons, the backscattered Stokes wave is downshifted in frequency. Additionally, the Stokes wave has a spectral distribution determined by the phonon lifetime in the optical fiber. Two fundamental parameters of the SBS nonlinear phenomenon are defined from these properties: the Brillouin frequency shift ν_B and the Brillouin linewidth $\Delta\nu_B$.

SBS has its roots in the study of nonlinear interactions between light and acoustic waves in a propagating medium. The phenomenon was first theoretically described by Léon Brillouin in 1922 [26], who proposed light scattering by thermally induced acoustic waves. Later, in 1930, E. F. Gross conducted the first experiments in liquids [27], which allowed him to validate the phenomenon. Several decades later, with the advent of laser technology, researchers began to observe and understand SBS in optical fibers [28]. In the beginning, in optical fiber communication systems, it was realized almost immediately that the backward reflection occurring in SBS would be the ultimate limit to the power levels that could be transmitted through fibers. In other words, SBS was considered to have a detrimental effect on optic communication systems, and some research was focused on its mitigation. In parallel, other valuable practical applications of SBS were investigated.

An explosive growth in SBS-related publications has been observed in the last 20 years, and it has widely expanded its applicability to different fields [29]. Besides all the technological background developed for fiber-based systems, two principal reasons justify such expansion: its narrow Brillouin linewidth (around 50 MHz in standard single-mode fibers) and the possibility of tuning the Brillouin frequency shift (around 10 GHz in standard single-mode fibers). SBS is being used to implement optical lasers and amplifiers with ultra-narrow linewidth [30], which can provide long coherence lengths in combination with wavelength tunability. These new light sources can be used for spectroscopy, seed waves for frequency combs, the generation of precision clocks, the synthesis of microwave signals, and coherent receivers for data communications. These characteristics of SBS also permitted the characterization of narrow-linewidth light sources [31] and the implementation of optical spectrum analyzers with unprecedented wavelength resolution in what is known as Brillouin optical spectrum analyzers (BOSA) [32][33].

Brillouin scattering allows for distributed and precise measurements of environmental parameters along optical fibers. Brillouin-based fiber sensing relies on the interaction between incident light and acoustic waves induced by temperature or strain variations in the fiber. This interaction is highly dependent on these environmental changes, producing variations in the Brillouin frequency shift of the scattered wave. These features have been used for the development of Brillouin Optical Time Domain Analysis (BOTDA) [34][35] to retrieve spatial information of temperature and strain along an optical fiber link. This method is commercially available for monitoring strain distributions in bridges [36], tunnels [37], as well as transmission lines [38]. SBS has also been applied to process microwave signals in the optical domain, for example, for phase control [39], filtering [40] and signal generation [41]. Brillouin scattering is also applied to implement narrowband optical delay lines in fiber [42]. Brillouin dynamic gratings (BDG), a subfamily of SBS interactions, permit the implementation of several types of analog

signal processing operations, such as time differentiation, time integration and true-time reversal (TTR), microwave photonic reconfigurable filters, phase-shifted BDGs, tunable optical delay lines, isolators, pulse compression, frequency combs, sensors, and reflectometers [43].

The demand for low-latency, high-density, and low-power dissipation devices is continuously growing. Optical signal processing can compete with electronics in very high-speed systems, overcoming some limitations associated with broadband parallel processing and power consumption. Moreover, some photonic applications, such as true-time reversal or high-Q microwave filtering, have no similar counterparts in electronics. Bragg gratings can implement these and other signal processing operations [44], which can consequently be replaced by SBS-based systems. These reasons motivated the intensive research on the excitation of SBS interactions in photonic chips to give rise to new possibilities in terms of integration and miniaturization of SBS processors [45][46]. Specific photonic integrated platforms able to embed chalcogenide materials allow the excitation of Brillouin scattering in a Photonic Integrated Circuit (PIC) [47] and multiple signal processing operations [48]. Thus, integrated Brillouin photonics can leverage the development of analog processors if large enough markets are developed. Design and test of new materials, such as special fibers and micro- and nano-waveguides, that aim at re-utilizing the well-established silicon-based chip foundries and fiber-optic components in industrial manufacturing, also contributes to the miniaturization of SBS interactions and the reduction of the power required to drive the acoustic wave [49][50].

Further details on the SBS mechanism are provided in Appendix A.

1.4. Stimulated Brillouin Scattering for Polarization Control

The advantages of SBS over other nonlinear electromagnetic wave-matter interactions permit the implementation of techniques for controlling light polarization. Despite SBS-related research that has been carried out for more than 100 years [51], so far in the literature, only two polarization control techniques using this nonlinear phenomenon can be found. Polarization pulling was the first technique proven to drag a light beam's state of polarization (SoP) using a strong pump [52]. The basis of the polarization pulling technique consists of considering the fiber as a polarization-dependent gain (or loss) medium with two orthogonal input and output orthogonal SoPs, which, respectively, provide the signal maximum and minimum SBS amplification (or attenuation). Under high Brillouin gain conditions, the output SoP of arbitrarily polarized input signals would tend to converge towards that of maximum SBS gain. In the case of

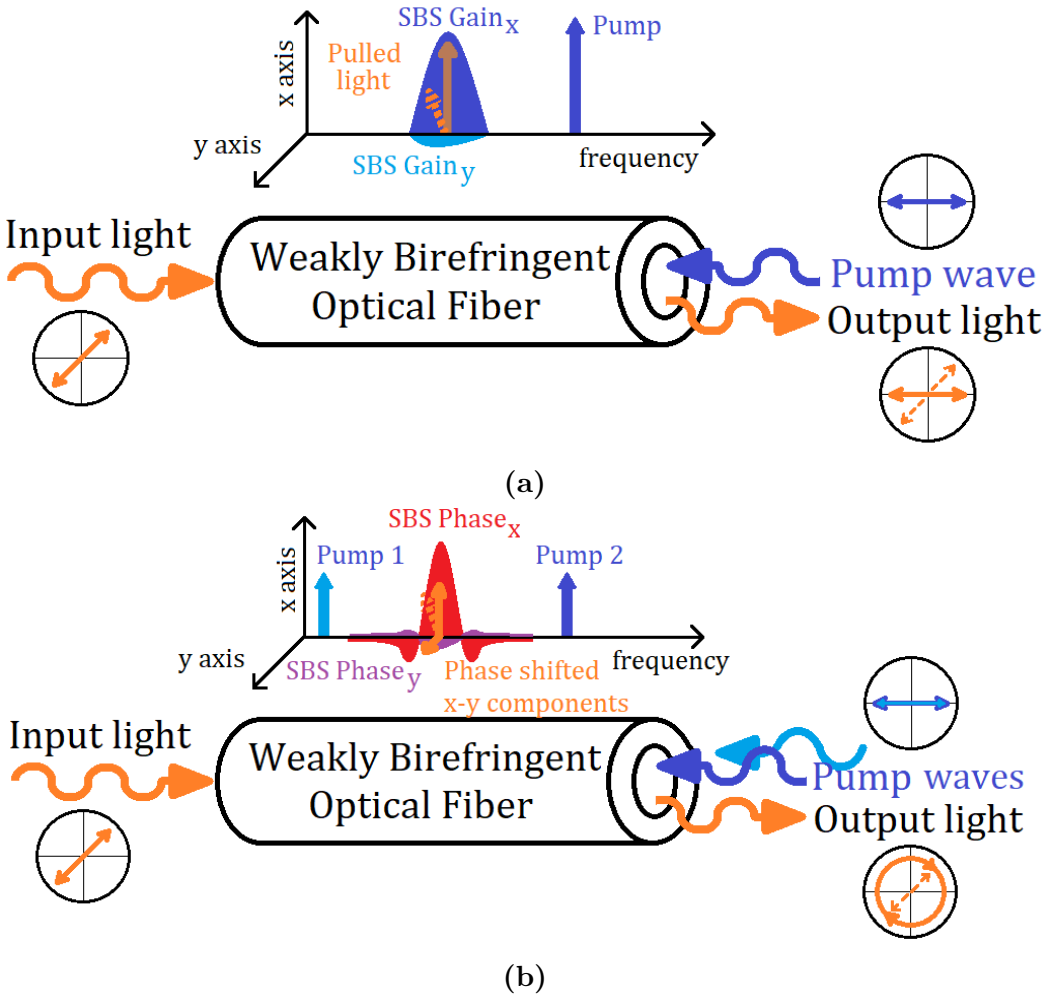

Figure 1.4: SBS-based polarization control mechanisms of (a) polarization pulling and (b) polarization conversion.

high SBS attenuation, the output SoP of an arbitrarily polarized signal would approach the output SoP corresponding to minimum attenuation. Recently, a new approach for controlling the polarization state of a light beam was presented [53] that, similarly to polarization pulling, exploits the polarization-dependent interactions that SBS offers in single-mode fibers with a fixed low birefringence [55], but at the same time is different, because it transparently performs the control of the signal SoP by combining gain and loss responses produced by two orthogonal pumps to change the relative phase between both orthogonal components of the signal polarization state. Both polarization control techniques are illustrated in Fig. 1.4a and Fig. 1.4b, respectively, and show how each one performs the polarization control. In this example, despite both schemes having the pump set at the x polarization axis, the effect induced by the SBS interaction on the signal is different, producing a dissimilar SoP in the output light beam. There are three principal reasons for focusing on the latter polarization control method, also known as SBS-induced polarization conversion, rather than polarization pulling:

- The signal's polarization state follows a well-defined path on the Poincaré sphere

as the pump power increases.

- It is based on the phase profile of the SBS response with gain and loss compensation, which, in principle, might avoid the induction of high SBS gains that could lead to pump depletion.

- The polarization conversion is performed transparently, i.e., it does not add gain or loss to the signal wave.

As it will be further seen, the first two properties become relevant to achieve reliable and complete polarization of light, and the third one will be important for some applications that can be derived from it.

1.5. Thesis Outlook

The objective of this Thesis propose and develop a method for full polarization control of light using Stimulated Brillouin Scattering polarization-dependent interactions and the search for technological applications using the polarization controller structure proposed in [53].

Full polarization control refers to controlling not only the amount and type of birefringence induced in the material but also the bandwidth and the spectral shape. By proving its feasibility, it will allow the development of practical all-optical nonlinear polarization controllers and pave the way to fully reconfigurable optical devices such as remote wavelength routers of signals for optical networks, new microwave photonics subsystems, fiber sensors, etc.

This Thesis is structured as follows: in Chapter 2, the basis for dynamically inducing birefringence in optical fibers is presented, where the control of both its amount and type, as well as differential group delay and differential group delay dispersion, is performed by exploiting the polarization dependence of SBS. In Chapter 3, a pump engineering technique that permits tailoring and extending the operational bandwidth of the SBS polarization controller is developed. Chapter 4 is devoted to giving guidelines on constructing some photonic devices based on the SBS full polarization controller. A dual notch/passband microwave photonic filter will be shown in concrete. The Conclusions and Future work derived from this Thesis are found in Chapter 5. Finally, this Thesis includes two appendices. In the first, Appendix A, the theory of Brillouin Light Scattering is briefly reviewed. Appendix B models used for describing the SBS gain spectrum are provided and then used to characterize our SBS-fiber system.

Chapter 2

Birefringence Control[†]

As discussed in the previous Section, birefringence is an essential property of optical materials that allows a different path for manipulating optical signals and can be dynamically changed through nonlinear effects. A theoretical description of the control of the polarization of a light wave using an auxiliary light wave (pump-probe scheme) via a nonlinear phenomenon was described in [54]. In a pump-probe scheme, the pump wave produces a change in the refractive index of the propagating media of the form $n = n_0 + k_n I_P$, where n is the new refractive index, n_0 the natural (non-excited) refractive index of the material, k_n is a proportionality factor, and I_P is the intensity of the pump wave. When the probe or signal wave passes through this nonlinear medium, it experiences this change in the refractive index as a phase shift. Suppose this pump-power-dependent refractive index exhibits different constants k_n depending on the states of polarization (SoP) of the signal and pump waves. Birefringence will be induced in that case, which is sufficient to achieve polarization control. From this reasoning, an analysis can be carried out by considering a nonlinear medium that presents two arbitrary orthogonal polarization axes, generically defined as parallel $\parallel$ and perpendicular $\perp$. In this case, the pump should induce a change in the refractive index such that

$$n_{\parallel} = n_0 + k_{\parallel} I_P \tag{2.1a}$$

$$n_{\perp} = n_0 + k_{\perp} I_P. \tag{2.1b}$$

From 2.1, the condition to produce a relative change in both refractive indexes of the nonlinear media, i.e., induce birefringence, and consequently achieve dynamic polarization control, is $k_{\parallel} \neq k_{\perp}$. The abovementioned process is illustrated in 2.1, where $\parallel$ and $\perp$ polarization axes correspond to the x and y Cartesian polarization axes, respec-

[†]This Chapter is based on: D. Samaniego, G. Zoireff and B. Vidal, «Brillouin-Induced Dynamic Arbitrary Birefringence», in *Journ. of Light. Technol.*, vol. 39, no. 7, pp. 1961-1967, 1 April, 2021.

tively. It can be seen that the y component of the probe wave results shifted $\pi/2$ from its initial state, provoking at the end of the propagation through the excited nonlinear medium a change of its polarization state from linear -45° SoP to left-handed circular SoP.

Now, finding a nonlinear phenomenon that provides the previous condition is necessary. Hopefully, light-to-matter interactions in Stimulated Brillouin Scattering (SBS) fit very well in this description. Here, the difference in the refractive indexes is achieved due to different induced Brillouin gains and phases according to the relative SoP of pump and probe waves [55].

This Chapter gives the fundamentals of the induction of arbitrary birefringence by using the nonlinear process of Stimulated Brillouin Scattering in optical fibers. Birefringence is generated in a controlled manner, allowing dynamic modification of its magnitude and type, such as, for example, going from linear to circular birefringence. Subsequently, the generation of differential group delay (DGD) and differential group delay dispersion (DGDD) using SBS is investigated, which could potentially be employed in polarization-mode dispersion (PMD) emulators and reconfigurable optical delay lines, giving support to those fiber-monitoring systems that combine the principle of polarization-nulling and BOSA [56].

2.1. Birefringence Control Using SBS

An isotropic transmission medium in which the refractive indexes of orthogonal propagation modes (LP_{01x} and LP_{01y} in a single-mode optical fiber), n_x and n_y, are different, is known as birefringent. Birefringence, B_m, is defined as

$$B_m = |n_x - n_y|, \tag{2.2}$$

In our case, the change in the refractive index between orthogonal axes is related to the polarization-dependent phase shifts produced in the propagating medium via

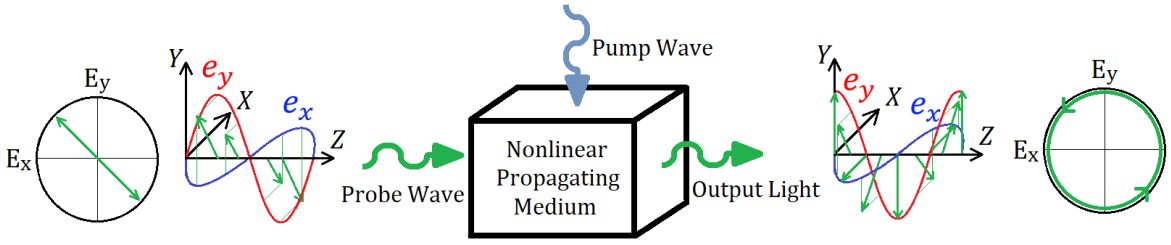

Figure 2.1: Pump-probe scheme for inducing birefringence via a nonlinear process. The probe wave experiences a phase shift on the y axis component of its electrical field, resulting in a change of the polarization state at the end of the propagation through the excited nonlinear medium. Note: $\parallel$ and $\perp$ polarization axes correspond to the x and y Cartesian polarization axes, respectively.

stimulated Brillouin scattering according to

$$n_x = n_0 + \Delta n_x = n_0 + \phi_x \frac{\lambda}{2\pi L} \tag{2.3a}$$

$$n_y = n_0 + \Delta n_y = n_0 + \phi_y \frac{\lambda}{2\pi L}, \tag{2.3b}$$

where L is the fiber length, n_0 is the effective refractive index, and ϕ_x, ϕ_y are the polarization-dependent phase shifts generated in the optical fiber. Thus, birefringence can be dynamically controlled via SBS polarization-dependent phase shifts as follows

$$B_m = |n_x - n_y| = \frac{\lambda}{2\pi L}|\phi_x - \phi_y|. \tag{2.4}$$

Let f_{P1} and f'_{P1} be a primary pair of pumps located at $f_0 \mp (\nu_B + \Delta\nu_B/2)$ from the band of interest f_0, where $\Delta\nu_B$ is the full width at half maximum (FWHM) bandwidth of the Brillouin gain response and ν_B is the Brillouin frequency shift. Each pump of the pair generates a gain/loss Brillouin response over the x polarization axis (see Fig. 2.2a). Each response causes a variation in the refractive index according to

$$\Delta n_1, \Delta n_1' = \mp\xi \frac{g_0 P_p L_{eff} c}{2A_{eff} 2\pi L f} \frac{\Delta\nu_B \left(f - f_0 \pm \Delta\nu_B/2\right)}{\left(f - f_0 - \Delta\nu_B/2\right)^2 + \left(\Delta\nu_B/2\right)^2}, \tag{2.5}$$

where g_0 is the Brillouin gain factor, P_p is the pump power, L_{eff} is the effective interaction length of the fiber, A_{eff} is the effective area of the fiber [53]. If SBS is induced in single-mode fibers with fixed low birefringence, its gain and phase responses have

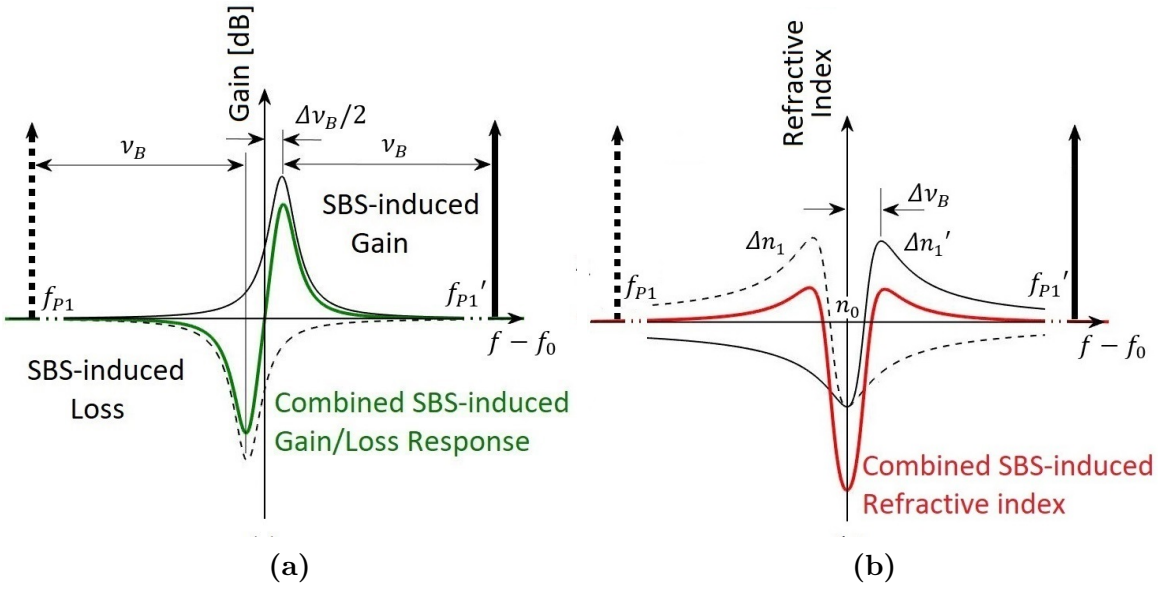

(a) **(b)**

Figure 2.2: Combined SBS-induced (a) gain (green) and (b) refractive index (red) responses generated by two pumps symmetrically placed at $f_0 \mp (\nu_B + \Delta\nu_B/2)$. Dashed and solid lines indicate the effects of f_{P1} and f'_{P1}, respectively.

polarization-dependent characteristics [55]. This polarization dependence of SBS is introduced by the ξ factor, which is 2/3 if the counterpropagating signal SoP is aligned to the pump SoP and 1/3 if it is orthogonal.

If a symmetric pair of pumps is used, a gain plus a loss SBS response can be combined, as shown in Fig. 2.2a. Thus, the combined amplitude response is always compensated, whereas the refractive index reaches a negative minimum at the frequency of interest f_0, as shown in Fig. 2.2b.

From the signal perspective, during its propagation through the fiber, it experiences different refractive indexes according to its SoP. At the frequency of interest f_0, the signal effectively experiences the following variations around the effective refractive index n_0

$$\Delta n_{1x} = -\xi_{1x} \frac{g_0 P_p L_{eff} c}{A_{eff} 2\pi L f_0} \tag{2.6a}$$

$$\Delta n_{1y} = -\xi_{1y} \frac{g_0 P_p L_{eff} c}{A_{eff} 2\pi L f_0}. \tag{2.6b}$$

When the SoP of the signal is aligned with the pump's SoP, i.e., the x axis, it turns out that $\xi = \xi_{1x} = 2/3$. On the other hand, when it is aligned to the y axis (orthogonal SoP) $\xi = \xi_{1y} = 1/3$. This difference in both factors, $\delta\xi = \xi_{1x} - \xi_{1y} = 1/3$ is sufficient to generate birefringence via SBS.

Now, let's consider a secondary pump pair, f_{P2} and f'_{P2}, at $f_0 \mp (\nu_B - \Delta\nu_B/2)$ set along the y polarization axis. Their SBS responses are similar to those in Fig. 2.2, but the induced refractive index variations reach a maximum positive value at f_0

$$\Delta n_{2x} = \xi_{2x} \frac{g_0 P_p L_{eff} c}{A_{eff} 2\pi L f_0} \tag{2.7a}$$

$$\Delta n_{2y} = \xi_{2y} \frac{g_0 P_p L_{eff} c}{A_{eff} 2\pi L f_0}. \tag{2.7b}$$

where $\xi_{2x} = 1/3$ and $\xi_{2y} = 2/3$. In this case, $\xi_{2x/y}$ values change with respect to $\xi_{1x/y}$ because the second pump pair is set along the y polarization axis. The variation in the refractive index induced by the primary and secondary pumps at the central frequency f_0 is

$$\Delta n_{x0} = \Delta n_{1x} + \Delta n_{2x} = -\delta\xi \frac{g_0 P_p L_{eff} c}{A_{eff} 2\pi L f_0} \tag{2.8a}$$

$$\Delta n_{y0} = \Delta n_{1y} + \Delta n_{2y} = \delta\xi \frac{g_0 P_p L_{eff} c}{A_{eff} 2\pi L f_0}. \tag{2.8b}$$

Thus, the total birefringence, defined in 2.2, can be maximized in the band of

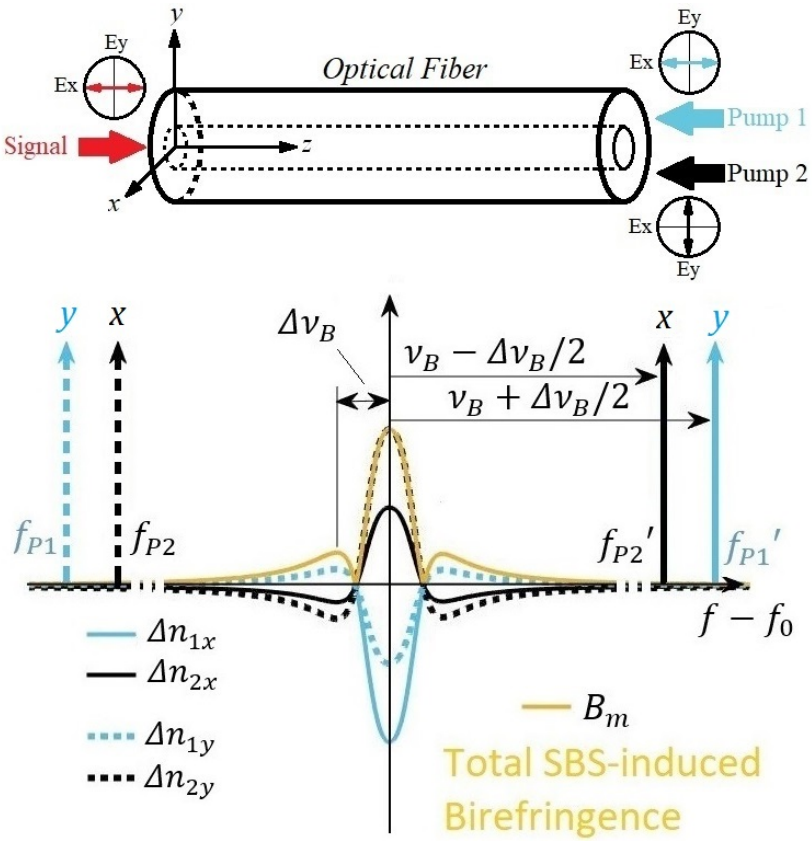

Figure 2.3: Maximization of birefringence in an optical fiber at f_0 using primary (f_{P1}, f'_{P1}) and secondary (f_{P2}, f'_{P2}) pairs of pumps. The refractive index variations induced along x and y axes are plotted in solid and dashed lines, respectively.

interest

$$B_{m0} = 2\,\delta\xi\,\frac{g_0 P_p L_{eff} c}{A_{eff} 2\pi L f_0}. \tag{2.9}$$

This process is illustrated in Fig. 2.3, using two pairs of orthogonal pumps to combine their responses to maximize the birefringence induced at f_0. Each pair of pump waves can easily be achieved by biasing an external modulator at the minimum transmission bias (MITB) with a microwave signal of frequency f_P, as shown in Fig. 2.4.

2.1.1. SBS-induced Dynamic Arbitrary Birefringence

The previous analysis considered the signal and pump in a $x-y$ basis state. It can be extended to any orthogonal basis in order to manipulate the system's birefringence arbitrarily.

The birefringence induced through SBS can be expressed using the generalized Jones matrix formalism as,

$$\mathbf{J} = \mathbf{F}^{-1}\mathbf{J}_{\mathbf{SBS}}\mathbf{F}; \tag{2.10}$$

where $\mathbf{J}$ is the Jones matrix of the nonlinearly induced birefringence, and $\mathbf{F}$ is the

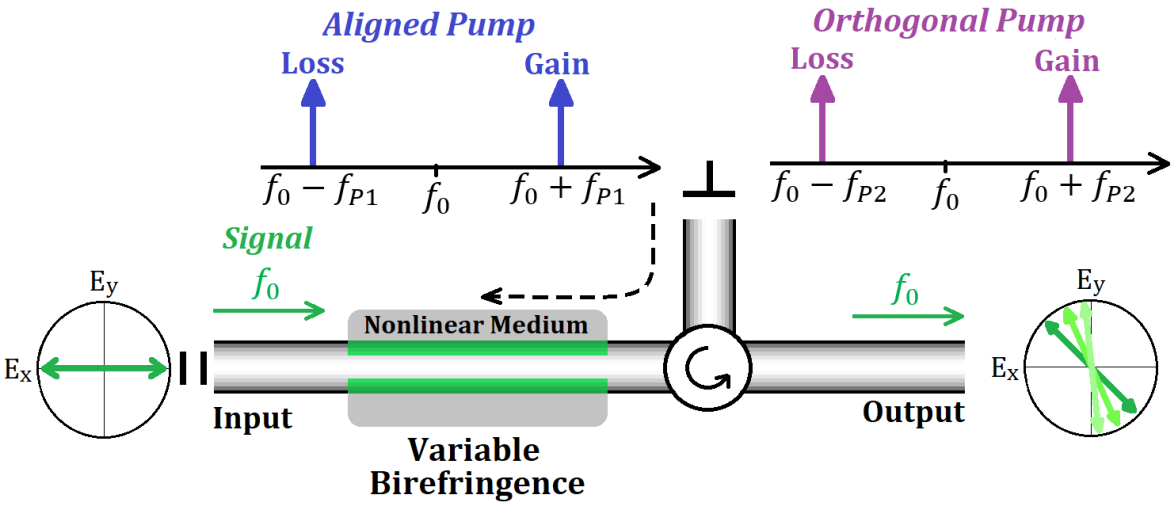

Figure 2.4: Brillouin-based variable birefringence device.

transformation matrix related to the arbitrary SoP of the pump. It can be calculated from the SoP of the orthogonal pumps as basis states [25], and $\mathbf{J_{SBS}}$. Considering the $x-y$ basis state, $\mathbf{J_{SBS}}$ is given by

$$\mathbf{J_{SBS}} = \begin{pmatrix} \exp\begin{pmatrix} G_{1x} + A_{1x} + G_{2y} + A_{2y} \\ +j\frac{\pi L f_0}{c} B_{m0} \end{pmatrix} & 0 \\ 0 & \exp\begin{pmatrix} G_{1y} + A_{1y} + G_{2x} + A_{2x} \\ -j\frac{\pi L f_0}{c} B_{m0} \end{pmatrix} \end{pmatrix} \tag{2.11}$$

where G_x and G_y are the maximum and minimum exponential Brillouin gains, respectively, while A_x and A_y are the maximum and minimum Brillouin loss, and B_{m0} is the maximum birefringence generated at f_0 from both the primary and secondary pumps. When the gain and loss amplitude responses overlap, they compensate each other, i.e., $G_x + A_x \approx 0$, and $G_y + A_y \approx 0$. Thus, the system behavior is equivalent to an isotropic retarder without significant power change at f_0, granting transparency to the nonlinear media.

The following transformation matrix gives the effect of the pump SoP on the induced birefringence:

$$\mathbf{F} = \begin{pmatrix} \cos(\delta + \pi/4)\exp(-j\phi_x) & -\sin(\delta + \pi/4)\exp(j\phi_y) \\ \sin(\delta + \pi/4)\exp(-j\phi_y) & \cos(\delta + \pi/4)\exp(j\phi_x) \end{pmatrix}; \tag{2.12}$$

where δ is the azimuth of the major axis of the ellipse of polarization of the pump and ϕ_x, ϕ_y represent the phases of the electric-field components along the x and y axes.

Linear birefringence is obtained when the pump pairs have linear SoPs (horizontal and vertical), as shown in Fig. 2.5a. For circular birefringence, pump pairs with left and right circular polarizations are used instead (Fig. 2.5b). In general, elliptical bire-

fringence is obtained when the SoP of the pump pairs is elliptical (Fig. 2.5c). Thus, arbitrary types of transparent birefringent elements can be implemented by choosing the pump's polarization state. The pump power determines the amount of birefringence, and the reconfigurability speed is mainly given by the length of the medium used for the Brillouin interaction.

2.1.2. SBS-induced Dynamic Differential Group Delay

The SBS-induced birefringence is associated with a variation in the group velocity of orthogonal polarization axes (τ_{gx}, τ_{gy}), i.e., it could induce a differential group delay (DGD)

$$DGD = |\tau_{gx} - \tau_{gy}| = \frac{\omega}{c}\frac{dB_m}{d\omega}, \tag{2.13}$$

with ω the angular frequency and c the speed of light. As it can be seen in Fig. 2.3, if only the primary pumps, f_{P1} and f'_{P1}, are applied, birefringence has a peak value at f_0, which corresponds to zero group delay at this frequency and consequently, no DGD. On the other hand, maximum/minimum group delay along x axis is located approximately at $f_0 \pm \Delta\nu_B/2$,

$$\tau_{gx-max/min} = \tau_{g1x} + \tau'_{g1x} = \pm\xi_x \frac{28}{25}\frac{g_0 P_P L_{eff}}{2\pi A_{eff}}\frac{1}{\frac{\Delta\nu}{2}}. \tag{2.14}$$

Similarly, the maximum/minimum group delay along the y axis at the same frequencies can be obtained

$$\tau_{gy-max/min} = \tau_{g1y} + \tau'_{g1y} = \pm\xi_y \frac{28}{25}\frac{g_0 P_P L_{eff}}{2\pi A_{eff}}\frac{1}{\frac{\Delta\nu}{2}}. \tag{2.15}$$

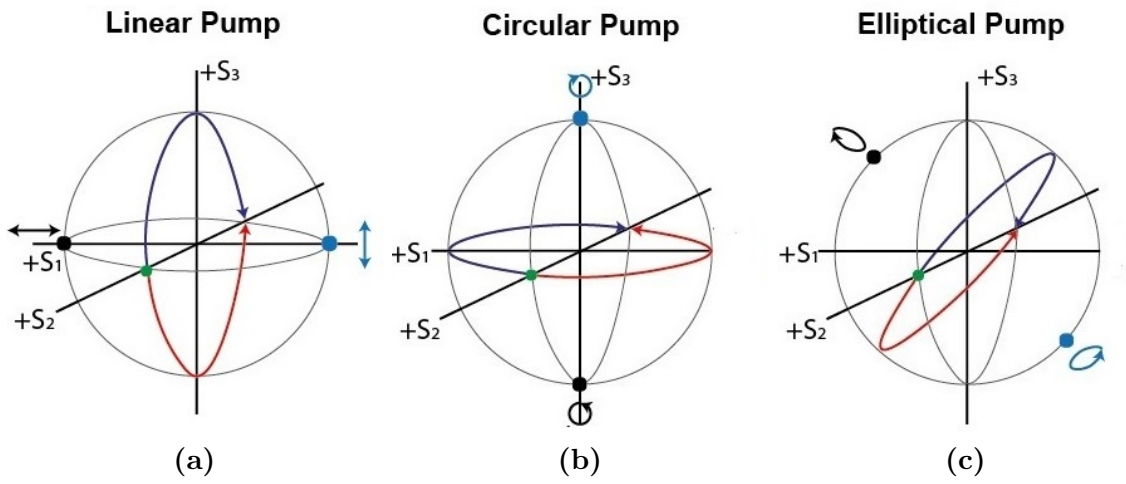

Figure 2.5: Dependence of the type of birefringence on the SoP of the pump signal: (a) linear birefringence with a linear pump, (b) circular birefringence with a circular pump, and (c) elliptical birefringence with an elliptical pump.

Figure 2.6a shows a graphical representation of both delays. By employing 2.13, the maximum induced DGD can be determined

$$DGD_{max} = \delta\xi \frac{28}{25} \frac{g_0 P_P L_{eff}}{2\pi A_{eff}} \frac{1}{\frac{\Delta\nu}{2}}. \tag{2.16}$$

For frequencies $f < f_0$, the y axis takes the role of the fast axis since its induced group delay is positive. Meanwhile, if a light beam with frequencies $f > f_0$ is set in the x polarization axis, it will propagate faster than in the y polarization axis. In other words, x and y axes act as a frequency-dependent fast/slow light generator pair. Thus, DGD can be easily manipulated by adjusting the power of pumps in the x and y axes. However, the SBS-induced gain/loss response (Fig. 2.2a) must also be considered. It affects the signal at $f_0 \pm \Delta\nu_B/2$ because the system intrinsically provokes a single sideband modulation. Therefore, using only a single pair of pumps, it is expected to experience only slow light signals.

2.1.3. SBS-induced Dynamic Differential Group Delay Dispersion

Another property derived from the DGD is the DGD dispersion (DGDD) or second-order DGD, which is determined as the difference between the slopes of the induced group delays on x and y axes. Each slope is, by definition, the induced group velocity dispersion (GVD) on the corresponding propagation axis. At f_0, it is

$$DGDD = GVD_x - GVD_y = \delta\xi \frac{28}{25} \frac{g_0 P_P L_{eff}}{(2\pi)^2 A_{eff}} \frac{1}{(\Delta\nu/2)^2}. \tag{2.17}$$

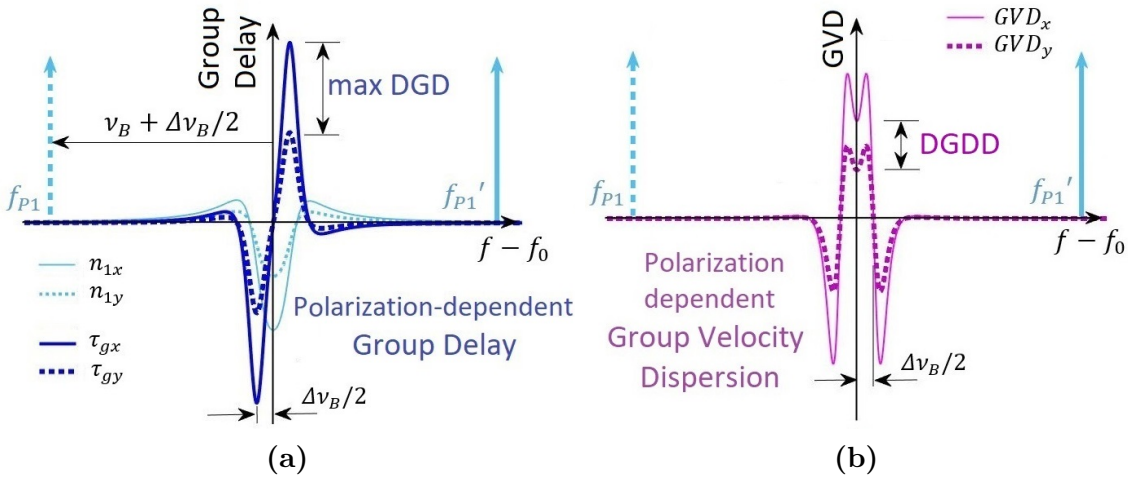

Figure 2.6: SBS-induced (a) group delay and (b) group velocity dispersion responses of two pumps symmetrically placed at $f_0 \mp (\nu_B + \Delta\nu_B/2)$. Effects produced along x and y axes are plotted in solid and dashed lines.

As shown in Fig. 2.6b, this value is not uniform over the bandwidth $\Delta\nu$ and is not the maximum value. DGDD can be controlled by modifying the pump power as in the previously studied cases. Analogous analysis can be carried out for the secondary pairs of pumps f_{P2} and f'_{P2}, resulting in the curves of Fig. 2.6 but inverted. Additionally, the transformation stated in Section 2.1.1 for a different pair of orthogonal pumps is also valid.

2.2. Experimental Setup

Experiments have been conducted to prove the concept of an arbitrary birefringent element, differential group delay, and differential group delay dispersion induced by SBS.

Figure 2.7 shows the block diagram used to demonstrate the feasibility of the nonlinearly-induced arbitrary birefringence and its properties. An optical signal at $\lambda = 1548.25$ nm is split into two paths: the upper one is used to generate the pump waves, whereas the lower one experiences variable birefringence. The pump is genera-

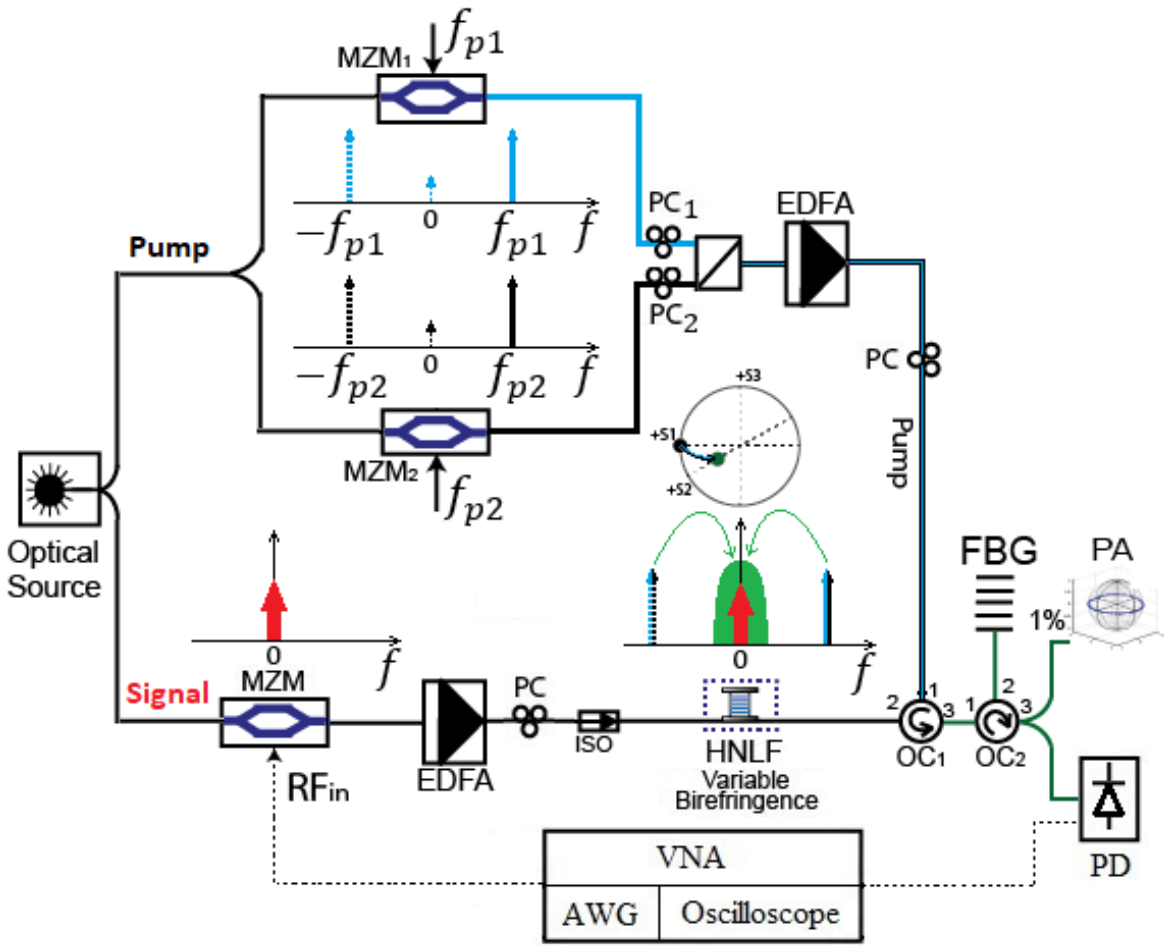

Figure 2.7: Experimental setup.

ted by amplitude modulation of the optical signal using two Mach-Zehnder modulators (MZM_1 and MZM_2) at minimum transmission bias (MITB) and fed by two microwave oscillators with frequencies $f_{P1} = 9.675$ GHz and $f_{P2} = 9.290$ GHz. An optical circulator (OC_1) directs the pump towards an optical fiber, where its induced birefringence is controlled. The fiber comprises 1 km of highly nonlinear fiber (HNLF). The Brillouin parameters for this fiber are $\Delta\nu_B = 70$ MHz, $g_0 = 7.19 \times 10^{-12}$ m/W, $A_{eff} = 11$ μm^2 and $\nu_B = 9.640$ GHz at 1548 nm. A second optical circulator (OC_2) directs the signal to a fiber Bragg grating (FBG) in reflection mode (bandwidth of 12.5 GHz), which is used to filter out backward residual pump waves. The induced birefringence is controlled by adjusting the pump power through the EDFA and changing the SoP of the pump wave. This induced birefringence provokes changes in the SoP of the signal wave, which is measured by a polarization analyzer (PA).

In experiments related to DGD, the SoP of the primary pair of pumps, f_{P1} and $f_{P1'}$, is set to horizontal linear polarization, and the SoP of the secondary pair of pumps, f_{P2} and $f_{P2'}$, in vertical linear. In the signal path, a Mach-Zehnder modulator (MZM) at the quadrature bias point fed by an arbitrary waveform generator (AWG, Rigol DG1062) is used to generate optical pulses. For inducing DGD by SBS, the signal is set in horizontal SoP by a polarization controller (PC), and the primary pump is turned on. Then, the primary pump is turned off, and the secondary pump is enabled. A photodiode (PD) receives the optical signal and converts it to the electrical domain. Finally, the output signal is analyzed by a Vector Network Analyzer (VNA, HP8510C), and its waveform is acquired by a digital oscilloscope (Tektronix TDS 3032) to be further processed.

Thermal variations change ν_B; consequently, it is necessary to readjust pumps' frequencies. Vibrations also affect the state polarization of the pump and signal, which is reflected as additional noise in the signal. This resetting of the system is done in periods of around 2 or 3 hours due to thermal and mechanical variations are much slower than measurements' acquisition time (hours vs. minutes). For this reason, there is no need to include fast or automated stabilizers in the setup. Despite this, no significant changes in the system's behavior have been observed during the experiments.

2.3. Results and Discussion

The Brillouin-induced birefringence grows with Brillouin gain, proportional to the effective length and pump power. This dependence can be seen in Fig. 2.8, where birefringence has been estimated from the retardance measured using the Poincaré sphere method [57]. It shows measurements of the SBS-induced birefringence for an input signal of 0.08 mW as a function of pump power for three types of birefringence: linear $\left([(1,0)]^T, [(0,1)]^T\right)$, circular $\left(\left[1/\sqrt{2}(1,j)\right]^T, \left[1/\sqrt{2}(1,-j)\right]^T\right)$ and elliptical

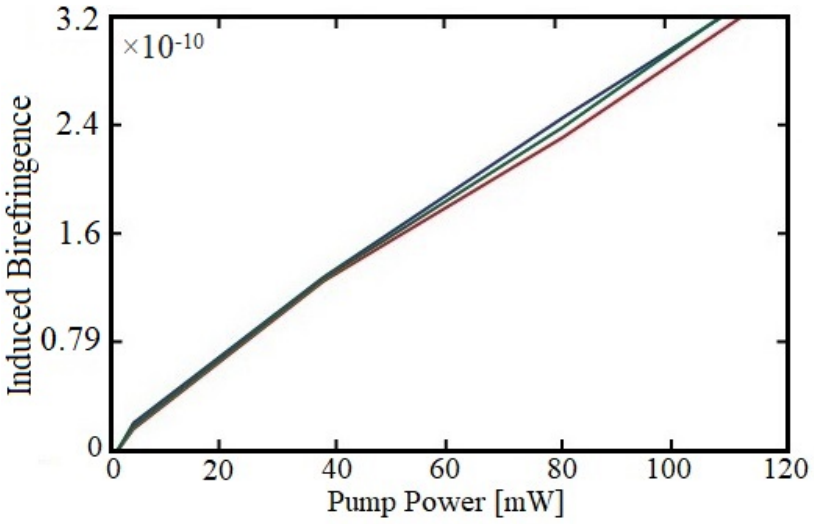

Figure 2.8: Measurement of birefringence as a function of pump power for (blue) linear, (red) circular, and (green) elliptical-induced birefringence.

$\left(\left[1/\sqrt{2}(1+j,0)\right]^T, \left[1/\sqrt{2}(0,1-j)\right]^T\right)$. Figure 2.8 also shows that this technique can provide different kinds of birefringence with the same efficiency, i.e., the same pump power induces the same retardance for linear, circular, and elliptical birefringence. In all cases, the relation is linear. The magnitude of the birefringence can be continuously tuned by changing pump power. For the sake of comparison, a value of induced birefringence of 3.87×10^{-10} is equivalent to performing a π rotation on the Poincaré sphere (considering $\lambda = 1548$ nm and $L = 1$ km). Also, the induced birefringence adds to the natural birefringence of the standard single-mode optical fiber, which is around 10^{-6} [8].

When a change in the birefringence is performed, only a slight variation in the SBS-induced gain is observed because of the combination of gain and loss responses,

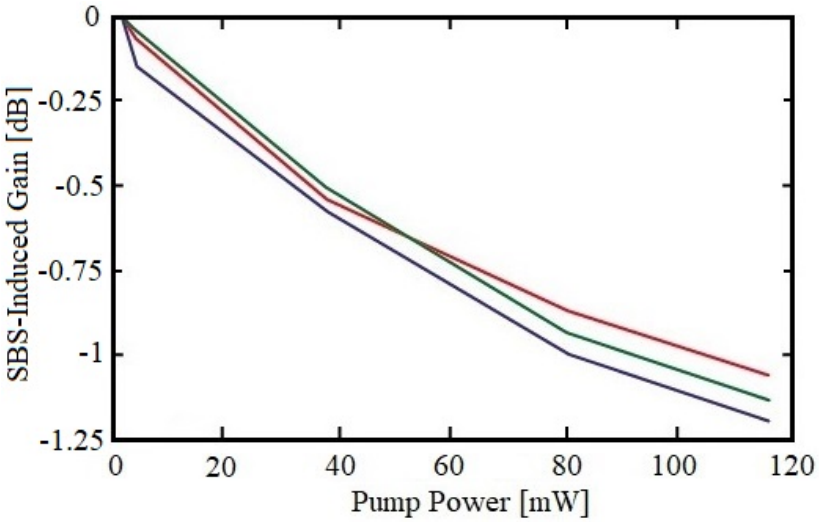

Figure 2.9: SBS-induced gain at the central frequency as a function of pump power for (blue) linear, (red) circular, and (green) elliptical-induced birefringence.

as shown in Fig. 2.9. Results show that the SBS-induced gain depends on the pump power and the type of induced birefringence, remaining below 1.1 dB in the full range of operation.

Figure 2.10a shows the evolution of the signal SoP at the output of the optical fiber when circular birefringence has been nonlinearly induced. It shows that when the power of the pump is changed from 5 mW to 90 mW (Fig. 2.8), half of the circumference (blue dots) of the Poincaré sphere is covered. The rest of the circumference is covered by swapping the pumps f_{P1} and f_{P2} (red dots), so in this way, an excessive increment of the pump power is avoided, which could compromise system linearity.

The rotation is obtained similarly for the linear birefringence, but the SoPs of the pump waves are linear at 90° and 0° (Fig. 2.10b). Finally, Fig. 2.10c and Fig. 2.10d show elliptical birefringence when the SoPs of the pump waves are elliptical with Jones vectors $\left(\left[1/\sqrt{2}(1+j,0)\right]^T, \left[1/\sqrt{2}(0,1-j)\right]^T\right)$ and $\left(\left[1/\sqrt{2}(0,1+j)\right]^T, \left[1/\sqrt{2}(1-j\,,\,0)\right]^T\right)$, respectively.

Figure 2.11 presents the results obtained for the SBS-induced group delay (blue) and

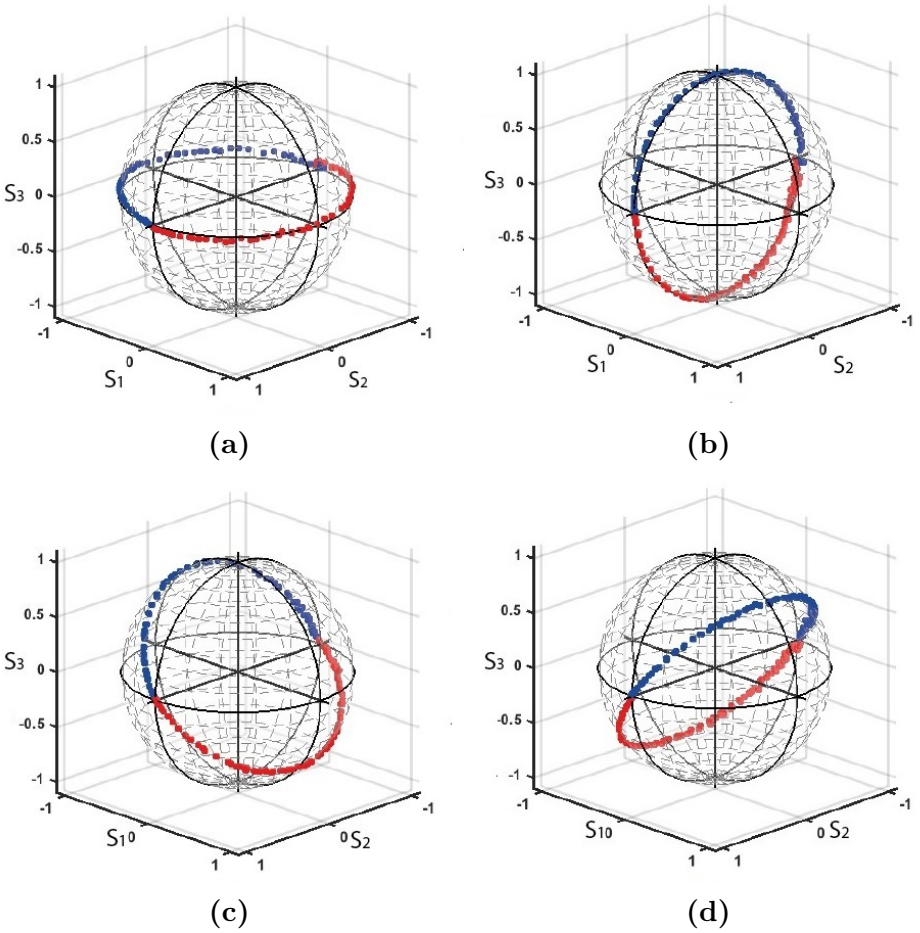

Figure 2.10: Evolution of the state of polarization represented on the Poincaré sphere for different types of nonlinearly induced birefringence: (a) circular, (b) linear, (c), and (d) elliptical.

group velocity dispersion (magenta). Again, the polarization-dependent characteristics of both responses can be appreciated. Maximum group delay is reached at 36.5 MHz for both exposed cases (when the signal SoP is aligned to the pump SoP and orthogonal to the pump SoP). The maximum differential group delay (DGD), which is 8.18 ns in a 1 km fiber reel using a pump power of 80 mW, can be extracted from this difference. For the sake of comparison, the PMD parameter value, D_{PMD}, associated with this SBS-induced DGD is around 16000 times higher than the root mean square (RMS) value of DGD produced by the propagation of a light beam through the same distance of standard single mode fiber, typically around $D_{PMD} = 0.5$ ps km$^{-1/2}$.

Group velocity dispersion (magenta), determined by the derivative of group delay responses, takes positive and negative values around 36.5 MHz at the point where group delay reaches a peak. The maximum negative value of GVD is -800 ns^2 at 45 MHz, when the signal SoP is aligned to the pump SoP. By considering that the length of the employed fiber is 1 km, the resultant GVD value is much greater than the typical value of the GVD parameter in a standard single-mode fiber ($\beta_2 = 20$ ps^2/km). When signal and pump SoPs are orthogonal, the GVD is reduced by 50 %. Located at the frequency of 50.9 MHz, the maximum measured DGDD value is 534.2 ns^2.

Additional tests were carried out using pulses with a full width at half maximum (FWHM) of 50 ns modulated in amplitude at a frequency of 35 MHz (in the region of maximum DGD as shown in Fig. 2.11), which were transmitted into the arbitrary birefringent system to test the DGD. As with other SBS-based systems, the limited time-bandwidth product limits the possibility of delaying narrower pulses [58]. The

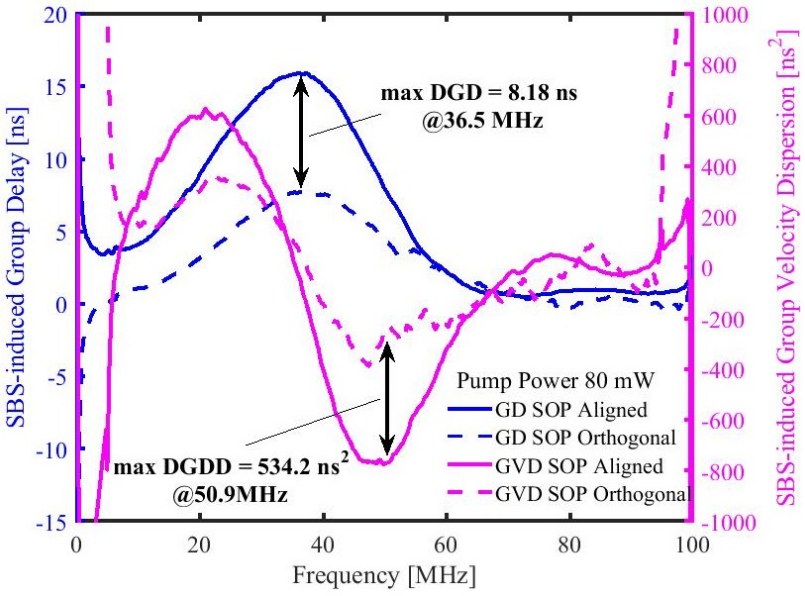

Figure 2.11: SBS-induced group delay (blue) and group velocity dispersion (magenta) frequency responses of a transmitted signal with SoP aligned (solid line) and orthogonal (dashed line) to the pump SoP.

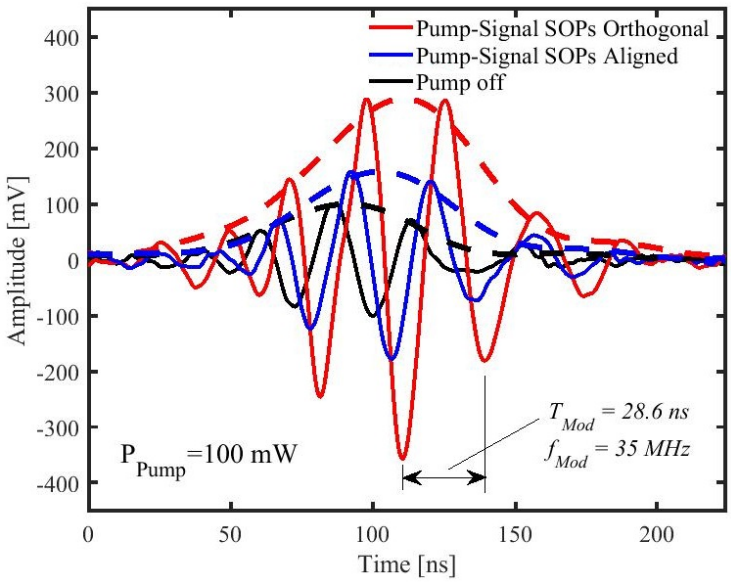

Figure 2.12: Measurement of modulated pulses of FWHM = 50 ns at 35 MHz transmitted through the optical fiber without pump (solid black line) and with SoP aligned (solid red line) and SoP orthogonal (solid blue line) to the pump SoP. The received baseband pulses are represented by modulated signals' envelope (dashed lines).

results are shown in Fig. 2.12.

When the pump is on, and its SoP is aligned to the signal, the signal experiences a longer delay (red solid line) compared to the signal without the pump (black solid line) and also to the signal orthogonal to the pump SoP (blue dashed line). The measured DGD was 7 ns using 100 mW of pump power. As discussed in Section 2.1.2, the sign of the group delay cannot be changed since it can only be induced using the gain response of the SBS. Unlike baseband signals, which are away from f_0, the SBS gain response alters the signal amplitude, which increases with pump power. The aligned

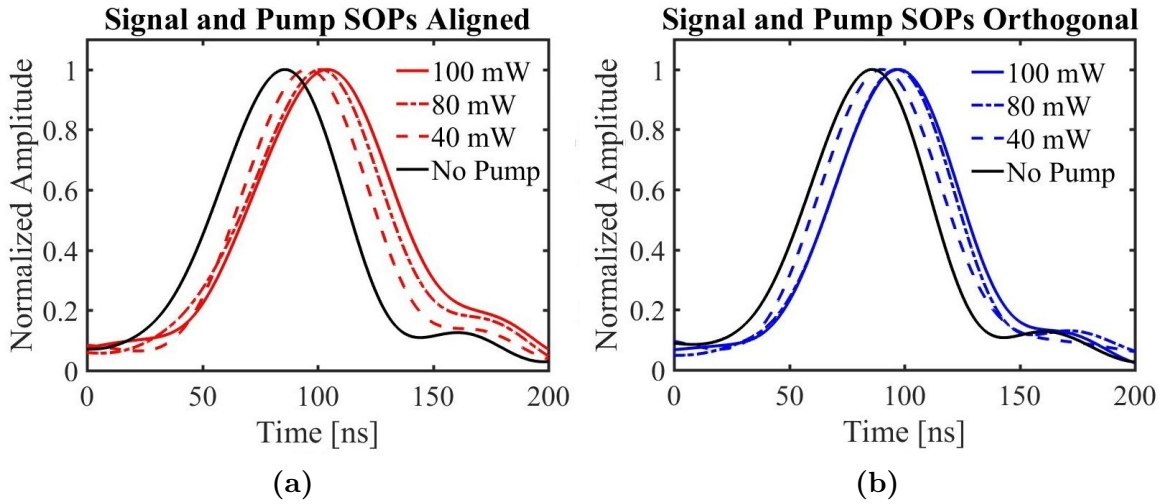

Figure 2.13: Baseband optical pulses (FWHM = 50 ns) normalized in peak amplitude are affected by SBS when signal and pump SoPs are (a) aligned and (b) orthogonal.

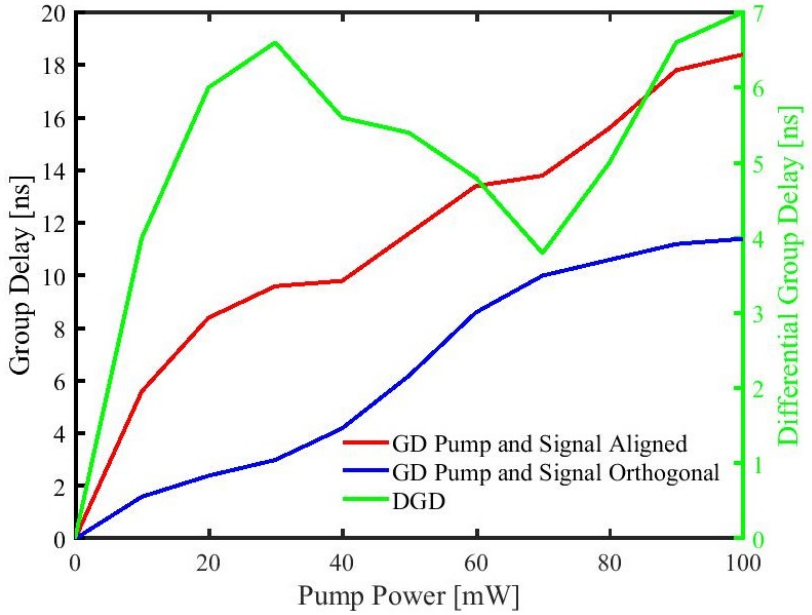

Figure 2.14: Group delay (blue and red) and differential group delay (green) as a function of pump power for baseband optical pulses of FWHM = 50 ns affected by SBS.

signal exhibits a higher amplitude than the orthogonal signal due to the polarization-dependent characteristics of SBS gain response [25][59]. The influence of pump power and its SoP on baseband optical pulses can be seen in Fig. 2.13. These pulses were demodulated by employing digital envelope detection. In the range of pump powers from 10 mW to 100 mW, the distortion of the pulses is moderate.

Figure 2.14 shows the measured group delay of baseband pulses for different pump powers. The DGD is more significant as the pump power increases. The maximum

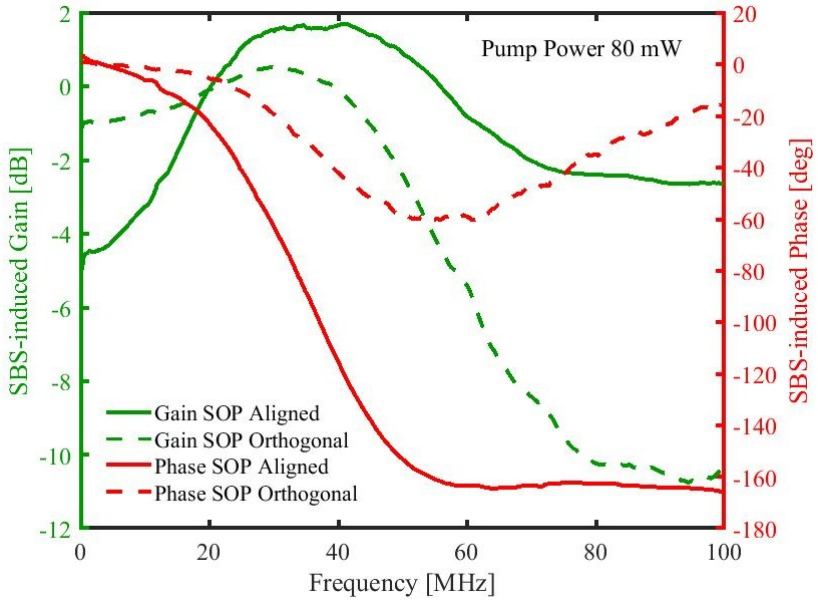

Figure 2.15: Frequency responses of the SBS-induced gain (green) and phase (red) of a transmitted signal with SoP aligned (solid line) and orthogonal (dashed line) to the pump SoP.

group delay obtained was 18.4 ns using a pump power of 100 mW when the signal and pump SoPs were aligned. When both are orthogonal, the group delay was 11.4 ns. The obtained delays are in line with previous results [58][59][60][48].

The system's behavior can be alternatively analyzed through its frequency response. The SBS-induced gain and phase frequency responses have been measured using a vector network analyzer, and the results are shown in Fig. 2.15. The polarization dependence of SBS-induced gain and phase frequency responses is demonstrated. When the signal SoP is aligned to the pump SoP (green line), gain and phase responses are enhanced, with a gain peak of nearly 2 dB and a phase shift of around -140 degrees at 40 MHz. On the other hand, the orthogonal case provides a modest maximum gain of less than 1 dB at 30 MHz and a minimum phase of -40 degrees at 55 MHz. In the range of 20 MHz to 45 MHz, phase responses present a well-defined slope. The difference between the slopes of both phase responses indicates the presence of DGD, which is consistent with the results depicted in Fig. 2.11.

The analyses and experiments presented in this Chapter demonstrate a novel method to transform an optical fiber into an arbitrarily manipulated birefringent, delay-generator, and highly dispersive propagating media.

Chapter 3

Retardance Spectrum Shaping[†]

Some operations, for example, filtering and routing signals, require a certain degree of flexibility in selecting the central frequency band and bandwidth. The technique presented in the previous Chapter for inducing arbitrary birefringence is constrained to operate with the natural Stimulated Brillouin Scattering parameters of Brillouin frequency shift ν_B and Brillouin linewidth $\Delta\nu_B$, which are in the range of GHz and MHz, respectively [8], limiting the applicability of SBS. However, the development of dynamic tuning of these parameters will open up new fields of application.

This chapter investigates how to tune the Brillouin frequency shift (associated with selectivity of the frequency band) and Brillouin linewidth (associated with bandwidth). Modifying the ν_B does not represent significant challenges because it can be done using a tunable laser source [61] or optical modulators [40]. The second option offers more frequency stability and could be required in, for example, microwave photonic filtering with high-frequency selectivity [62]. Given that the broadened Brillouin gain and loss spectra are related to the pump spectrum through the linear convolution operation between the natural SBS response (usually modeled as a Lorentzian function), the pump is spectrally shaped to obtain the desired effect on the probe wave. For example, spectral broadening of the amplitude response [64] and, similarly, of the delay response (slow light) [42][58][65], is straightforwardly achieved by broadening the pump. Slow-light systems employ the spectral broadening of the Brillouin amplitude frequency response to induce nearly a linear phase response over a wider bandwidth, whose derivative results in a flat time delay. In contrast, the spectral broadening in the birefringence, or equivalently, the retardance, requires, ideally, a flat phase response since the Brillouin-induced phase is directly translated into the retardance.

As discussed in Chapter 1: Introduction, Section 1.4, not many techniques perform the control of the polarization of light using SBS. To the best of our knowledge, there

[†]This Chapter is based on: G. Zoireff, and B. Vidal, «Light-by-light polarization control using Stimulated Brillouin Scattering with retardance spectrum shaping», in *Opt. Laser Technol.*, vol. 169, 110036, Feb. 2024.

are only two techniques for polarization control based on SBS: Polarization Pulling and controlling phase retardance. In Chapter 2, it has been demonstrated that the latter approach has the property to generate arbitrary birefringence dynamically. An additional improvement will be to expand its capabilities for controlling the polarization (or birefringence) over broadened SBS spectra, which is a point not yet clear at all since the broadening approaches conventionally used in SBS are not directly applicable. Hence, it will pave the way for developing applications based on this device, such as remote routing of signals and active polarization beam splitters, which can have potential interest in different areas, such as optical networks.

This Chapter describes a method to engineer the pump wave that allows for increasing and tailoring the frequency response of the SBS-based polarization controller based on polarization-dependent interactions, which was developed in the previous Chapter. As it will be further seen, this technique provides a simplification in relation to the experimental setup presented in 2.2 by using a single-arm architecture and includes a feedback loop aimed at controlling the principal variables of the system and addressing the saturation of Brillouin gain. Thus, an additional degree of freedom is given to the SBS-based polarization controller, which will be fundamental to achieving practical full-polarization control.

3.1. Fundamentals of Spectral Broadening of SBS Polarization-Dependent Interactions

As described in the Chapter 1: Introduction, Section 1.3, Stimulated Brillouin Scattering is caused by the interaction between an electromagnetic and an acoustic wave via electrostriction, which results in a variation in the refractive index of the propagation medium [8]. In a pump-probe scheme, due to the change in the refractive index, the probe (also known as signal) wave experiences exponential gain, A_G, as well as a phase change, ϕ_G, both induced by a counter-propagating pump wave. These gain and phase responses are linked by Kramers-Kronig relations [63][66]

$$H_B(f) = \exp A_G(f) + j\phi_G(f) \tag{3.1a}$$

$$\phi_G(f) = \mathcal{H}\{A_G(f)\} \tag{3.1b}$$

where H_B is the transfer function induced by the pump wave that affects the signal wave, and $\mathcal{H}\{\cdot\}$ denotes the Hilbert transform operator.

When the pump signal is a single tone located at frequency f_P (see Fig. 3.1a), under a non-saturated regime, the gain response can be expressed as a Lorentzian-shaped power spectrum located at $-\nu_B$ ($\sim$10.8 GHz for standard Single Mode Fiber),

$$A_G(f) = G_B \frac{\left(\frac{\Delta\nu_B}{2}\right)^2}{(f+\nu_B-f_P)^2+\left(\frac{\Delta\nu_B}{2}\right)^2}, \tag{3.2a}$$

$$\phi_G(f) = -G_B \frac{\frac{\Delta\nu_B}{2}(f+\nu_B-f_P)}{(f+\nu_B-f_P)^2+\left(\frac{\Delta\nu_B}{2}\right)^2}, \tag{3.2b}$$

$$A_L(f) = -G_B \frac{\left(\frac{\Delta\nu_B}{2}\right)^2}{(f-\nu_B-f_P)^2+\left(\frac{\Delta\nu_B}{2}\right)^2}, \tag{3.2c}$$

$$\phi_L(f) = G_B \frac{\frac{\Delta\nu_B}{2}(f-\nu_B-f_P)}{(f-\nu_B-f_P)^2+\left(\frac{\Delta\nu_B}{2}\right)^2}, \tag{3.2d}$$

with $G_B = g_0 P_p L_{eff}/A_{eff}$ being the Brillouin exponential gain, where g_0 is the Brillouin gain of the medium, P_p the pump power, L_{eff} the effective length of the fiber, A_{eff} the effective area of the fiber, and $\Delta\nu_B$ (∼50 MHz for standard Single Mode Fiber) the linewidth or FWHM bandwidth of the Brillouin gain response. In parallel, a loss SBS response is generated at a frequency of ν_B. Both gain and loss responses are illustrated in Fig. 3.1a

An enhanced phase response can be obtained using a double-pumped scheme to add the phase of each SBS response constructively. If the pumps are set at $-\nu_B + \frac{\Delta\nu_B}{2}$ and $\nu_B - \frac{\Delta\nu_B}{2}$, the total phase shift is maximized and gain and loss are compensated at the central wavelength ($f = 0$), as it is shown in Fig. 3.1b. SBS can be broadened by engineering the pump wave [58][65][42], which affects the gain and loss power spectra

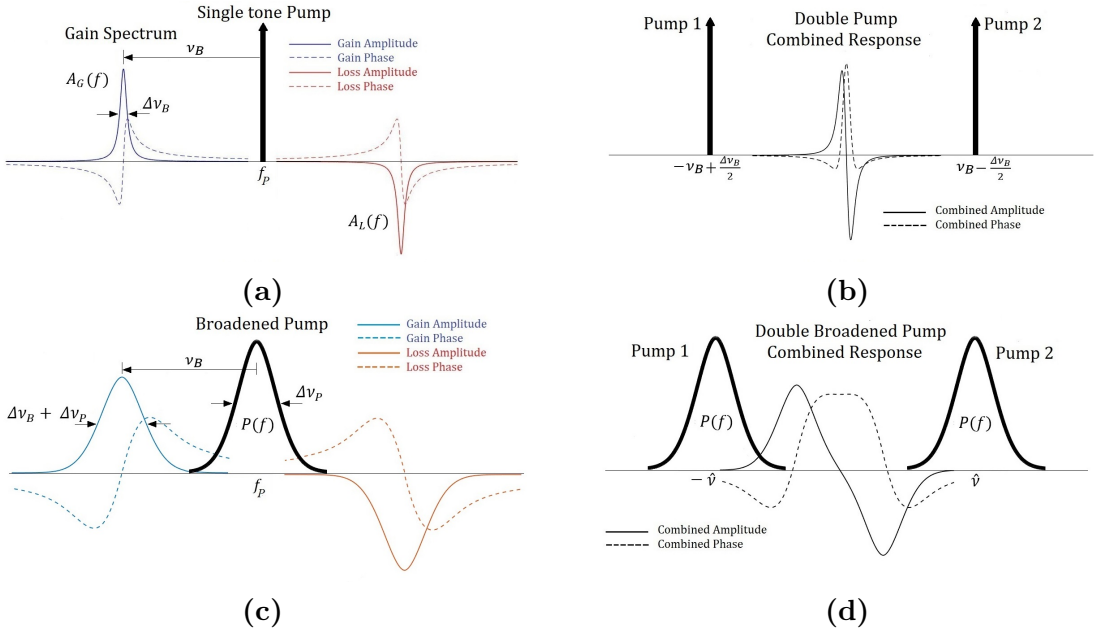

Figure 3.1: Amplitude and phase responses of Stimulated Brillouin Scattering using (a) single pump, (b) double pump combined, (c) single broadened pump, and (d) double broadened pump combined SBS frequency response.

through the convolution between the pump and the SBS frequency response as follows:

$$\tilde{A}_{G/L}(f) = A_{G/L}(f) * P(f). \tag{3.3}$$

From it, a new phase profile can be determined using Kramers-Kronig relations

$$\tilde{\phi}_{G/L}(f) = \mathcal{H}\left\{\tilde{A}_{G/L}(f)\right\} = \mathcal{H}\left\{A_{G/L}(f) * P(f)\right\}. \tag{3.4}$$

The broadening effect of SBS is shown in Fig. 3.1c, where a pump profile, $P(f)$, is depicted. The linewidth of the SBS-induced gain is broadened from the natural linewidth $\Delta\nu_B$ to an approximate value of $\Delta\nu_P + \Delta\nu_B$, with $\Delta\nu_P$ the linewidth of the pump profile. If the linewidth of the pump is much greater than the natural linewidth $\Delta\nu_B$, the shape of SBS gain and loss interactions approximates the spectral profile function of the pump, $P(f)$.

Thus, arbitrary amplitude and phase profiles can be obtained by selecting an adequate $P(f)$. Moreover, the double pump scheme can be combined with the broadened pumping scheme to induce a more complex phase spectrum. A combination of two broadened SBS responses, where the resulted phase profile is flat in a band of frequencies much wider than the linewidth of the natural SBS response, is shown in Fig. 3.1d. To achieve this phase response, a new value for the frequency spacing between the pumps, $\hat{\nu}$, must be determined. Since the effect of the broadened combined SBS phase response is generated by the inner half of the pump profile $P(f)$ (see Fig. 3.1d), the latter can be reduced to one symmetrical portion using single-sideband modulation. An exact expression for the exponential gain assuming Lorentzian profiles by a broadened pump can be obtained [42]

$$\tilde{G}_B = \frac{g_0 P_p L_{eff}}{A_{eff}} \frac{\Delta\nu_B}{\Delta\nu_B + \Delta\nu_P}. \tag{3.5}$$

This expression, which also affects the phase SBS response in the same quantity, conceptually indicates that the pump power must be increased in the same amount to compensate for the effect of broadening to obtain the same phase shift for the case of the natural SBS response. This calculation does not consider other nonlinear behaviors inside SBS, such as saturation of the gain response. Hence, to obtain high values of phase shift (>60°) with a broadened pump with linewidth $\Delta\nu_P$, the pump power must be increased at least by a factor $(\Delta\nu_B + \Delta\nu_P)/\Delta\nu_B$. For example, if a Dispersion-Shifted Fiber ($g_0 = 7.19 \times 10^{-12}$ m/W, $A_{eff} = 50$ μm^2, $L_{eff} = 1$ km, $\Delta\nu_B = 50$ MHz) is considered, the maximum phase shift that can be obtained with a pump power of 10 mW is $\phi_{Max} = 82^{\text{o}}$. If the pump is broadened to 500 MHz, the required power to obtain the same maximum phase would be around 100 mW if no other nonlinear effects are

present. The power levels required to operate the system with phase shifts near 90^{o} will likely provoke saturation in the SBS gain spectrum.

3.1.1. Phase-to-Retardance Conversion

The Brillouin gain, g_0, has different values according to the alignment of the SoPs of the signal and the pump light sources. When they are aligned, g_0 is maximum; when they are orthogonal, g_0 is reduced in half [67]. Different values of g_0 imply that a probe signal will experience polarization-dependent phase shifts due to SBS, which is equivalent to the signal suffering the cause of being propagated through a material with nonlinearly induced birefringence. Assuming a signal with an electrical field of amplitude E_S is aligned to the x-axis of the fiber, and pumps are set in the right-handed circular polarization (RHCP) state, the system behaves as a circular retarder and phase shifts are converted into retardance. This process is illustrated in Fig. 3.2, where the input signal is aligned to the polarization x-axis (red spectrum), and a broadened pump wave with right-handed circular polarization is counter-propagated. A part of the spectrum of the signal wave experiences the SBS-induced circular birefringence by being rotated from the x to the y polarization axis. At the output of the fiber, a new signal is generated with x and y polarization components, which can be further processed. This process can also be interpreted through the Jones calculus, where the Jones matrix associated with this system, $\mathbf{J}$, can be determined by using the transformation matrix of $\mathbf{F}$ (see Eq. 2.12), that for a circularly polarized pump ($\delta = \pi/2$, $\phi_x = 0$ and $\phi_y = \pi/2$) it results:

$$\mathbf{F} = \frac{1}{2}\begin{pmatrix} 1 & -j \\ -j & 1 \end{pmatrix}. \tag{3.6}$$

The Jones matrix of the SBS-induced birefringence in the x-y coordinate basis system is

$$\mathbf{J_{SBS}} = \begin{pmatrix} \exp\begin{pmatrix} G_{1x}(f) + A_{1x}(f) \\ +j\left(\phi_{1xG}(f) + \phi_{1xA}(f)\right) \end{pmatrix} & 0 \\ 0 & \exp\begin{pmatrix} G_{1y}(f) + A_{1y}(f) \\ j\left(\phi_{1yG}(f) + \phi_{1yA}(f)\right) \end{pmatrix} \end{pmatrix}. \tag{3.7}$$

Note that this last expression is slightly different from Eq. 2.11 because here it is considered only a single pair of orthogonal pumps and written in terms of the induced SBS phase shift. Recalling that $G_{1x}(f) + A_{1x}(f) \approx 0$ and $G_{1y}(f) + A_{1y}(f) \approx 0$ in the overlapped region of the SBS spectra, $G_x, A_x(f) = 2G_y, A_y(f)$, $\phi_{xG,A}(f) = 2\phi_{yG,A}(f)$

and using Eq. 2.10, the Jones matrix for this SBS-based circular can be expressed as

$$\mathbf{J} = \mathbf{F}^{-1}\mathbf{J}_{\mathbf{SBS}}\mathbf{F} \approx$$
$$\mathbf{J} \approx \exp\left[G_{SBS-Circular}(f)\right] \begin{pmatrix} \cos\left(\phi_{SBS-Circular}(f)\right) & \sin\left(\phi_{SBS-Circular}(f)\right) \\ -\sin\left(\phi_{SBS-Circular}(f)\right) & \cos\left(\phi_{SBS-Circular}(f)\right) \end{pmatrix}, \tag{3.8}$$

where the total SBS-induced circular phase shift and exponential gain are defined by

$$\phi_{SBS-Circular}(f) = \frac{3}{4}\phi_{1x}(f) = \frac{3}{4}\left[\phi_{1xG}(f) + \phi_{1xA}(f)\right] \tag{3.9a}$$
$$G_{SBS-Circular}(f) = \frac{3}{4}\left[G_{1x}(f) + A_{1x}(f)\right], \tag{3.9b}$$

that results from combining the gain and loss SBS phase and gain spectra. Thus, the Jones matrix of the system takes the form of a rotational matrix composed of the SBS-induced circular phase shift.

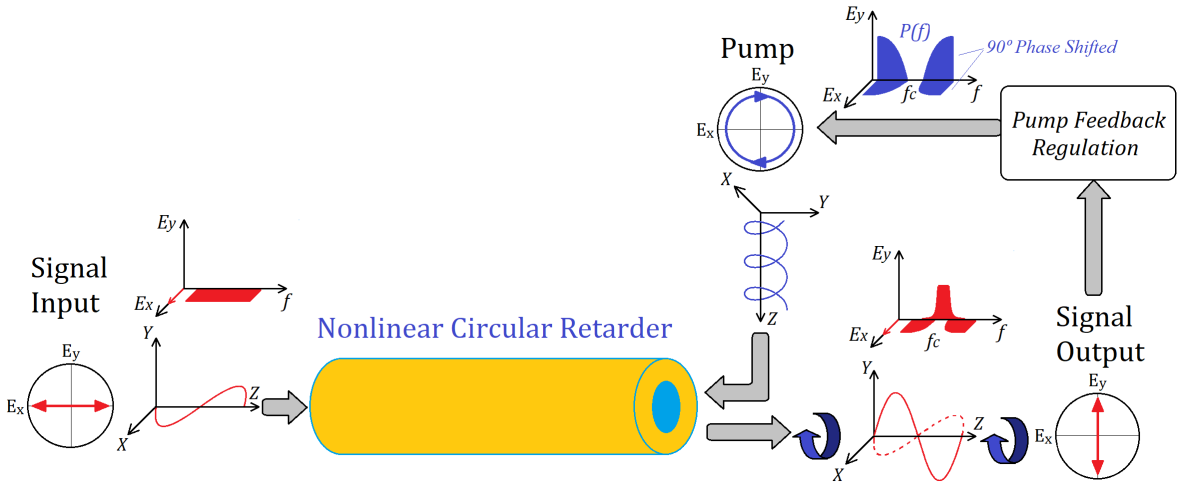

Figure 3.2: Nonlinear circular retarder generated by SBS polarization-dependent interactions.

3.1.2. Engineering Retardance

Unlike conventional Brillouin-based slow light schemes where the target is to achieve a linear phase response over a broad bandwidth to have a flat time delay, the aim is to produce a broadened, ideally flat top, phase response that will induce a broadened retardance. By choosing a proper pump profile $P(f)$ and combining the gain and loss power spectra, we extend the natural bandwidth of SBS, which is around 50 MHz for standard single-mode fibers.

The broadening process of the pump can be done by performing a frequency sweep of a single pump line [68]. This pump broadening method provides several advantages over conventional pump broadening using a broadband signal. Among these advantages, it can be first mentioned that the minimum bandwidth can be considerably low

(because the Brillouin bandwidth is around 50 MHz). Consequently, the precision obtained is very high. Second, the AWG generates the electrical signal accurately within a specific frequency range, ensuring a good representation of the pump profile. Third, the number of the comb line can be dynamically changed to adjust the retardance bandwidth precisely. Fourth, the central frequency of the pump can be shifted by tuning the wavelength of the comb electrically and optically. Fifth, the four-wave mixing (FWM) effect caused by the multiple pump lines can be mitigated by randomly setting the frequency interval of the electrical spectral lines around the natural SBS gain bandwidth instead of an equal interval. In this case, the FWM-induced gain will no longer superpose on the original lines. In summary, the chosen pump spectral-shape generation method can reconfigure bandwidth, central frequency, and, most importantly, shape with very high precision.

The maximum retardance is achieved when a gain and a loss spectrum are overlapped to combine both phase responses, and these need to be engineered to follow a given profile. The desired phase profile is achieved by controlling the amplitude and offset of each frequency line, as well as the span of frequency. Following this approach, only one pump line is present at each instant, and therefore, nonlinear beats are avoided in the external modulator.

Small changes are strongly magnified since the Brillouin gain increases exponentially with the pump power. Additionally, the saturation of the SBS response adds another level of complexity. Thus, an iterative process is needed to define the amplitude profile of the frequency sweep from experimental feedback to consider the effects of the nonlinear growth of the Brillouin gain.

Due to the lack of direct access to the retardance in the experiment, its value and bandwidth are derived from the amplitude measured after a polarizer, which is placed after the nonlinear circular retarder. The retardance can be inferred from the amplitude-frequency response measured after a photodiode. If the polarizer is aligned to the x-axis, the intensity of the measured photocurrent at the output of a photodiode with responsivity $\Re$ is related to the retardance through Malus' law:

$$i = \Re \left| \begin{pmatrix} 1 & 0 \\ 0 & 0 \end{pmatrix} \mathbf{J} \begin{pmatrix} E_S \\ 0 \end{pmatrix} \right|^2 = \Re\, E_S \, \exp\left[2G_{SBS-Circular}(f)\right] \cos\left(\phi_{SBS-Circular}(f)\right) |^2. \tag{3.10}$$

The equation above implies that polarization changes are transformed into amplitude changes observed at the photodiode output, and the phase-to-retardance conversion can be straightforwardly extracted from the intensity of measured photocurrent by using Eq. 3.10.

3.2. Experimental Setup

The experimental setup used to validate the proposed technique is shown in Fig. 3.3. Two independent light sources, one with fixed wavelength (FLS) and the other with tunable wavelength (TLS), configure the pump-probe scheme to induce SBS. This approach is preferred over a single laser and an external modulator to show the technique's feasibility, which is a well-representation of a condition where an optical signal controls another that comes from a different source.

The signal path is single-sideband (SSB) modulated with a dual-drive Mach-Zehnder (DD-MZM) modulator and then amplified by an Erbium-Doped Fiber Amplifier (EDFA). The SoP of the signal source is controlled by the polarization controller PC_S and is set to horizontal SoP.

On the pump path, the light is modulated using a Mach-Zehnder modulator at the minimum transmission bias point and fed by an Arbitrary Waveform Generator (AWG), which contains the pump profile $P(f)$ generated by the software. The pump signal is amplified, and PC_P modifies its polarization state to right-hand circular SoP.

The signal is propagated, and the pump is counter-propagated through 1.2 km of a HNLF, that is, a Dispersion-Shifted Fiber with measured parameters $g_0 = 7.19 \times 10^{-12}$ m/W, $A_{eff} = 50\ \mu m^2$, $L_{eff} = 1.15$ km, $\Delta\nu_B = 42$ MHz, and $\nu_B = 9.636$ GHz. A portion of the power spectrum of the signal experiences circular rotation induced by SBS. The signal lightwave affected by SBS comprises two power spectra, one aligned

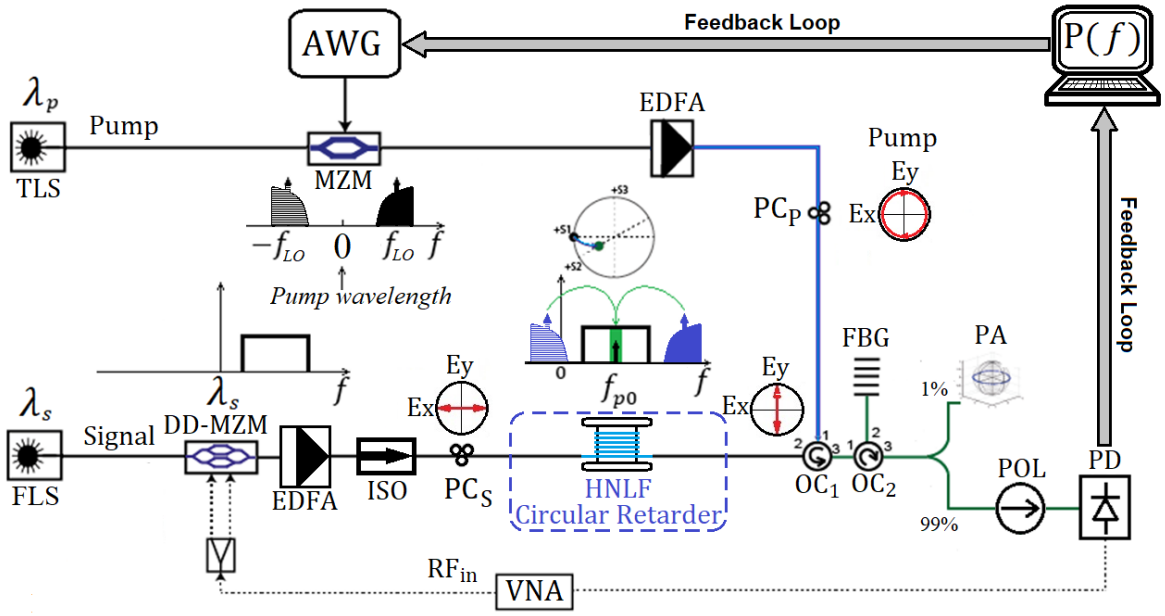

Figure 3.3: Experimental setup. TLS: Tunable Light Source, AWG: Arbitrary Waveform Generator, MZM: Mach-Zehnder Modulator, EDFA: Erbium-Doped Fiber Amplifier, PC: Polarization Controller, FLS: Fixed Light Source, DD-MZM: Dual Drive Mach-Zehnder Modulator, ISO: Isolator, HNLF: Highly Nonlinear Fiber, OC: Optical Circulator, FBG: Fiber Bragg Grating, PA: Polarization Analyzer, POL: Polarizer, PD: Photodetector, VNA: Vector Network Analyzer.

to the horizontal axis and another to the vertical axis. The polarizer, POL, which is aligned to the horizontal axis, removes the component of the vertical axis, and a photodiode detects the horizontal component. A 99/1 power coupler delivers 1 % of the light beam to a polarization analyzer PA, which measures the polarization states of the signal, the pump, and the optical power.

The pumps, frequency shifted around ±9.6 GHz from the central frequency, generate a Rayleigh backscattered wave that travels towards the photodetector. The Rayleigh wave is used to determine the SoP of the pump, but it might cause damage to the photodetector or generate unwanted oscillations, particularly when pumps with high power levels are used. For this reason, before photodetection, a 12.5 GHz bandwidth FBG is placed to remove the Rayleigh backscattering induced by the pump.

Finally, the RF transmitted and detected signals are generated from and introduced to a Vector Network Analyzer (VNA) that provides a linearly swept electrical signal with a mean power of 10 dBm to study the transmission response of the system.

3.3. Results and Discussion

3.3.1. Design of the Pump Profile

The Kramers-Kronig relations impose that the SBS phase profile, which will be further transformed into a retardance frequency response, is linked to a defined SBS gain profile. Thus, an amplitude pump response that induces the desired SBS phase response is needed to tailor the retardance effectively. In addition, as this technique employs combined gain and loss SBS power spectra, the frequency spacing between signals should be chosen appropriately to obtain the desired retardance frequency response. This method is unlike time delay schemes where just a broadened Brillouin gain response with a broader bandwidth is pursued since it provides a linear phase over a more extensive range of frequencies, and, therefore, its slope (derivative), i.e., time delay, is broadened.

The first step to designing a pump profile to achieve a broadened retardance is to find a theoretical model that accurately represents SBS gain and loss power spectra under a determined pump power condition. Appendix B presents these models for the fiber-based SBS system used in this Thesis. Equation 3.1 must be applied to obtain the expected phase profile. Thirdly, Eq. 3.10 describes the phase-to-retardace conversion. Figure 3.4 shows measurements and theoretical predictions, where two tones generated with a microwave local oscillator of $f_{LO} = \nu_B - \Delta\nu_B/2 = 9.615$ GHz were used as pumps. In the inset of Fig. 3.4, the power spectrum of the pump profile is shown. The optical pump power was set to 15.5 dBm.

As shown in Fig. 3.4, results show good agreement between theory and measure-

ments. The model proposed for the combined response (blue solid line) fits the measurement (solid red line) and exhibits the saturation in the gain spectrum induced by the SBS response. The gain (dashed yellow line) and the retardance (dotted violet line) spectra can be extracted from it. This model also predicts the frequency value, which presents maximal retardance.

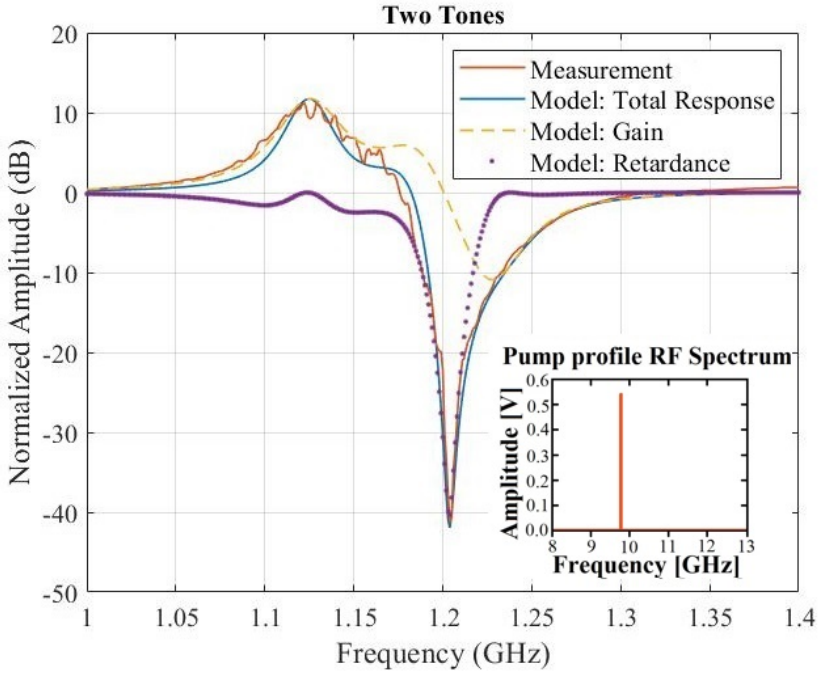

Figure 3.4: The normalized amplitude response of the measured system (red solid line) after a polarizer and the nonlinear model proposed (blue solid line) to infer Brillouin-induced retardance, which is the result of the combination of gain (dashed yellow line) and phase-to-retardance conversion (dotted violet line) models. Inset: spectrum of the pump profile.

3.3.2. Feedback Loop Regulation

Gain saturation also implies that the outcome of the system will not scale linearly with pump power. This phenomenon becomes more evident when high retardance values are required, for example, to perform a 90^{o} of signal SoP rotation, as shown in the measurements in Fig. 3.4. Moreover, the frequency spacing of the pumps, in combination with the pump spectrum shaping, are critical parameters of the system that must be controlled to obtain a desired retardance frequency response. Consequently, these variables are dynamically monitored and controlled, as indicated in the scheme of Fig. 3.5, where the extracted data are compared against the desired response, constituting a feedback loop regulation. Iteratively, the model is readjusted, and the pump profile is reconfigured until a determined retardance frequency response is obtained.

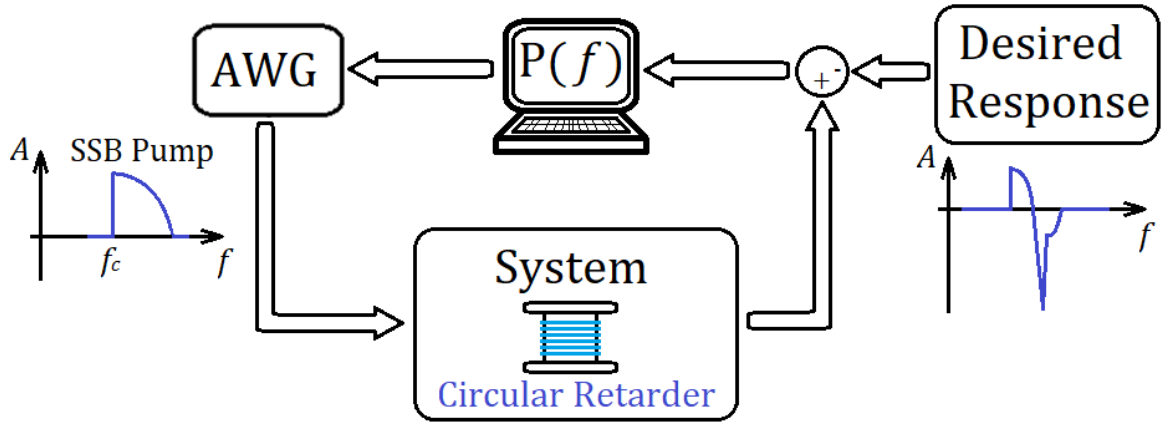

Figure 3.5: An iterative process was followed to determine the pump profile.

3.3.3. Broadening Retardance

The proposed technique has been validated via measurements of the system's response using SSB pumps built from frequency sweep signals of 500 MHz and 1 GHz bandwidths. The iterative process presented in Section 3.1.2 resulted in triangular-shaped pump profiles, consistent with the results shown in [68].

Measurements are shown in Fig. 3.6a jointly with the model. In the inset, the power spectrum of various pumps employed is depicted. The difference in voltage between them is due to the AWG, which provides a fixed mean RF power. Hence, as the signal's bandwidth increases, the voltage is reduced. In each case, the model has a good agreement with the measured response. The retardance is maximized at a frequency value that is not necessarily the central frequency of the combined SBS gain and loss spectra ($f_{central}$).

Following Eq. 3.10, the induced retardance is derived from the amplitude frequency response. Figure 3.6b depicts the extracted retardance from the model versus the frequency deviation from the central frequency for three pump cases: non-broadened response based on two tones (pump power of $P_{Pump} = 15.5$ dBm) and two frequency sweeps of 500 MHz ($P_{Pump} = 22.4$ dBm) and 1 GHz ($P_{Pump} = 25$ dBm). The retardance of the two-tone case nearly reaches 90°, as does the 500 MHz case. Meanwhile, in the 1 GHz case, the retardance is around 80°. The bandwidth of the retardance is increased from 51 MHz for the two-tone pump to 566 MHz and 913 MHz for 500 MHz and 1 GHz sweeps, respectively. It is noticeable that there is an asymmetry around the peak of retardance because of gain saturation. Alternatively, this asymmetry can be interpreted as a detuning of the expected central frequency in the ideal case.

These results were obtained by performing offline processing. For real-time applications, the propagation velocity in the nonlinear medium mainly restricts the maximum loop speed. For a fiber length of 1.2 km, the system will have a polarization modulation speed of approximately 170 kHz, or equivalently, a minimal loop time of 5.8 ns.

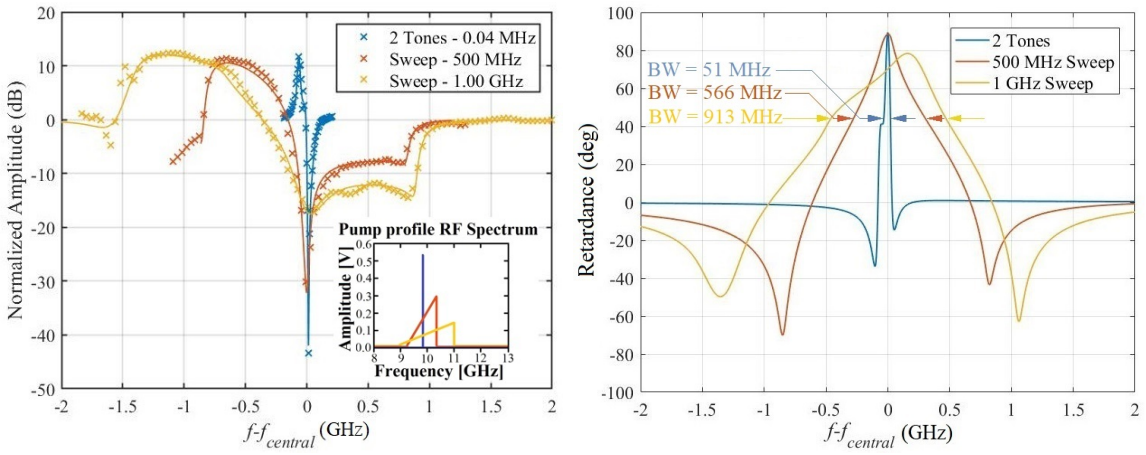

(a) **(b)**

Figure 3.6: (a) Amplitude frequency response (solid line) and theoretical model (cross markers) when a polarizer is used after the circular retarder using a 500 MHz and 1 GHz bandwidth swept pump scheme; the inset shows the spectrum of the pump profile; and (b) retardance extracted from experimental results shown in Fig. 3.6a as a function of deviation from the central frequency for two tones (blue), 500 MHz (red) and 1 GHz swept pump schemes (yellow).

As a metric for evaluating the deviations between the expected retardance response (model) and measurement, the relative root mean squared error (RRMSE) was chosen. A minimization process for the RRMSE was done, establishing an exit condition for the feedback loop when RRMSE<20 %. This value represents a good trade-off between the number of iterations and the proposed model's accuracy. It was required to obtain these triangular-like pump profiles at about 20 iterations, where the desired retardance profile was set as a squared window with a bandwidth equal to the pump bandwidth. Simultaneously, the central frequency of the pump was modified by steps of 1, 25, and 50 MHz for the two-tones, 500 MHz sweep and 1 GHz sweep cases, respectively.

According to Eq. 3.5, a pump power increase of around ten times with respect to the two-tone case would be needed to obtain an increment in the bandwidth of retardance from 51 MHz (two tones) to 566 MHz. This increase in pump power would need to be around 20 times when retardance bandwidth is increased up to 913 MHz. Instead, in the experiment, the pump power has been increased 4.9 times to obtain a retardance bandwidth of 566 MHz and 9.8 times to get 913 MHz. This difference can be attributed to the fact that Eq. 3.5 was derived by considering a Lorentzian-shaped broadened pump, an assumption that is quite different from the case described here. In this work, the combination of multiple single sidebands broadened pumps using a frequency sweep is carried out rather than an idealized Lorentzian pump. This discrepancy, combined with experimental deviations, makes it hard to derive a closed-form expression of the required power needed to obtain a given retardance bandwidth. Nevertheless, Eq. 3.5 can be used to estimate the power levels needed for the experiment.

3.3.4. Flattened Retardance

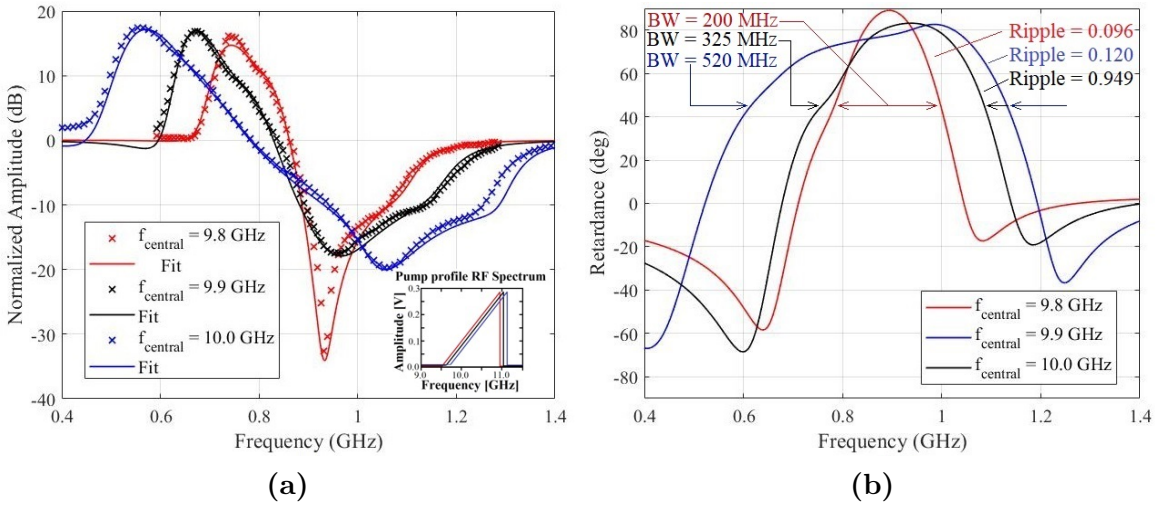

Figure 3.7: (a) Measurements (cross markers) and fitting (solid line) of system outcome for different carrier frequencies; the inset shows the spectrum of the pump file; and (b) extracted retardance for a 300 MHz linearly swept pump profile.

A flat-top retardance frequency response can also be achieved by controlling the pump profile. The pump profile can be engineered to provide a flattened response by increasing the frequency spacing among pump lines. Results for a linearly swept pump profile with a 300 MHz bandwidth are shown in Fig. 3.7. The inset of Fig. 3.7a depicts the power spectrum of the triangular pump profiles employed, whose central frequency has been shifted. In this experiment, the carrier frequency of the pump profile has been modified from the condition of maximum retardance with $f_{central}$ = 9.8 GHz to 9.9 GHz and 10.0 GHz. In Fig. 3.7a, as the carrier frequency increases, gain and loss spectra reduce the overlap, and the peak of absorption is reduced.

Consequently, in Fig. 3.7b, it can be appreciated that peak retardance starts to flatten, but bandwidth is increased. The maximum retardance is slightly reduced when the overlap is reduced. It goes from nearly 90^{o} for $f_{central}$= 9.8 GHz, with a bandwidth of 200 MHz, to a retardance of around 82^{o} with carrier frequencies of 9.9 GHz and 10.0 GHz that result in a bandwidth of 325 MHz and 520 MHz, respectively. Ripple is also observed because of gain saturation caused by high power levels (in this experiment, the pump power was set to P_{Pump} = 22.3 dBm). A ripple factor, indicated in the retardance curves of Fig. 3.7b, determined by the frequency range in which the retardance (ϕ) drops to half of its peak value, can be defined as

$$Ripple\ Factor = \frac{\sqrt{\phi_{RMS}^2 - \phi_{Mean}^2}}{\phi_{Mean}}. \tag{3.11}$$

Ripple can be considerably reduced while obtaining a symmetrical frequency response of retardance by decreasing pump power levels, as seen in Fig. 3.8. In Fig. 3.8a, measu-

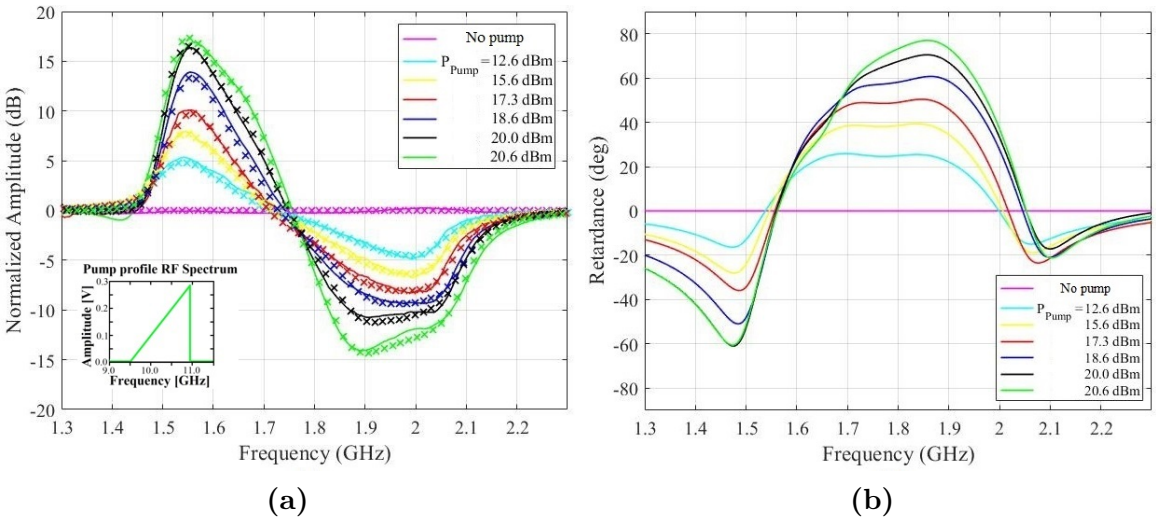

(a) **(b)**

Figure 3.8: (a) Measurements (cross markers) and fitting (solid line) of amplitude frequency response after a polarizer for different pump power levels, and (b) extracted retardance using 3.10 versus frequency using a 300 MHz linearly swept pump profile.

rements of the system outcome for different pump power levels using a linearly swept pump profile with a carrier frequency of 9.9 GHz are presented with the respective model fitted. In Fig. 3.8b, extracted retardance is shown, and the distortion or ripple introduced by high power pump levels can be clearly seen.

Next, it is demonstrated that the value of retardance can also be tuned by controlling the pump power, as shown in Fig. 3.9, where mean retardance and ripple factor are shown as a function of pump power. The ripple factor (associated with nonlinear distortion) is reduced when the pump power is reduced. Saturation could be mitigated

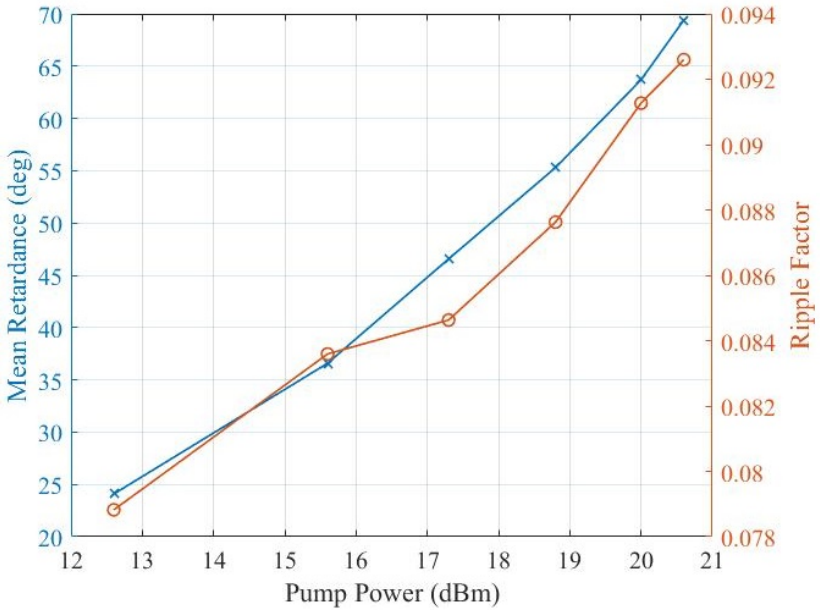

Figure 3.9: Mean retardance and ripple factor versus pump power using a 300 MHz linearly swept pump profile.

by including a second set of two orthogonal pumps with left-handed circular polarization with another sideband of the pump profile, which would partially compensate a gain with a loss and, at the same time, add retardance to the system [69][53]. Thus, the system could operate at higher power values with reduced nonlinear distortion.

The impact of noise on retardance is analyzed. Since Brillouin gain G_B is proportional to the pump power P_p (as shown in Eq. 3.3 and Eq. 3.4), the Brillouin gain will be directly affected by random amplitude variations of the pump, and, in consequence, these random variations will be translated as noise in the Brillouin-induced phase response and thus on the retardance. Consequently, any amplitude noise from the pump, such as relative intensity noise (RIN) and amplified spontaneous emission (ASE) noise, will result in fluctuations in retardance. Given that the power used in these experiments was considerably high, ASE noise is the dominant noise contribution in this system. Simulations have been carried out to test the effect of the amplitude noise of the pump light beam on the retardance by considering the model of SBS polarization-dependent interactions with gain saturation and a spectral broadening of 300 MHz (following the conditions of measurements shown in Fig. 3.8).

The results are depicted in Fig. 3.10, which shows the relation between $\sigma^2_{Retardance}$ (the variance of the mean retardance in the bandwidth of interaction) and the signal-to-noise ratio of the pump and the ASE noise ($SNR_{Pump} = P_{Pump}/P_{ASE}$) at different pump power levels through 10000 realizations of a numerical simulation of the system. A nonlinear dependence between $\sigma^2_{Retardance}$ and SNR_{Pump}, that rapidly grows for

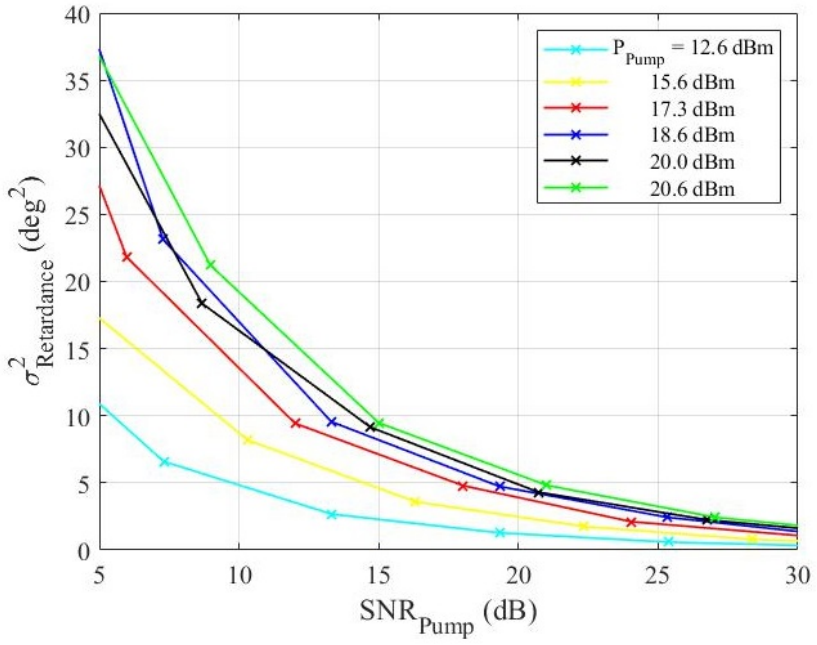

Figure 3.10: The variance of retardance $\sigma^2_{Retardance}$ vs. signal-to-noise ratio of the pump SNR_{Pump} obtained from simulations of the model of SBS polarization-dependent interactions with gain saturation and a spectral broadening of 300 MHz.

SNR_{Pump} less than 15 dB, is observed. In addition, as pump power increases, the noise of the retardance is less affected for each SNR_{Pump}, showing a particular effect of saturation of noise, accordingly to the saturation of the SBS gain spectra.

Finally, Fig. 3.11 shows histograms of the mean retardance under different conditions of SNR and pump powers. SNR values of 5 dB and 30 dB and pump power levels of 12.6 dBm and 20.6 dBm have been selected to obtain these histograms. For all cases, even though SBS polarization-dependent interactions constitute a nonlinear system, it is observed that the noise distribution in the mean retardance follows a Gaussian-like distribution, which is likely that it comes from the Gaussian distribution of the ASE noise considered for simulations. When comparing the histograms of Fig. 3.11a and Fig. 3.11c to the histograms of Fig. 3.11b and Fig. 3.11d, it is observed that the samples of the mean retardance are more dispersed around their mean value, which means that with a pump with high power, the variance of the mean retardance is increased regardless of the pump's SNR. This last statement is consistent with the results pre-

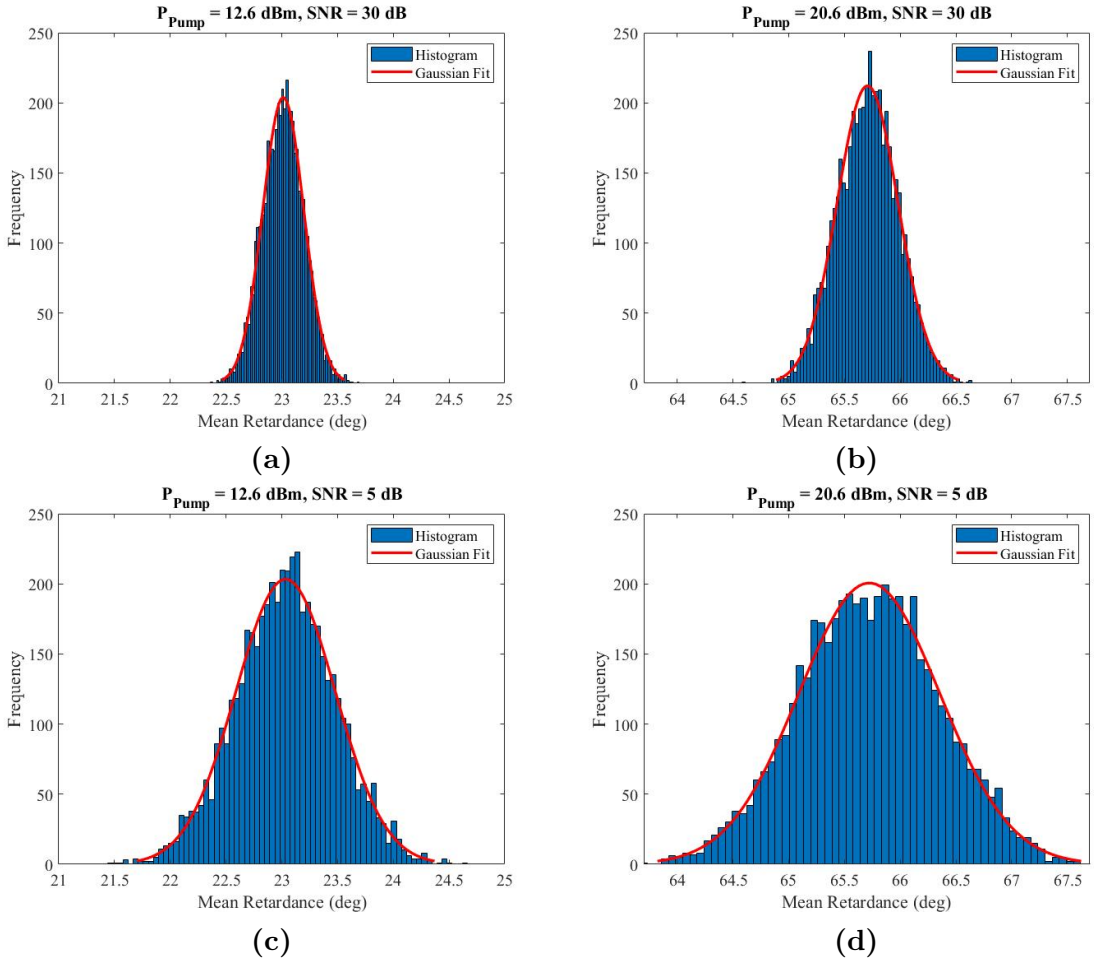

Figure 3.11: Histograms of the mean retardance obtained from the SBS polarization controller under different noise and power conditions: (a) P_{Pump} = 12.6 dBm and SNR = 30 dB; (b) P_{Pump} = 20.6 dBm and SNR = 30 dB, (c) P_{Pump} = 12.6 dBm and SNR = 5 dB, (d) P_{Pump} = 20.6 dBm and SNR = 5 dB.

sented in Fig. 3.10 and implicates that under high pump power conditions (i.e., high retardance), the performance of the system in terms of the variance of the retardance is slightly affected by the purity of the pump light source and, consequently, low-cost lasers could be used as a pump for this circular retarder nonlinear device.

The methodology developed in this Chapter allowed us, for the first time and to the best of our knowledge, to present and demonstrate a light-by-light polarization control scheme via a nonlinear interaction with bandwidth extension and spectral shaping .

Chapter 4

Applications

In previous chapters, methods for full polarization control based on SBS have been discussed. It has been proven that it is possible to manipulate the state-of-polarization (SoP) of an optical signal with the properties mentioned before. This Chapter applies the concept of SBS-based polarization control to perform optical signal processing functionalities in fiber optic systems. In particular, this search for new applications focuses on optical signal routing and photonic microwave filtering.

4.1. Signal Routing

Signal distribution is one of the main tasks of optical networks. Additionally, devices such as optical power splitters and combiners are crucial for sensing [70], monitoring [71], and delivering optical signals to different subsystems in photonic circuits [72]. In some cases, the signal needs to be split into its fundamental polarization components, a procedure that can be done straightforwardly by a polarization beam splitter (PBS). The effect of separating signals that are coded in different polarization axes can be interpreted as a signal routing operation, where input signals aligned to the principal polarization axis of the PBS come out to one of its output ports and signals orthogonal to the principal polarization axis comes out to the second output port. Due to the capacity of the SBS-based polarization controller to change the SOP of a light beam, it can potentially become in the core subsystem, in combination with the PBS, of an optical router.

Moreover, by using this configuration and leveraging the frequency and bandwidth tuning properties of this system, if the input signal is composed of different sub-signals (aligned to the principal axes of the PBS) placed at a determined wavelength, one of these sub-signals can be selected and delivered to the orthogonal port of the PBS. This routing signal operation is similar to a Wavelength Selective Switch (WSS), as shown in Fig. 4.1, with the principal difference in the operating bandwidth: a commercial

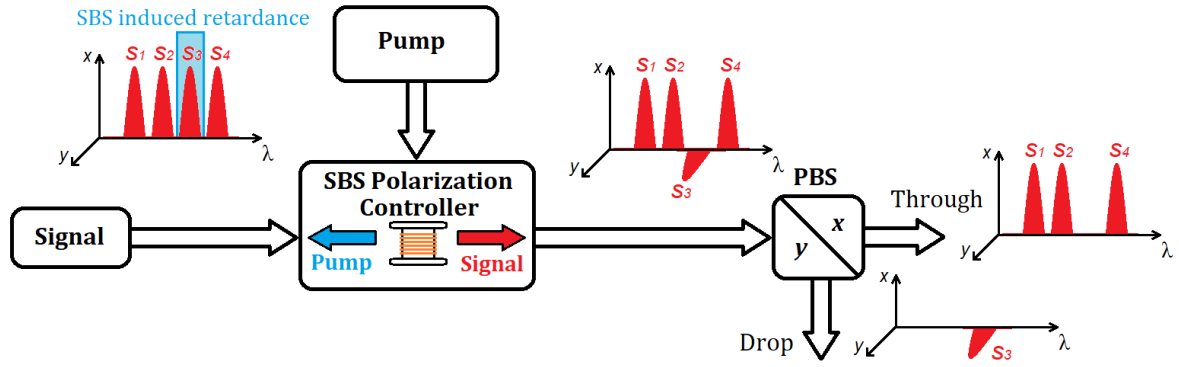

Figure 4.1: Use of the SBS-based polarization controller for selecting and delivering to the Drop port (y polarization axis output of the PBS) the sub-signal S_3 which is part of a set of signals S_1, ...,S_4 that are wavelength division multiplexed and aligned to x polarization axis.

WSS operates with bandwidths of 50 GHz and 100 GHz. An SBS-based optical router can complement present WSS technology based on MEMs (Micro-Electromechanical Systems) or LCoS (Liquid Crystals on Silica) since they can provide this functionality with narrower band channels. Schemes for splitting signals with lower bandwidth can be constructed with optical filters [73]. Still, the possibility of fine frequency tuning (i.e., the MHz/GHz range) is minimal. Meanwhile, the SBS-based polarization controller is proven to operate in the GHz range, representing an improvement in frequency selectivity.

On the other hand, other types of devices exhibit altered transmission characteristics if the input and output channels are interchanged [74], called nonreciprocal devices. Examples of them are optical circulators [75], isolators [76], and amplifiers[77], and their use is widely spread in photonic systems. Backward Stimulated Brillouin Scattering is a nonlinear, nonreciprocal phenomenon, where amplitude and absorption spectra are induced only under frequency, phase, and direction (counter-propagating pump and signal waves) matching conditions [78]. From the direction condition, it is derived that the typical backward SBS gain and loss spectra do not appear when pump and signal waves are co-propagated. There is a forward Brillouin scattering phenomenon [79], which is activated using a co-propagating signal and pump waves pair. However, it only induces phase modulation [80], and Brillouin frequency shifts are around several MHz, so it can be neglected when direct detection is employed, and the pump-signal pair is separated in the range of GHz.

Thus, the nonreciprocal property of the SBS-based polarization controller can be considered when designing active circulators and isolators with high isolation between ports. In Fig. 4.2, a scheme of an active optical wavelength selective circulator whose core component is the SBS-based polarization controller is shown. Here, a signal that enters port 1, which is co-propagating with the pump wave, travels to port 2, avoiding being affected by the SBS-induced retardance. While considering a signal entering port

2, the operation of polarization rotation is performed, and the signal from port 2 is derived to port 3, corresponding to other outputs of the polarization beam splitter. It can be seen that ports 1 and 3 and ports 2 and 1 are strongly isolated, in one case by the PBS and in the other by the change of the SoP induced by the SBS. As mentioned, bandwidth and central frequency can be modified to select a portion of a signal spectrum and transmit it to port 3. Furthermore, an active-frequency selective optical isolator can be built if a polarizer is placed instead of a PBS.

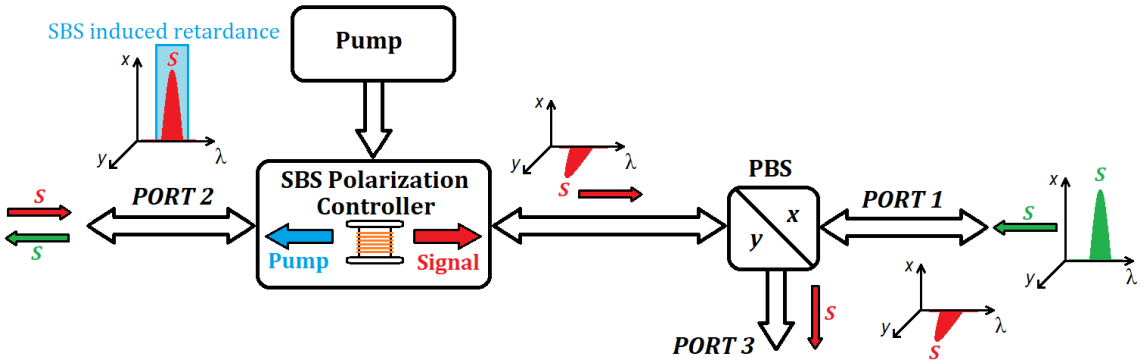

Figure 4.2: A scheme of a wavelength selective optical circulator constituted by the SBS-based polarization controller: a signal that travels from port 1 to port 2 is not affected by SBS-induced retardance; meanwhile, a signal entering port 2 suffers from polarization conversion in order to be split to the y polarization axes and delivered to port 3. If a polarizer replaces the PBS, the optical circulator will be transformed into an optical isolator.

4.2. Photonic Microwave Filtering

In the last Section, it was mentioned that if a portion of a signal wave changes its SoP by using the SBS polarization controller. Then, this signal is spatially separated or blocked using a polarization-sensitive device, e.g., a PBS or a polarizer, and the remaining signal will result in a part of its power spectrum absorbed. This process resembles the working principle of a polarization-sensitive optical filter, where the bandwidth of the absorbed spectrum is determined by the total retardance induced by the SBS polarization controller. This concept is graphically described in Fig. 4.3. Moreover, if the optical signal carries the information of an electrical microwave signal, the overall system will constitute a microwave photonic filter after reconversion to the electrical domain. For instance, the results showed in Chapter 3 Fig. 3.11a can be interpreted as a microwave photonic reject band filter based on the SBS polarization controller with adjustable central frequency and bandwidth, where the absorbed power spectrum is strictly related to the induced SBS retardance. Aiming to go beyond, if the rotated signal is not lost but instead is handled in order to maintain optical coherence and obtain frequency stability, it could be made a microwave photonic passband filter from a single SBS-polarization controller.

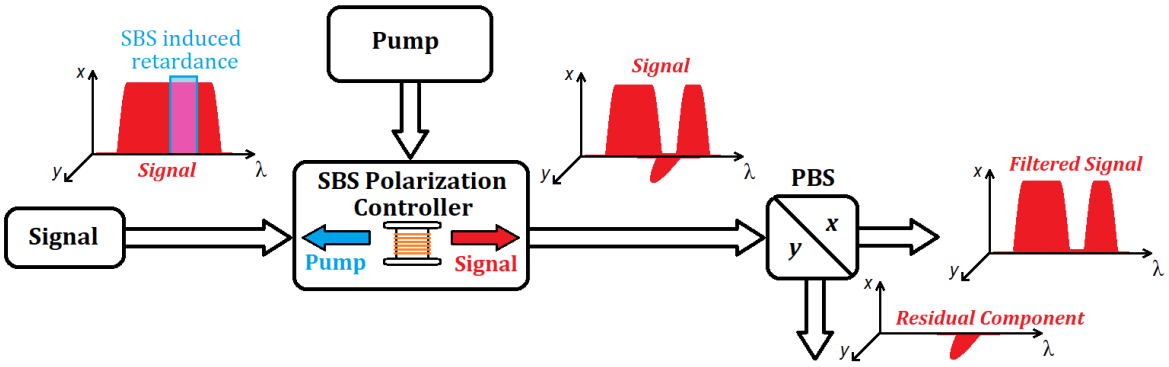

Figure 4.3: SBS-based polarization controller as the core subsystem of a microwave photonic filter.

The concepts mentioned above were considered to develop and test an application in the field of Microwave Photonics [81]. The polarization control method described in Chapter 2, in combination with a polarization-sensitive balanced detection scheme, allowed the implementation of versatile photonic microwave filters with frequency tunability and bandform, i.e., notch and passband responses, using a single-fiber stage SBS-based polarization controller. It will be further seen that the stopband filter derived from the SBS-based polarization controller outperforms other implementations in terms of stopband attenuation and simultaneously provides interchangeability with the passband filter. The obtained passband filter has a similar stopband rejection compared to those that only use one stage of optical fiber.

4.2.1. Microwave Photonic Filter Based on Polarization-Sensitive Balanced Detection[†]

The filter architecture relies on performing a polarization-dependent balanced photodetection on an optical signal whose polarization has been changed in a band of interest in the SBS-based polarization controller. As seen in previous Chapters, this polarization control method exploits the fact that if the pump is aligned with one eigenmode of the signal, SBS induces a controlled phase shift between eigenmodes. Thus, SBS can introduce an optically controlled phase retardance between linearly polarized eigenmodes. An enhanced phase response can be obtained if two SBS responses, namely one gain plus one loss, are combined, as shown in Fig. 4.4a. The phase shift from both responses is added, while the amplitudes of the gain and loss are mainly compensated. It is analogous to an optical all-pass filter. This process is achieved by generating a pair of pumps at frequencies $\pm\omega_{p1} = \pm 2\pi(\nu_B + \Delta\nu_B/2)$, where ν_B is the Brillouin frequency shift and $\Delta\nu_B$ the gain bandwidth, around the band of interest Ω_c that must be filtered.

[†]This Subsection is based on: G. Zoireff, D. Samaniego and B. Vidal, «Dynamic Filtering of Microwave Signals Through Brillouin-Based Polarization-Sensitive Balanced Detection», in *IEEE J. Sel. Top. Quantum Electron.*, vol. 27, no. 2, pp. 1-6, Art no. 7500206, March-April 2021.

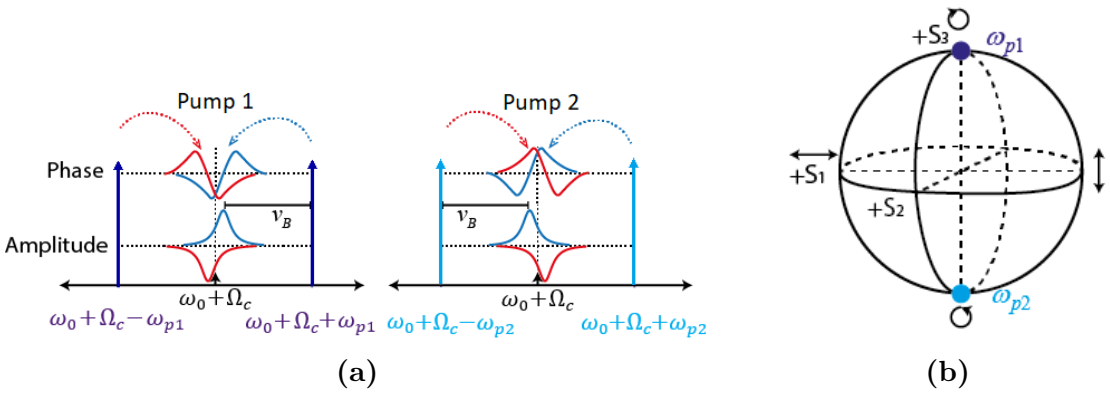

Figure 4.4: Mechanism and pump waves for polarization control based on SBS-induced retardance. a) Phase and amplitude responses from the combination of gain and loss responses by using a pair of pump waves at $\pm\Omega_{p1}$ and $\pm\Omega_{p2}$; b) Representation on the Poincaré sphere of the pump waves for circular rotation: one pair has right-handed circular polarization Ω_{p1} and the other left-handed circular polarization Ω_{p2}.

To minimize the spontaneous noise contribution and center the peak of the retardance at Ω_c, a second pump pair is used at $\pm\omega_{p2} = \pm 2\pi(\nu_B - \Delta\nu_B/2)$. Depending on the SoP of the pump waves, different types of polarization control can be achieved if pumps are set in each pole on the Poincaré sphere (see Fig. 4.4b), and a circular retarder can be implemented. The amount of polarization rotation is controlled by the pump power.

If a microwave signal is modulated onto an optical carrier through a single sideband modulation with carrier (SSB+C), light-by-light polarization control can be used to selectively rotate the SoP of a band of interest, as given by

$$E_s(t) \propto \exp(j\omega_0 t)\,[A_c + m_{SSB}(t)]\,, \tag{4.1}$$

where ω_0 and A_c are the angular frequency and amplitude of the optical carrier, respectively, and $m_{SSB}(t)$ is the microwave signal modulated in SSB.

The SoP of the band of interest within the sideband Ω_c is rotated at 45^{o} relative to the SoP of the carrier and single sideband (SSB+C), as shown in Fig. 4.5a and given by

$$E'_s(t) = \begin{pmatrix} E_{\hat{x}} \\ E_{\hat{y}} \end{pmatrix} \propto \exp(j\omega_0 t)\,[A_c + \tilde{m}_{SSB}(t)] \begin{pmatrix} 1 \\ 0 \end{pmatrix} + \frac{1}{2} M_{SSB}(\Omega_c) \exp(j(\omega_0 + \omega_c)t) \begin{pmatrix} 1 \\ 1 \end{pmatrix}, \tag{4.2}$$

where M_{SSB} is the Fourier transform of $m_{SSB}(t)$ and $\tilde{m}_{SSB}(t)$ is its unrotated remaining part along the $\hat{x}$ axis.

If 4.2 is rotated with a conventional broadband fiber polarization controller to enter a polarization beam splitter (PBS) at 45^{o} of its principal polarization axes, as shown in Fig. 4.5b, in each PBS output, the input signal is projected to one its axes.

If the PBS output corresponding to its $\hat{x}$ axis, given the convention assumed in Fig.

4.5b, is connected to one input of a balanced photodiode and the output corresponding to its $\hat{y}$ axis of the PBS is blocked before entering the balanced photodiode, a stop-band filter response will be obtained at the output of the photodiode, i.e. polarization rotation is transformed to optical loss. This process is shown in Fig. 4.5c and Fig. 4.3. As can be seen, the sideband suffers a 3 dB loss, whereas the band of interest is highly attenuated due to the PBS

$$E'_{\hat{x}}(t) \propto \frac{1}{\sqrt{2}} \exp\left(j\omega_0 t\right) \left[A_c + \tilde{m}_{SSB}(t)\right], \tag{4.3}$$

$$E'_{\hat{y}}(t) \propto \exp\left(j\omega_0 t\right) \left[A_c + \tilde{m}_{SSB}(t) + \sqrt{2} M_{SSB}(\Omega_c) \exp\left(j\Omega_c t\right)\right]. \tag{4.4}$$

On the other hand, if the signal in the $\hat{y}$ axis is not blocked, a passband response 4.4 is achieved from the subtraction in the balanced photodiode between the optical notch response shown in Fig. 4.5c and the response of Fig. 4.5d. Thus, outside the band of interest, both signals are canceled by the balanced detection, while within this band, the passband with the 3 dB gain is not canceled because the PBS has filtered the signal in this band.

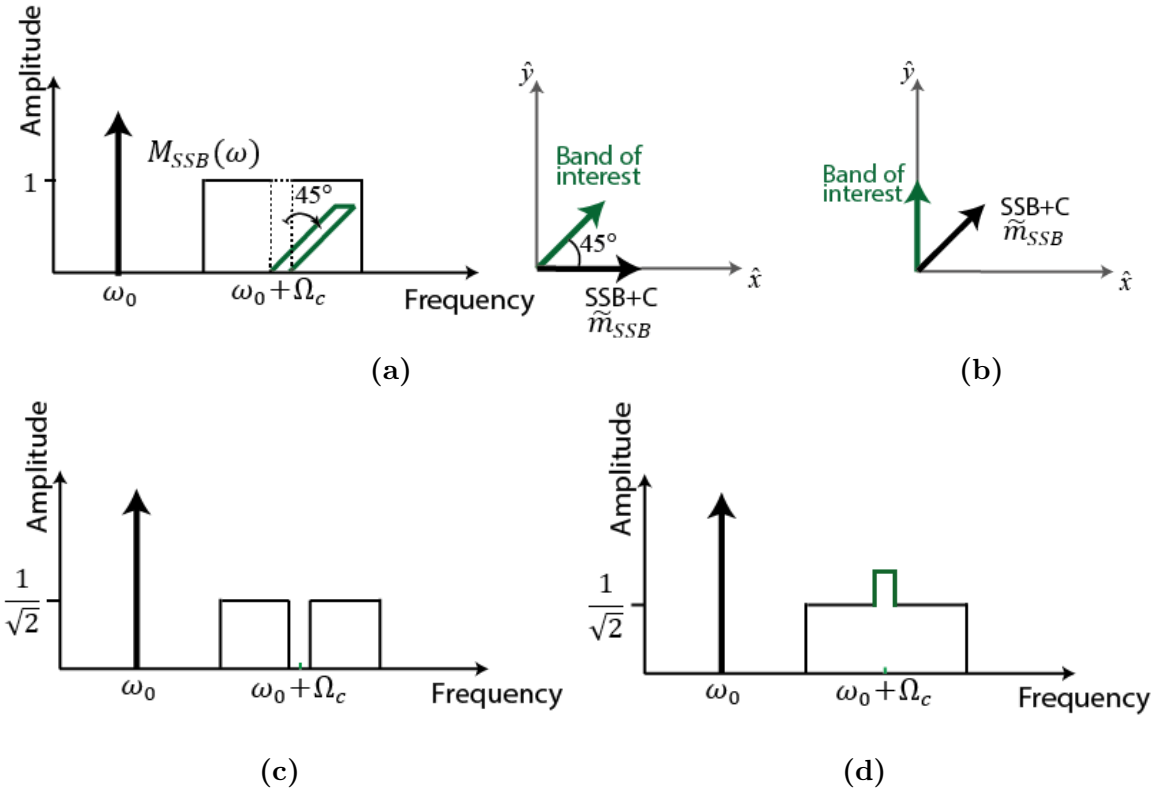

Figure 4.5: The operating principle of the proposed photonic microwave filter. a) Single sideband modulated signal with carrier (SSB+C) at the output of the nonlinear polarization where the band of interest has been rotated 45º; b) Rotation of the SSB+C signal to enter at 45º relative to the fast and slow axes of the PBS; c) Optical signal at the output $\hat{x}$ of the PBS showing a stopband response; d) Optical signal at the output $\hat{y}$ of the PBS showing an all-pass response but in the band of interest where the architecture applies a 3 dB gain.

Thus, a filter response not constrained by the conventional SBS gain in optical fibers of around 20 dB can be implemented, which forces multi-stage architectures to achieve filter response with significant out-of-band rejection.

4.2.2. Experimental Setup

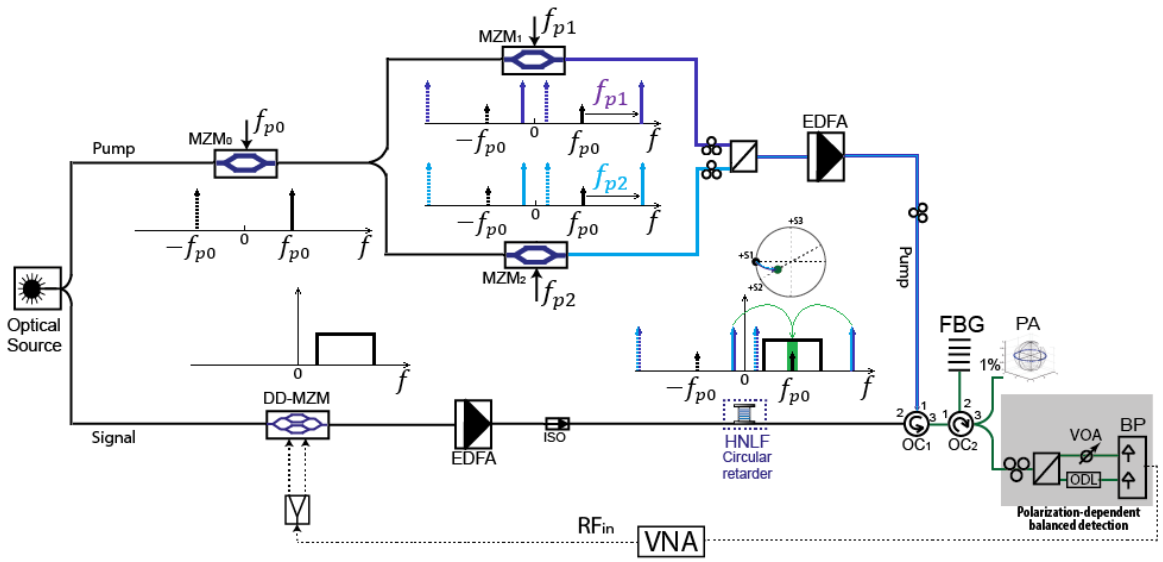

Figure 4.6: Block diagram of the experimental setup of the proposed photonic microwave filter. HLNF: highly nonlinear fiber. OC: optical circulator; ISO: isolator. FBG: fiber Bragg grating. PA: polarization analyzer. ODL: optical delay line. VOA: variable optical attenuator. BP: balanced photodetector. VNA: vector network analyzer.

The experimental setup used to validate the concept of photonic microwave filtering based on all-optical polarization control is shown in Fig. 4.6. An optical signal (1548 nm) is split into two paths. The upper path is used to generate the central pump angular frequency Ω_c of the optical carrier (by the Mach-Zehnder modulator MZM_0 biased at Minimum Transmission Bias -MITB) of the Brillouin polarization control stage that acts as a circular retarder. It is implemented by two Mach-Zehnder modulators (MZM_1 and MZM_2) biased at MITB and fed by two microwave oscillators with frequencies f_{p1} (9.607 GHz) and f_{p2} (9.677 GHz). An optical circulator (OC_1) directs the SBS pump (Pump#1) toward the circular retarder through 1 km of highly nonlinear fiber (HLNF). The Brillouin parameters for this fiber are $\Delta\nu_B = 40$ MHz, $g_0 = 7.19 \times 10^{-12}$ m/W, $\nu_B = 9.64$ GHz, and $A_{eff} = 11$ μm^2. In the lower path, an RF signal modulates the light signal using a dual-drive Mach-Zehnder modulator (DD-MZM) at quadrature bias to implement an SSB+C. This pumping scheme could be replaced by an arbitrary waveform generator (AWG) to simplify the system hardware and extend the bandwidth, as done in Chapter 3.

The Brillouin polarization control was optimized by adjusting the polarization of the two counter-propagating signals at frequencies f_{p1} and f_{p2} to the right and left

circular SoP, respectively. A fiber Bragg grating (FBG) in reflection mode (bandwidth of 12.5 GHz) filters out backward residual pump waves. The pump power control is done by adjusting the pump power through the Erbium-doped fiber amplifier (EDFA) until it is matched to the orthogonal SoP relative to the transmission axis of PBS output by stopband filter. The polarized signal is set to be 45° linear at the input of the PBS. The power of the required pump is 8 dBm, reaching a retardance of $-\pi/2$, which changes the signal's polarization state until horizontal linear polarization. The retardance has been measured with a polarization analyzer (PA) following the Poincaré sphere method [57]. A good linear dependence between retardance in the $\pi/4$ to π range and pump power from 1 mW to 6.5 mW has been observed [53].

The filtered modulated signal reaches a balanced photodiode, where a variable optical attenuator (VOA) is used to select the filter response's bandform (notch or passband) by blocking one path. The balanced photodetector is a Teleoptix 43 Gbps DPSK photoreceiver with limiting TIA, with a typical small signal differential conversion gain of 1500 V/W, 0.5 ps of optical path delay, and an OSNR performance of 19 dB. Also, an optical delay line (ODL) is employed to compensate for the balanced photodetector's optical path delay. Finally, the filter's frequency response is measured with a vector network analyzer (VNA) HP8510C. Unlike other stopband filters, the filter's great depth is performed in the optical domain.

Experimental measurements show that the performance is stable after the configuration of the polarization states of the signal and pumps.

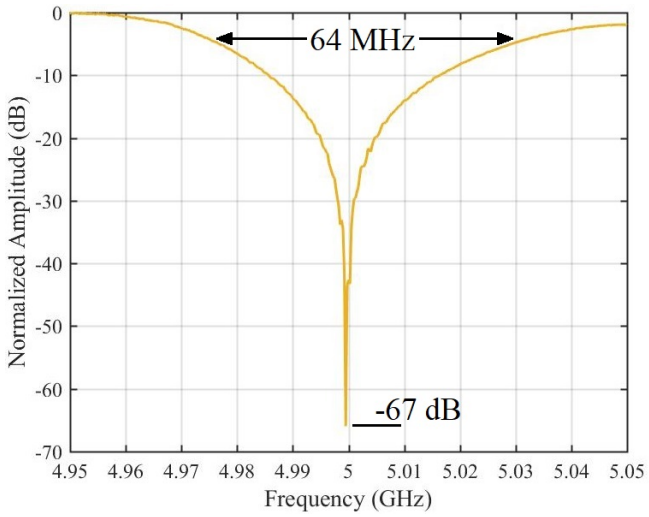

Figure 4.7: Measured normalized frequency response of the photonic microwave stopband filter centered at 5 GHz.

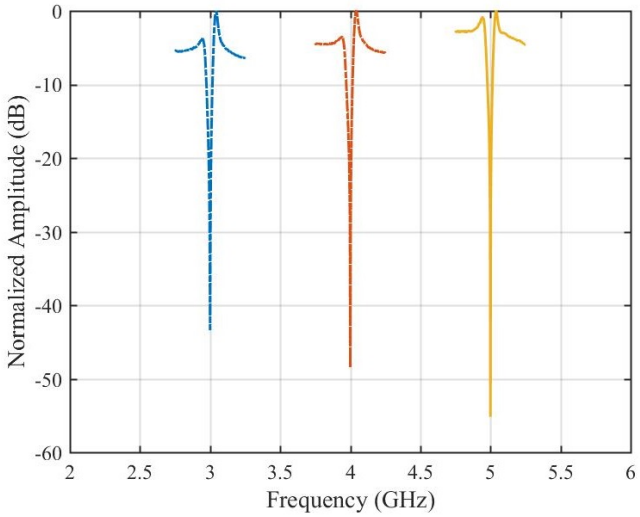

Figure 4.8: Measurement of the tunability of the frequency response of the stopband filter response by changing the pump frequency f_{p0}.

4.2.3. Results and Discussion

Figure 4.7 shows the normalized response (S_{21}), which has been measured with the VNA at the output of the balanced photodetector when the strong attenuation of the VOA blocks one path. In this configuration, a notch filter response filter designed to operate with a center frequency of 5 GHz is obtained.

Measurements show a very large stopband rejection of 67 dB with a FWHM of 64 MHz. To the best of our knowledge, it is the highest stopband rejection reported for a photonic microwave stopband filter. The filter central frequency is given by the pump's frequency, controlled by a microwave oscillator. As shown in Fig. 4.8, the filter response can be tuned by changing the pump frequency f_{p0}. Due to the frequency response of the overall system and the lack of equalization, the insertion loss changes with central frequency in this proof of concept.

Additionally, the setup shown in Fig. 4.6 allows for the dynamic switch between a notch and a passband response by blocking one input to the balanced photodetector. The experimental setup was done using a VOA, but high-speed switching of the type of filter response could be done if a fast-optical switch replaces the VOA. Fig. 4.9 shows a passband filter response obtained using this technique. The passband has a bandwidth of 95 MHz, with a maximum ripple of 0.5 dB and an out-of-band rejection better than 30 dB. In a similar way as with the stopband response, the central frequency of the passband can be tuned by changing the pump frequency, as shown in Fig. 4.10, where the range of tunability has been limited by the bandwidth of the microwave oscillators available at the laboratory. The out-of-band rejection is determined by the amplitude and phase imbalances of the optical signals applied to the balanced PD and the common-mode rejection ratio of the balanced PD. Additional degrada-

tion was experienced due to imperfections during the generation of the dual-sideband suppressed-carrier pump signal and spontaneous noise. Consequently, when the central frequency is tuned, the filter exhibits a reduction in the out-of-band rejection, but the shape and bandwidth are preserved.

Additionally, the setup shown in Fig. 4.6 allows for the dynamic switch between a notch and a passband response by blocking one input to the balanced photodetector. The experimental setup was done using a VOA, but high-speed switching of the type of filter response could be done if a fast-optical switch replaces the VOA. Fig. 4.9 shows a passband filter response obtained using this technique. The passband has a bandwidth of 95 MHz, with a maximum ripple of 0.5 dB and an out-of-band rejection better than 30 dB. In a similar way as with the stopband response, the central frequency of the passband can be tuned by changing the pump frequency, as shown in Fig. 4.10, where the range of tunability has been limited by the bandwidth of the microwave oscillators available at the laboratory. The out-of-band rejection is determined by the amplitude and phase imbalances of the optical signals applied to the balanced PD and the common-mode rejection ratio of the balanced PD. Additional degradation was experienced due to imperfections during the generation of the dual-sideband suppressed-carrier pump signal and spontaneous noise. Consequently, when the central frequency is tuned, the filter exhibits a reduction in the out-of-band rejection, but the shape and bandwidth are preserved.

The idea of using Stimulated Brillouin Scattering for microwave filtering purposes is not new. This nonlinear phenomenon offers interesting features over other implementations because the filter's central frequency and bandwidth can be tuned without much effort, and the natural bandwidth of SBS is around 20 MHz. Thus, very narrow filter responses (i.e., high-quality factors) can be obtained. At the same time, by broa-

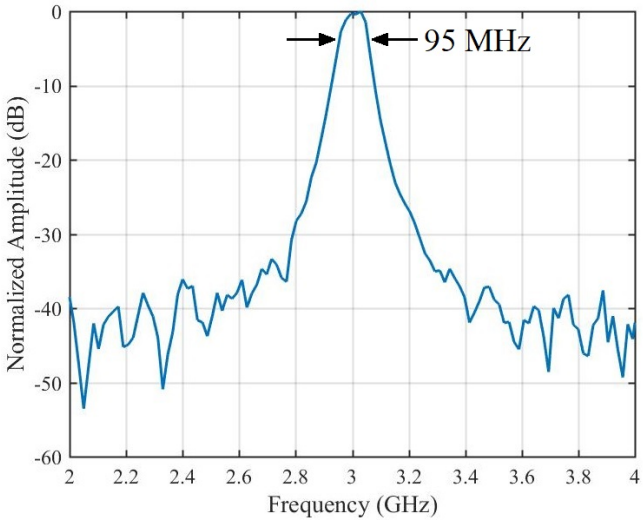

Figure 4.9: Measured normalized frequency response of the photonic passband filter centered at 3 GHz.

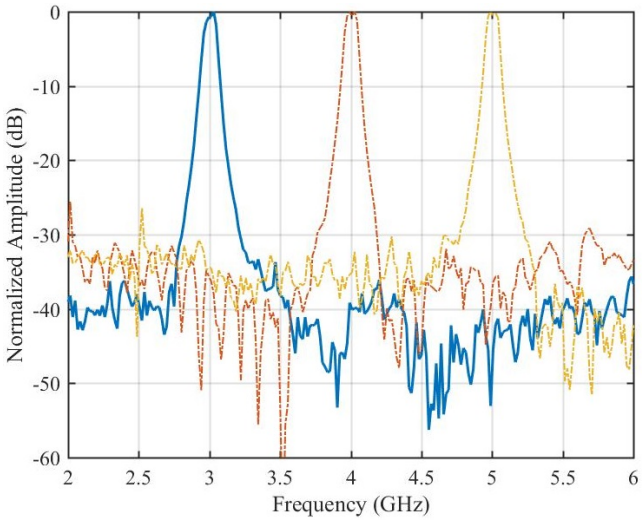

Figure 4.10: Measurement of the tunability of the frequency response of the passband filter response by changing the pump frequency f_{p0}.

dening the pump wave, it is possible to implement GHz-wide flat-top responses with fine granularity and large skirt selectivity. Unlike previous photonic microwave filters, primarily based on FIR structures, e.g., in [92], SBS avoids the tradeoff between bandpass bandwidth and free spectral range (FSR). Brillouin-based photonic microwave filters usually provide only two bandpass responses in the 0–20 GHz band, although a single response can be obtained [93]. This implementation departs from FIR filters, which have periodic frequency responses with a bandpass bandwidth related to the FSR. Tunability is also much simplified with SBS in relation to previous FIR photonic microwave filters since it is done just by tuning the pump. Despite some schemes that have been proposed to avoid this limitation, [94] SBS offers a much more versatile solution for filtering.

Additionally, Brillouin-based photonic microwave filters can be tailored to comply with a given filter mask [86][88].

Finally, SBS has the lowest activation power of all nonlinear effects in silica fibers, so it can be easily induced, reducing the power consumption of the filter. This property will also permit the miniaturization of SBS-based filter architectures through photonic integration [95][96], which has a great potential to reduce the cost and footprint of photonic solutions for microwave signal processing.

From the original concept of SBS-based photonic microwave filtering, a subfamily of filter architectures evolved towards those that rely on polarization pulling [25][90][91][97]. SBS is based on the interference between two counter-propagating waves, which, through electrostriction, induce an acoustic wave that generates a traveling grating. This interference process is highly polarization-dependent. Suppose the pump and the signal do not have their states of polarization (SoP) perfectly aligned. In that case, SBS amplification, although not getting maximum gain, applies a selective gain

Table 4.1: Performances of Microwave Photonic Filters based on SBS effect.

Reference	Method	Fiber Stages	Filter Type	Bandwidth	Stopband Attenuation
[40]	Gain and Loss	1	Passband / Stopband	24.4 MHz	22 dB / -
[82]	Gain and Loss	1	Passband / Stopband	32 MHz	30 dB / 58 dB
[83]	Phase	1	Stopband	13 MHz	60 dB
[84]	Gain	2	Passband	1 to 3 GHz	40 dB
[85]	Polarization Pulling	1	Passband	250 MHz to 1 GHz	40 dB
[86]	Phase	1	Passband	84 MHz	30 dB
[87]	Loss + Polarization Pulling	1	Passband	0.5 to 9.5 GHz	20 dB
[88]	Gain	1	Passband	30 MHz	40 dB
[89]	Gain and Loss	1	Stopband	33 to 89 MHz	60 dB
[90]	Polarization Pulling	1	Passband	700 MHz	30 dB
[91]	Polarization Pulling	2	Passband	7.7 MHz	80 dB
This work	**Polarization Conversion**	**1**	**Passband / Stopband**	**95 MHz / 64 MHz**	**30 dB / 67 dB**

on the polarization eigenmode aligned with the pump. Thus, the SBS effect pulls the signal SoP toward the pump SoP. This mechanism can implement photonic microwave filters if the polarization is converted to loss over a sideband spectrum that carries a microwave signal. Photonic microwave filters based on polarization pulling showed enhanced out-of-band rejection of the filter response, avoiding the need for multiple cascading stages.

Table 4.1 reviews the performance of state-of-the-art microwave photonic filters based on different strategies related to the SBS effect using a single stage of optical fiber. This comparison reflects that the architecture presented here outperforms other implementations regarding stopband attenuation, achieving a record of 67 dB. At the same time, it is given the chance to swap from stopband to passband filter types. The out-of-band attenuation in the obtained passband SBS filter is comparable to other filters but below 40 dB. However, as mentioned before, this property can be improved by reducing imbalances at the balanced PD and other mismatches due to the components employed in the experiment. Finally, the bandwidths obtained for passband and stopband implementations are consistent with using a double pump scheme, where, as discussed in Chapter 3, the total bandwidth is related to the phase-to-retardance conversion process. As this technique combines two phase responses of around 35 MHz (Brillouin bandwidth) and shifted ± 17.5 MHz, it will result in a bandwidth of retardance greater than the natural SBS response.

The different applications for the SBS-based polarization controller proposed in this Chapter merge as alternative approaches for traditional optical devices. An innovative microwave photonic filtering method has been developed from these proposals, which offers versatility in dynamic switching between notch and passband configurations. When comparing its performance against similar SBS-based microwave photonic implementations, the tremendous attenuation in the rejection band of the notch filter must be highlighted.

Chapter 5

Conclusions

From the theory of inelastic scattering predicted by L. Brillouin precisely one hundred and one years ago and the first experiments carried out in liquids by Gross in 1930 to the present, where Stimulated Brillouin Scattering (SBS) is excited in photonic chips to serve for multiple purposes, as well as in the most advanced systems of distributed sensing of temperature and strain, the role of this nonlinear phenomenon in modern and future photonic technology is highly relevant. Around this vast universe created based on SBS, the research focus of this Thesis has been on the study of the possibilities that it offers for light-by-light polarization control of light in optical fiber systems. The starting point has been to set specific targets that an SBS-based polarization controller has to accomplish: firstly, the ability to produce arbitrary types of birefringence and, secondly, to extend its natural bandwidth of operation. This way, full-polarization control of light would be achieved. A third objective has been finding technological applications for this device, which emerged as an opportunity to extend and improve the current state-of-the-art of SBS-based signal processing tools, if possible.

The first step to achieving full polarization control using SBS was to develop a method that allowed for arbitrarily controlling the birefringence experienced by light as it propagates through an optical fiber. As far as we know, it is the first technique experimentally proven to achieve dynamic change in the birefringence type and magnitude in optical fibers in an all-optical fashion, allowing well-defined trajectories on the Poincaré sphere, which are very hard or even impossible to accomplish using mechanically adjustable polarization controllers or waveplates. Thus, a polarization controller has been presented based on SBS polarization-dependent interactions with the ability to perform changes in a nonlinear medium's birefringence dynamically. Additional properties derived from this method were extensively studied, including SBS-induced group delay and group velocity dispersion. Their strong dependence on the polarization states of the pump and signal, which allowed the generation and manipulation

of differential group delays and differential group delay dispersion, has also been demonstrated. Thus, an optical fiber has been transformed via SBS into an arbitrarily manipulated birefringent, delay generator, and highly dispersive propagating medium.

The next step towards full-polarization control of light was to enhance the operating bandwidth of the polarization controller based on Brillouin polarization-dependent interactions. Phase-to-retardance conversion of a light source with a horizontal polarization state was achieved by combining the gain and loss power spectra of two broadened pumps with a right-handed circular polarization state. Unlike previous Brillouin broadening schemes aimed at amplitude or time delay control, retardance broadening requires engineering the phase frequency response of SBS interaction to have a constant flat phase frequency response that results in a flat-induced birefringence. An iterative method based on pump feedback allowed the engineering of the pump profile to reach a given Brillouin-induced retardance frequency response. The control of the main variables of the system, such as pump power, frequency spacing, bandwidth, and shape of the pump, permitted the operation of broadened polarization control even though the SBS gain response was under a saturation regime. From this, the pump profile was designed to provide flat-top retardance with an absolute value that can be controlled through the pump gain.

After reaching full-polarization control, two possible applications for this SBS-based polarization controller have been analyzed. The properties of bandwidth, central frequency, and birefringence tuning of the polarization controller have given place to signal routers, nonreciprocal devices such as active and wavelength-selective circulators and isolators, and optical or microwave photonic filters, on which the SBS-based polarization controller, in combination with polarization-sensitive structures, is the core subsystem.

Despite having presented a few alternatives for applying the SBS-based polarization controller, only one has been tested. This application in the Microwave Photonics field is a novel microwave filter architecture that offers tremendous versatility since it can be used to implement filters that are frequency tunable and completely reconfigurable by dynamically shaping the response, the bandwidth, and even the type of filter (stopband, passband). Experiments with this SBS-based filter using a single stage of highly nonlinear optical fiber exhibited a record-high stopband rejection. Meanwhile, the passband configuration presented a performance similar to other single-stage SBS filter implementations. This approach enhances the architecture's flexibility since a single design could be applied to various scenarios.

Finally, and to conclude, the main contribution of this Thesis has been the increase in the collection of tools available to achieve a better understanding of the control of light propagation in guided media and rethink traditional optical devices. Other issues that should have been discussed but are very important in most applications are

power consumption and the possibilities of implementing the concepts developed here in photonic integrated circuits. A viable way to reduce the power consumption of the SBS-based polarization controller is to consider using other non-traditional fiber-guided media with enhanced nonlinearity, such as photonic crystal fibers. These waveguides could also help overcome some limitations of SBS as its restricted time-bandwidth product opens up a chance for obtaining a broader retardance frequency response. Recent developments in On-Chip SBS pave the way for implementing this device in integrated photonic systems. Additionally, a window of opportunity opens for other opto-acoustic interactions, such as forward or inter-polarization Brillouin scattering, where polarization control of light has yet to be explored.

Appendix A

Theory of Brillouin Light Scattering

Brillouin Light Scattering (BLS) is a nonlinear process represented by the light-matter interaction between an optical wave (photons) and an acoustic wave (acoustic phonons), defined by the vibrational modes determined by the geometry of the propagating media. Fluctuations in the optical properties of a dielectric material system produce the acoustic wave. It provokes a modulation in the refractive index of the nonlinear medium, creating a diffraction grating that scatters the incident light beam. At the end of the interaction, scattered photons produce less energy than incident photons, which defines Brillouin light scattering as inelastic. This phenomenon is different from Raman light scattering, where the interaction is between photons against the vibrational modes of the lattice structure of the molecules of a nonlinear medium, and Rayleigh scattering, which is a linear light scattering from non-propagating density fluctuations and represents a fundamental propagating loss process [8][7]. These three fundamental scattering mechanisms are depicted in A.1.

Brillouin light scattering (BLS) is very relevant in optical fibers. In these waveguides, the nonlinear phenomenon requires the least power to be activated. For comparison, the BLS power threshold in optical fibers is around 1 mW, whereas Raman power thresholds are around 1 W [8]. Additionally, BLS manifests its influence at frequencies around ± 10 GHz of the pump frequency. It might be a problem for communication systems where linear transmission is usually required. However, this relatively low frequency of influence and low power threshold, in combination with other properties such as its sensitivity to strain and temperature, makes BLS suitable for sensing and signal processing applications.

Brillouin light scattering can be classified as spontaneous or stimulated, depending on whether the presence of the incident light beam alters the optical properties of the material system. Also, similar to other nonlinear processes in optical fibers, fulfilling phase-matching conditions are required to produce an efficient nonlinear interaction. The following sections will analyze these two types of BLS and the phase-matching

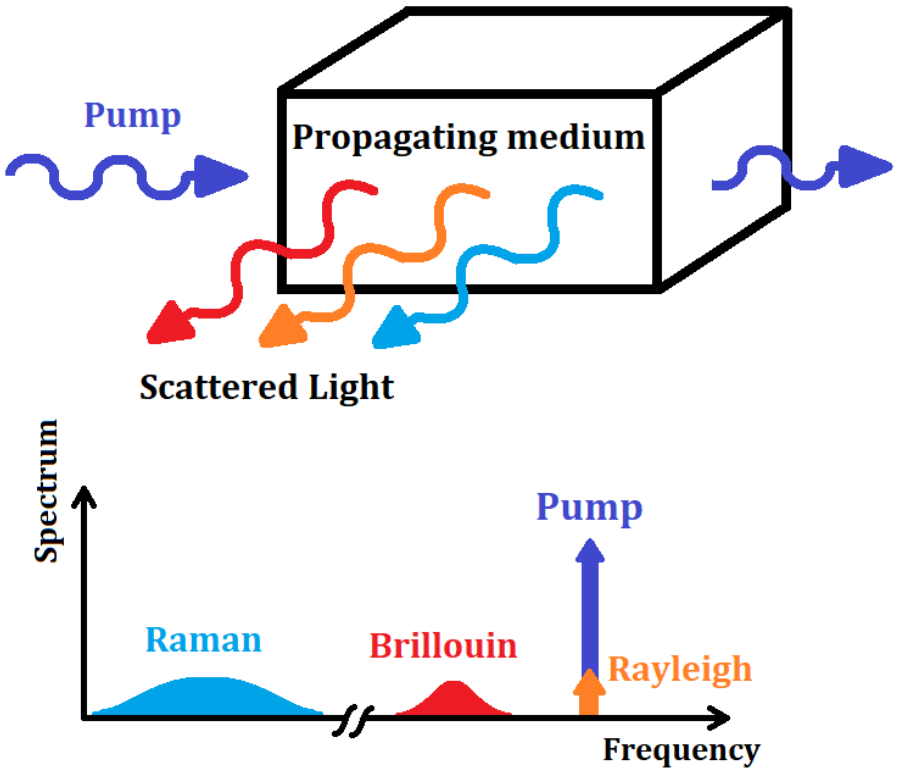

Figure A.1: Fundamental scattering processes in a nonlinear propagating medium.

conditions.

A.1. Spontaneous Brillouin Scattering

A light-scattering process is said to be spontaneous if the fluctuations (typically in the dielectric constant) that cause the light-scattering are caused by thermal or quantum mechanical zero-point effects [7]. These fluctuations generate thermal phonons or, equivalently, sound waves. Subsequently, the pump wave is scattered, creating a Stokes wave. In Fig. A.2a is shown the dispersion diagram where the optical and acoustic modes of the fiber are illustrated. The energy and momentum conservation conditions are satisfied when the pump and Stokes waves are related by

$$\Omega_B = \omega_P - \omega_S \tag{A.1a}$$

$$q = k_P - k_S. \tag{A.1b}$$

where ω_P and ω_S are the angular frequencies of the pump and Stokes waves with their associated wavenumbers k_p and k_S; and Ω_B and q are the angular frequency and the wavenumber of the acoustic wave. The dispersion relation of the longitudinal acoustic

modes is given by:

$$\omega_A(k) \approx v_A k, \tag{A.2}$$

where v_A is the acoustic velocity of the sound wave in silica. As $\omega_P \approx \omega_S \approx \omega_0$, from the dispersion diagram, it can be seen that $q \approx 2k_P = 2\omega_P n/c$, with n the refractive index of the optical fiber and c the speed of light in vacuum. Thus, when it is evaluated $\omega_A(k = q)$ it follows

$$\Omega_B = \omega_A(q) = \frac{2v_A n}{\lambda_0}. \tag{A.3}$$

$\nu_B = \Omega_B/2\pi$ is one fundamental parameter of the BLS, and it is named Brillouin frequency shift. For $v_a = 5900$ m/s and $n = 1.45$, $\nu_B = \lambda_0 = 1550$ nm, $\nu_B = 10.8$ GHz. Another important conclusion that can be extracted from the dispersion diagram is that to support the interaction of pump and Stokes waves; they must travel in opposite directions. For this reason, this interaction is also known as backward Brillouin

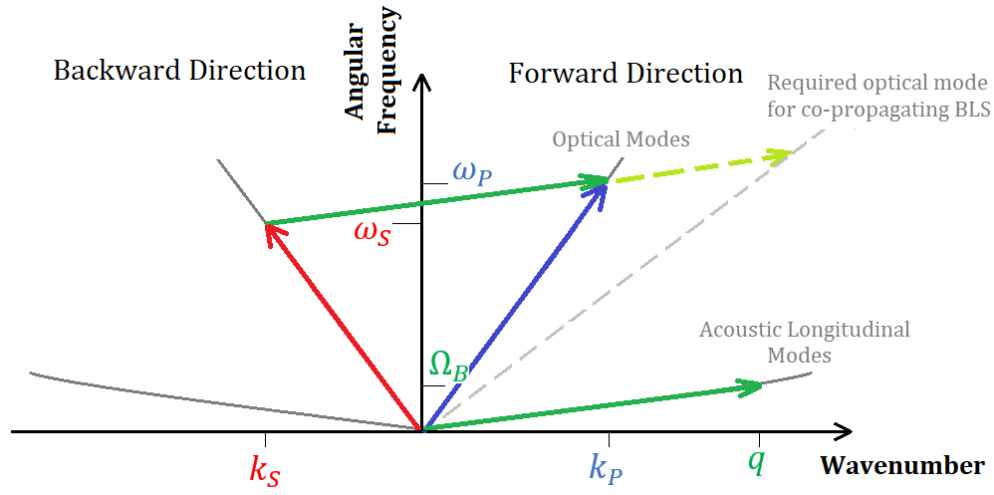

(a)

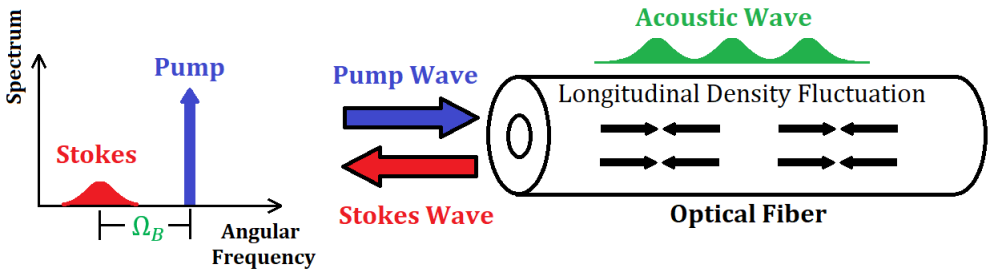

(b)

Figure A.2: (a) Dispersion diagram of spontaneous Brillouin light scattering, where frequencies and wavenumbers of the optical and longitudinal acoustic modes of the optical fiber match between them by energy and momentum conservation, and (b) backward Brillouin scattering in an optical fiber with counter-propagating pump and Stokes waves.

scattering, and it is derived from the excitation of longitudinal variations in the material density of the optical fiber, as can be appreciated in Fig. A.2b.

A.2. Stimulated Backward Brillouin Scattering

A light-scattering process is said to be stimulated if the presence of the light field induces fluctuations in the propagating media [7]. From the spontaneous BLS analysis, the main result of the scattering process of photons and thermally generated phonons was the creation of the Stokes wave. The Stokes wave is downshifted in frequency from the pump wave by the amount given by Ω_B. As the beating between the pump and sound waves reinforces the Stokes wave, the beating between the pump and Stokes waves reinforces the acoustic wave. This way, a positive feedback loop is established, producing an exponential increment in the power of the Stokes wave. Electrostriction is the primary mechanism that contributes to reinforcing the driving of the acoustic wave by the interaction of the pump and Stokes wave or, equivalently, increasing the efficiency of BLS. Electrostriction is the tendency of a material to become compressed in the presence of an electric field and the coupling mechanism that leads to stimulated Brillouin scattering. The feedback process of Stimulated Brillouin Scattering (SBS) is shown in Fig. A.3.

Under steady-state conditions, SBS is usually mathematically described by two coupled differential propagation equations for the amplitude of pump A_P and signal

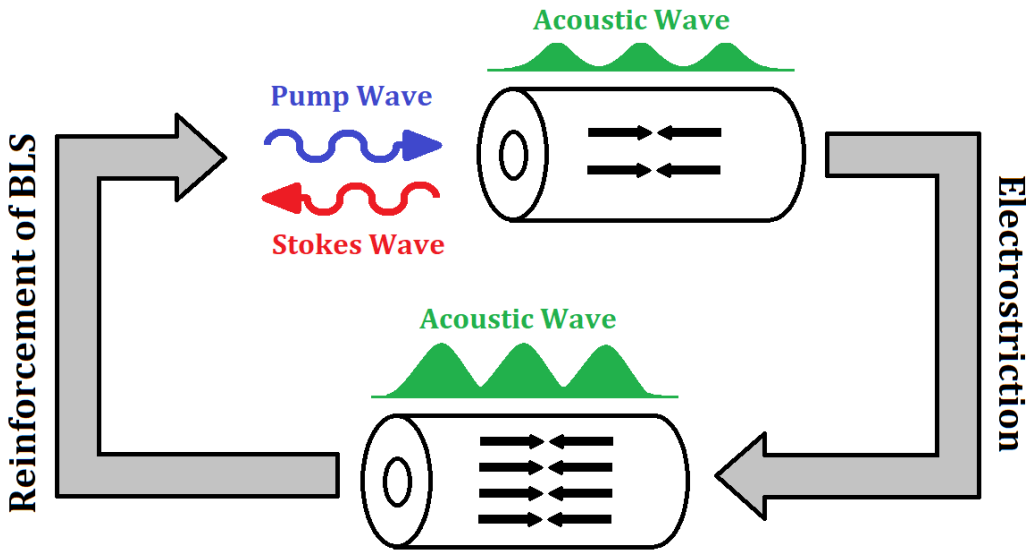

Figure A.3: Stimulated Brillouin scattering is represented by a feedback loop, whose principal coupling mechanism is electrostriction.

waves A_S as follows:

$$\frac{dA_P}{dz} = jg_0\frac{v_A c^2\Gamma_B}{2\omega_0}\frac{|A_S|^2 A_P}{\Omega_B - (\omega-\omega_0)^2 - j\Omega\Gamma_B} \tag{A.4a}$$

$$\frac{dA_S}{dz} = -jg_0\frac{v_A c^2\Gamma_B}{2\omega_0}\frac{|A_P|^2 A_S}{\Omega_B - (\omega-\omega_0)^2 + j\Omega\Gamma_B}, \tag{A.4b}$$

where two new fundamental parameters of SBS have been introduced: the Brillouin gain g_0 and the Brillouin linewidth Γ_0, which is inversely proportional to the phonon lifetime. The Brillouin bandwidth $\Delta\nu_B = \Gamma_B/2\pi$ is more commonly found in literature instead of the Brillouin linewidth. Typical values of g_0 and $\Delta\nu_B$ in optical fibers are around $10^{-11}/10^{-12}$ m/W and 50 MHz, respectively.

Assuming the intensity of the pump wave I_P remains constant during propagation, a solution for the intensity of the Stokes wave as a function of the propagated distance $I_S(z)$ can be derived from A.4

$$I_S(z) \approx I_S(L)\exp\left[gI_P(L-z)\right]. \tag{A.5}$$

where $I_S(L)$ is the initial intensity of the Stokes wave at the propagating length L (in optical fibers, it can be approximated to the effective length [8]), and $g = g(\omega)$ is the Brillouin gain spectrum. The latest can be approximated to a Lorenztian function, as follows:

$$g = g(\omega) = g_0\frac{(\Gamma_B/2)^2}{(\Omega_B - \omega - \omega_P)^2 + (\Gamma_B/2)^2}. \tag{A.6}$$

Note that g does not depend on the pump intensity. But as the Stokes wave propagates in the negative z, it experiences exponential gain determined by the product gI_P.

By changing indexes, P for S in Eq. A.4a and S for P in Eq. A.4b, a new set of coupled equations for the anti-Stokes wave is generated, whose solution, matched to $\omega_{AS} = \omega_P + \Omega_B$, is expressed as

$$I_{AS}(z) \approx I_{AS}(0)\exp\left[-gI_P z\right]. \tag{A.7}$$

Since the anti-Stokes wave at frequency ω_{AS} propagates in the positive z direction, it can be seen that it experiences attenuation due to the SBS process.

A priori, generating photons with energy higher than the pump photons violates energy conservation in a scattering process. However, the anti-Stokes wave indicates a mechanism for the absorption of photons that travels in the opposite direction of the pump wave and is frequency-shifted in $+\Omega_B$. These photons are annihilated to be reconverted into acoustic phonons.

SBS also presents a phase spectrum. Due to the refractive index modulation, the Kramers-Kronig relations express this phase spectrum is linked to the gain spectrum

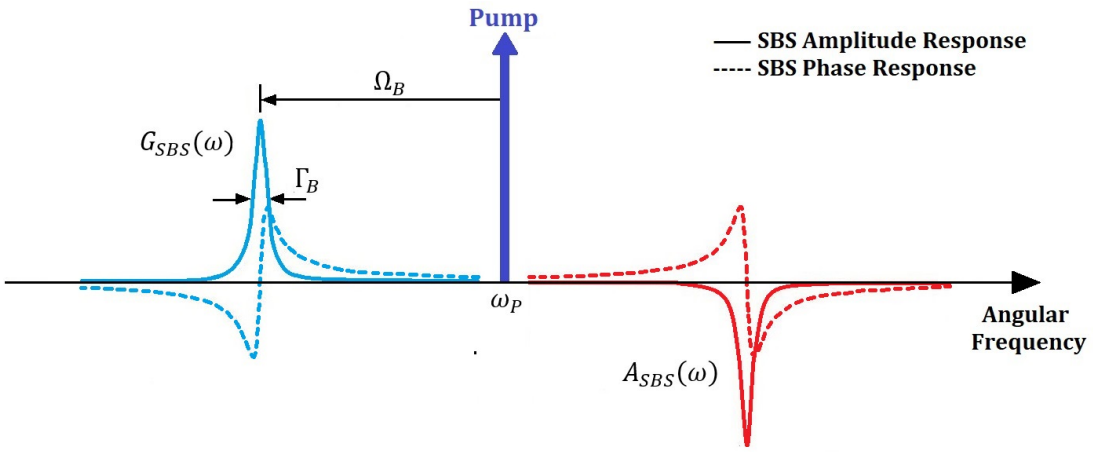

Figure A.4: Amplitude and phase responses induced by SBS.

by a Hilbert transform operation [63][66]. By applying this to A.6, it is obtained

$$\phi(\omega) = -g_0 \frac{\Gamma_B}{2} \frac{(\omega + \Gamma_B - \omega_P)}{(\omega + \Omega_B - \Omega_P)^2 + (\Gamma_B/2)^2}. \tag{A.8}$$

Thus, the exponential complex gain and loss of an SBS nonlinear interaction can be written as

$$G_{SBS}(\omega) = g_0 I_P \left[\frac{(\Gamma_B/2)^2}{(\omega + \Omega_B - \omega_P)^2 + (\Gamma_B/2)^2} - j \frac{\Gamma_B/2\,(\omega + \Omega_B - \omega_P)}{(\omega + \Omega_B - \Omega_P)^2 + (\Gamma_B/2)^2} \right], \tag{A.9a}$$

$$A_{SBS}(\omega) = -g_0 I_P \left[\frac{(\Gamma_B/2)^2}{(\omega - \Omega_B - \omega_P)^2 + (\Gamma_B/2)^2} - j \frac{\Gamma_B/2\,(\omega - \Omega_B - \omega_P)}{(\omega - \Omega_B - \Omega_P)^2 + (\Gamma_B/2)^2} \right]. \tag{A.9b}$$

These power and phase spectra are illustrated in Fig. A.4.

Due to the creation of the Stokes wave, SBS can lead to two different basis configurations. The first is SBS as a signal generator, where only a single light source is used as a pump wave to interact with thermally generated phonons present in the optical fiber, resulting in a back-scattered Stokes wave that grows exponentially by a feedback process mediated by electrostrictive forces and is downshifted in frequency from the pump in Ω_B. The second configuration is SBS as an amplifier, where, in addition to the pump, a second light source is counter-propagated at a frequency $\omega_p - \Omega_B$. The SBS process provides photons to the signal wave (matched to the Stokes wave), which induces gain. Analogously, an attenuator can be implemented by matching the frequency of the signal wave to the anti-Stokes wave at $\omega_p + \Omega_B$.

It is worth mentioning that experiments with SBS in the generator configuration exhibit an apparent threshold. An expression for this threshold in optical fibers is given

by

$$G_B^{th} = \frac{g_0 P_{cr} L_{eff}}{A_{eff}}; \tag{A.10}$$

where P_{cr} is the critical pump power, L_{eff} the effective length of the fiber and A_{eff} the effective area of the fiber. For typical parameters of optical fibers used for telecommunications, $G_B^{th} \approx 21$ ($g_0 = 5 \times 10^{-11}$ m/W, $P_{cr} \sim 1$ mW, $L_{eff} \approx 20$ km, $A_{eff} = 50$ μm^2) [8]. Such a low threshold value makes SBS the dominant nonlinear phenomenon in optical fibers.

Finally, no physical system can provide infinite gain, and SBS is no exception. In the amplification configuration, a significant amount of power is transferred from the pump to the Stokes wave. As their intensities are comparable, the gain no longer experiences exponential growth but starts to flatten. At this point, the Stokes wave starts to suffer from the SBS generated by itself because of its high power level, acting similarly to a pump wave. When the pump can no longer provide more energy to the Stokes wave, it is said that the pump is depleted, leading to saturation of Brillouin gain.

In the context of fiber optics, SBS can have both positive and detrimental effects. On the positive side, it is employed in Brillouin optical time-domain analysis (BOTDA) for distributed sensing applications, enabling precise temperature and strain measurements along the fiber [98]. Conversely, SBS poses a challenge in high-power fiber laser systems, where it can impose limitations on the achievable output power due to the risk of nonlinear effects [99]. In optics communications, particularly in multicarrier systems, as the Brillouin frequency shift ν_B is around $\pm$10 GHz, the effect of SBS can be detrimental to other channels [100].

A.3. Other Acousto-Optic Scattering Interactions

In backward Stimulated Brillouin Scattering, the light is scattered contrary to its original propagating direction as a consequence of the modulation of the refractive index due to a change in the density of the core of the optical fiber. These changes in density correspond to longitudinal vibrations caused by thermal or electrostrictive phonons. From the dispersion diagram of Fig. A.2a, it has been derived that forward scattering is prohibited if no other optical modes are present in the optical fiber that could support this interaction because it would violate the phase matching conditions.

However, standard optical fibers support several groups of guided acoustic modes. One is the radial acoustic modes, denoted as $R_{0,m}$. These modes can be driven via electrostriction by co-propagating two optical waves that must be detuned $\Omega_{0,m}$. Consequently, changes in the material density are radial, producing an effect of "breathing" of the core of the optical fiber. As can be seen in the dispersion diagram of Fig. A.5a,

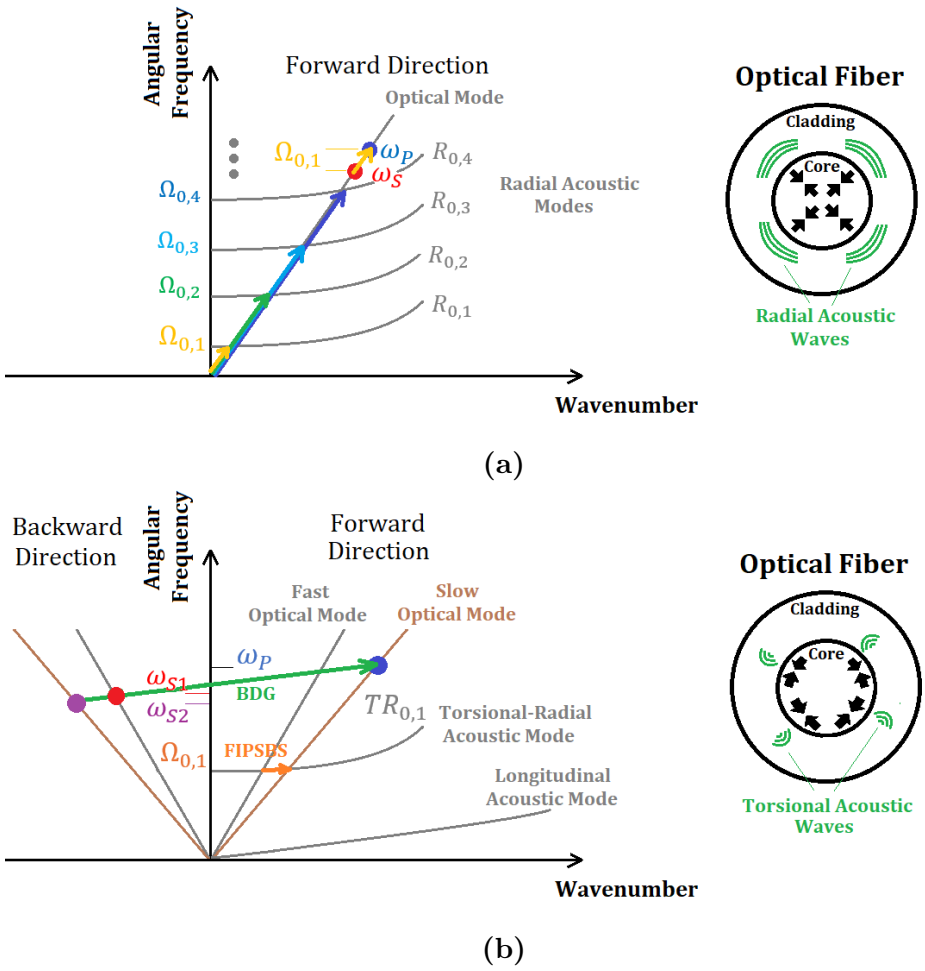

Figure A.5: (a) Dispersion diagram of forward (or Raman-like) stimulated Brillouin light scattering (FSBS) and (b) inter-polarization stimulated Brillouin scattering (IPSBS). In FSBS, the acoustics modes in the optical fiber represent a "breathing" of the core, whereas in IPSBS, they represent a "squeezing" of the core.

the phase matching condition for, e.g., $R_{0,1}$ requires that ω_S and ω_P are frequency shifted in $\Omega_{0,1}$ and also both are traveling in the forward direction. The Brillouin frequency shift of this forward-stimulated Brillouin Scattering (also known as Raman-like Brillouin scattering [101]) is found in standard optical fibers in the MHz range and induces only phase modulation to the Stokes wave [102]. Exciting applications of FSBS are in distributed sensors of liquids, where most advanced techniques have proven to measure, outside the cladding of a bare standard optical fiber, the properties of liquids such as ethanol or salted water [103].

Inter-modal SBS processes are also possible when the two optical fields are guided in different spatial modes. These peculiar SBS processes are exploited in, for example, polarization-maintaining (PM) optical fibers, where, because of the high birefringence induced by strain in the core, there are two optical modes with different slopes in the dispersion relation $\omega(k)$. This interaction, illustrated in Fig. A.5b, is usually found in the literature as inter-polarization stimulated Brillouin scattering (IPSBS).

Two coupling IPSBS mechanisms are possible: forward and backward. The first process, forward IPSBS, couples two co-propagating optical signals that travel in the slow and fast axes of a PM fiber and are frequency shifted in $\Omega_{0,m}$, the angular frequency correspondent to the Torsional-Radial modes. Then, electrostriction is induced, and the fiber is "squeezed" [101]. The second process, backward IPSBS, is responsible for producing a phenomenon called Brillouin Dynamic Gratings (BDG), whose principal characteristic is that it generates two Stokes waves in different polarization axes of the optical fiber. The frequency shifts of these Stokes waves are distinct, creating diffraction gratings centered at various frequencies and located in different spatial modes of the optical fiber. BDG is mainly employed for optical signal processing (delay lines, microwave photonic filters, and optical mathematical operations such as differentiation, integration, and time reversal) [104]. In contrast, forward IPSBS is mainly utilized for distributed sensing devices [105].

Appendix B

Models and Characterization of SBS Gain and Loss Spectra

In the nonlinear optics literature [7][8], the coupled equations that describe electro-acoustic interactions of a light-wave and a sound-wave in Stimulated Brillouin Scattering (SBS) provide a solution for the SBS gain and loss spectra that conveniently takes the form of Lorentzian distributions. This result is obtained by assuming steady-state conditions, the amplitude of the sound wave varying slowly in space and time, and the hypersonic phonons being strongly damped. However, experimental evidence proves that the Lorentzian distribution is not entirely an accurate description of the SBS power spectrum because it is highly dependent on the power of the pump wave.

The main objective of this Appendix is to provide a precise mathematical representation of the SBS gain and loss spectra of the SBS system presented in this Thesis. Many empirical models were proposed to precisely describe the SBS gain/loss distributions under different power conditions. The first characterization of SBS power spectra at different pump power levels was done by Villafranca et al. [106]. Then Wiatrek et al. [69] studied the SBS gain spectrum under a gain saturation regime. These analyses will be considered to perform a complete characterization and modeling of the SBS power spectrum necessary to develop the technique shown in 3.

B.1. Models for SBS Gain Spectrum

The SBS gain distributions proposed by Villafranca [106] are defined under low-gain and high-gain regimes. In the former, the SBS gain spectrum is determined by a Lorentzian distribution:

$$g_1(f) = g_0 \frac{(\nu_B/2)^2}{(f_B - f - f_P)^2 + (f_B/2)^2}, \tag{B.1}$$

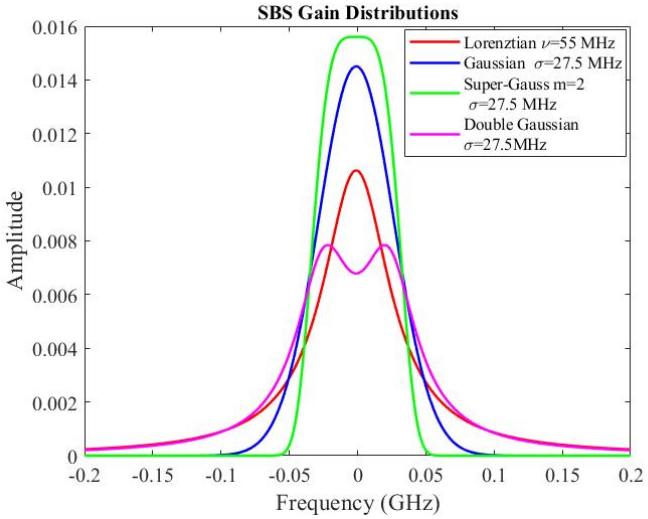

Figure B.1: Models for SBS gain distributions.

where g_0 is the Brillouin gain, ν_B the FWHM of the Lorentzian distribution, f_B the Brillouin frequency shift, and f_P the frequency of the pump. In the latter, a Gaussian function is employed to describe the SBS gain distribution as follows:

$$g_2(f) = \frac{g_0}{\sigma\sqrt{2\pi}} \exp\left[-\left(\frac{f_B - f - f_P}{\sqrt{2}\sigma}\right)^2\right]. \tag{B.2}$$

The Brillouin bandwidth is defined by the standard deviation σ in this Gaussian distribution.

Wiatrek proposes modeling the SBS gain distribution under the saturation regime as a superposition of two spectrally shifted Gaussian gains [69] as follows:

$$g_3(f) = \frac{g_0}{2\sigma\sqrt{2\pi}} \left\{ \exp\left[-\left(\frac{f_B - f - f_P - \delta f}{\sqrt{2}\sigma}\right)^2\right] + \exp\left[-\left(\frac{f_B - f - f_P + \delta f}{\sqrt{2}\sigma}\right)^2\right] \right\}, \tag{B.3}$$

where δf is the shift between these two non-saturated Gaussian distributions. The gain distribution departs from Gaussian, and as pump power increases, it changes to a double-shifted Gaussian distribution. In the transition, the Gaussian distribution exhibits flattening at its peak. This process can be modeled by a higher-order Gaussian (or super-Gaussian) distribution according to:

$$g_4(f) = g_0 A \exp\left[-\left(\frac{f_B - f - f_P}{\sqrt{2}\sigma}\right)^{2m}\right], \tag{B.4}$$

where A is a constant for normalization and m is the order of the super-Gaussian distribution.

These distributions are illustrated in Fig. B.1, where $f_P = f_B$ and a Brillouin

bandwidth of 55 MHz have been considered for all cases.

B.2. Experimental Characterization of SBS Gain and Loss Spectra

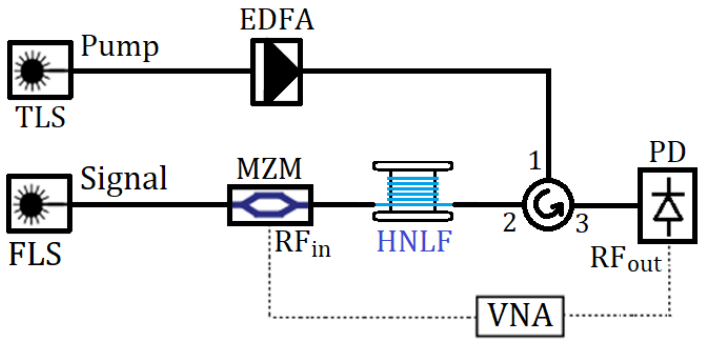

Figure B.2: Experimental setup.

The characterization of the SBS gain spectra of the optical fiber used throughout this Thesis has been carried out to find the power distribution that best fits measurements under different operating pump power levels. The experimental setup shown in Fig. B.2 is a typical pump-probe scheme for inducing SBS in a dispersion-shifted fiber (HNLF). The pump wave is a wavelength-tunable laser source (TLS) amplified by an erbium-doped fiber amplifier (EDFA), and the signal wave is a fixed-wavelength light source (FLS) that is AM modulated by a Mach-Zehnder Modulator (MZM). An optical circulator is placed to propagate pump and signal waves in opposite directions. A vector network analyzer (VNA) generates the electrical stimulus that drives the MZM and receives the RF photocurrent of the photodetector (PD) to obtain the normalized response of the direct transference (parameter S_{21}).

The HNLF has been excited using four different pump power levels: 12 dBm (3 dB above the Brillouin threshold), 15 dBm, 20 dBm, and 25 dBm (the power output level of the EDFA). Results are shown in Fig. B.3. It can be observed that there are four different gain responses for each pump power level, centered at 5 GHz. Cross markers on each response indicate the model fitted. Experimental results confirm the statements made in the previous Section, where a Lorenztian distribution best describes the low-gain regime (red) and a Gaussian distribution the high-gain regime (blue). In the transition to gain saturation, the SBS gain is fitted by a 2nd-order Gaussian distribution (green). The presence of two peaks characterizes the highly saturated gain regime shifted around the central frequency of the SBS gain response (magenta), which is well represented by the Double-Gaussian distribution.

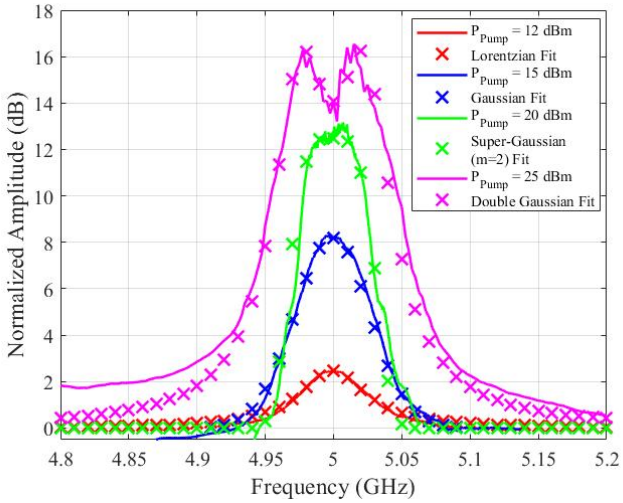

Figure B.3: Measurements of SBS gain response at different pump power levels (solid lines) and fitted models (cross markers).

Contrarily to the SBS gain case, the SBS loss response does not change its distribution when modifying the pump power, which produces an asymmetry between both spectra. This effect can be observed in Fig. B.4a, showing measurements of the gain and loss SBS responses in the highly saturated gain regime (blue). In this case, the loss response is fitted by a Lorentzian distribution.

Finally, the joint model for these interactions is presented in Fig. B.4b, where the combined gain and loss responses of the double Gaussian gain and Lorentzian loss distributions (red) are depicted, and the total phase (blue) is determined from Kramers-Kronig relations.

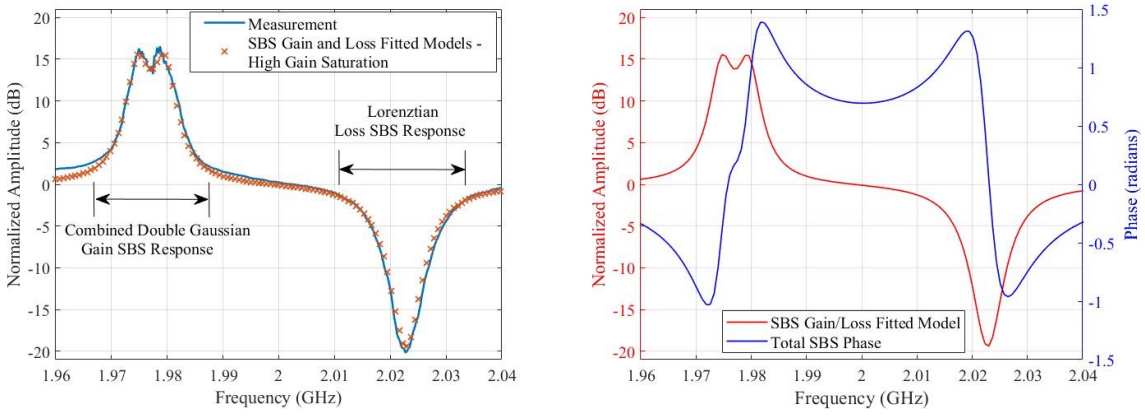

(a) **(b)**

Figure B.4: (a) Measured SBS saturated gain and loss power spectra (solid blue line) and fitted model (cross red markers) and (b) model of SBS total amplitude (red line) and phase (blue line) spectra.

References

[1] K. Kikuchi, «Fundamentals of Coherent Optical Fiber Communications», in *J. Light. Technol.*, vol. 34, no. 1, pp. 157-179, 1 Jan. 1, 2016. 1

[2] M. A. Báez-Chorro, and B. Vidal, «Single trace terahertz spectroscopic ellipsometry», in *Opt. Express*, 27, 35468-35474 (2019). 1

[3] J. F. De Boer, C. K. Hitzenberger, and Y. Yasuno, «Polarization sensitive optical coherence tomography – a review», in *Biomed. Opt. Express*, 8.3 (2017): 1838-1873. 1

[4] B. Vidal, T. Mengual, C. Ibanez-Lopez, and J. Marti, «Optical Beamforming Network Based on Fiber-Optical Delay Lines and Spatial Light Modulators for Large Antenna Arrays», in *IEEE Photonics Technol. Lett.*, vol. 18, no. 24, pp. 2590-2592, Dec.15, 2006. 1

[5] A. Rogers, in *Polarization in Optical Fibers*, Artech House Inc., 2009. 1, 2

[6] E. Collett, in *Field Guide to Polarization*, Vol. FG05, SPIE Field Guides, 2005. 2, 3

[7] R. W. Boyd, in *Nonlinear Optics*, 3rd ed., Academic Press, 2008. 3, 58, 59, 61, 67

[8] G. P. Agrawal, in *Nonlinear Fiber Optics*, 3rd ed., Ed. San Diego, California: Academic Press, 2001. 3, 5, 20, 26, 27, 58, 62, 64, 67

[9] M. Morant, J. Prat, and R. Llorente, «Radio-Over-Fiber Optical Polarization-Multiplexed Networks for 3GPP Wireless Carrier-Aggregated MIMO Provision», in *J. Light. Technol.*, vol. 32, no. 20, pp. 3721-3727, 2014. 3

[10] G. Zoireff, P. A. Costanzo Caso, L. A. Bulus Rossini, and B. Vidal, «Transparent Multichannel Wireless Bridge for Optical Fiber Links based on a Two-Stage Up-conversion», in *Opt. Commun.*, vol. 5006, 127585, March 2022. 3

[11] A. Crespi, R. Ramponi, R. Osellame, et al., «Integrated photonic quantum gates for polarization qubits», in *Nat. Commun.* 2, 566, (2011). 3

[12] Z. Huang, C. Wu, Y.Chen, X.Lin, and X. Tan, «Faithful reconstruction in orthogonal elliptical polarization holography read by different polarized waves», in *Opt. Express* , 28, 23679-23689, (2020). 3

[13] S. G. Demos, and R. R. Alfano, «Optical polarization imaging,» in *Appl. Opt.*, 36, 150-155, (1997). 3

[14] G. T. Reed, F. Y. Gardes, B. D. Timotijevic, G. Z. Mashanovich, W. R. Headley, and N. G. Emerson, «Waveguides and devices in silicon photonics: Polarisation independence», in *Proc. SPIE*, vol. 6476, pp. 647602-1–647602-10, Jan. 2007. 4

[15] L. H. Nicholls, F. J. Rodríguez-Fortuño, M. E. Nasir, et al., «Ultrafast synthesis and switching of light polarization in nonlinear anisotropic metamaterials,» in *Nature Photon*, 11, 628–633, 2017. 4

[16] A. J. Danner, T. Tyc, and U. Leonhardt, «Controlling birefringence in dielectrics,» in *Nature Photon.*, 5, pp. 357-359, Nov. 2013. 4

[17] Y. J. Tsai, S. Larouche, T. Tyler, A. Llopis, M. Royal, N. M. Jokerst, and D. R. Smith, «Arbitrary birefringent metamaterials for holographic optics at $\lambda = 1.55$ μm,» in *Opt. Express*, vol. 21, no. 22, pp. 26620-26630, Nov. 2013. 4

[18] A. Cerjan, and S. Fan, «Achieving arbitrary control over pairs of polarization states using complex birefringent metamaterials,» in *Phys. Rev. Lett.*, 118, 253902, May 2011. 4

[19] S. Biswas, et al., «Broadband electro-optic polarization conversion with atomically thin black phosphorus,» in *Science*, 374, 448-453, (2021). 4

[20] J. Shi, X. Chen, Y. Xia, and Y. Chen, «Polarization control by use of the electro-optic effect in periodically poled lithium niobate,» in *Appl. Opt.*, 42, 5722-5725, (2003). 5

[21] N. Moroney, L. Del Bino, S. Zhang, et al., «A Kerr polarization controller», in *Nat. Commun.*, 13, 398, (2022). 5

[22] J. Fatome, S. Pitois, P. Morin, and G. Millot, «Observation of light-by-light polarization control and stabilization in optical fibre for telecommunication applications», in *Opt. Express*, 18, 15311-15317, (2010). 5

[23] W. Xiong, C. W. Hsu, Y. Bromberg, et al., «Complete polarization control in multimode fibers with polarization and mode coupling,» in *Light Sci. Appl.*, 7, 54, (2018). 5

[24] M. Ferrario, V. Gilardone, P. Martelli, L. Marazzi, and M. Martinelli, «Effective all-optical polarization control induced by Raman nonlinear amplification,» in *European Conference and Exhibition on Optical Communication*, Turin, Italy, pp. 1-3. 2010. 5

[25] A. Zadok, E. Zilka A. Eyal, L. Thévenaz, and M. Tur, «Vector analysis of stimulated Brillouin scattering amplification in standard single-mode fibers», in *Opt. Express*, 16(26), 21692-21707. 5, 15, 24, 53

[26] L. Brillouin, «Diffusion de la lumière et des rayons X par un corps transparent homogène - Influence de l'agitation thermique,» in *Ann. Phys.*, vol. 9, no. 17, pp. 88-122, (1922). 6

[27] E. F. Gross, «Change of Wavelength of Light due to Elastic Heat Waves at Scattering in Liquids,» in *Nature*, 126, 201–202 (1930). 6

[28] E. P. Ippen, and R.H. Stolen, «Stimulated Brillouin scattering in optical fibers,» in *Appl. Phys. Lett.*, 1 December 1972; 21 (11): 539–541. 6

[29] E. Gamire, «Perspectives on stimulated Brillouin scattering,» in *New J. Phys.*, 19, 011003, (2017). 6

[30] H. H. Diamandi, and A. Zadok, «Ultra-narrowband integrated Brillouin laser,» in *Nature Photon.*, 13, 9–10 (2019). 6

[31] P. Sevillano, J. Subías, C. Heras, J. Pelayo, and F. Villuendas, «Brillouin induced self-heterodyne technique for narrow line width measurement,» in *Opt. Express*, 18, 15201-15206 (2010). 6

[32] J. M. Subías Domingo, J. Pelayo, F. Villuendas, C. D. Heras, and E. Pellejer, «Very High Resolution Optical Spectrometry by Stimulated Brillouin Scattering,» in *IEEE Photonics Technol. Lett.*, vol. 17, no. 4, pp. 855-857, Apr. 2005. 6

[33] F. Mihélic, D. Bacquet, J. Zemmouri, and P. Szriftgiser, «Ultrahigh resolution spectral analysis based on a Brillouin fiber laser,» in *Opt. Lett.*, 35, 432-434 (2010). 6

[34] T. Horiguchi, K. Shimizu, T. Kurashima, M. Tateda, and Y. Koyamada, «Development of a distributed sensing technique using Brillouin scattering,» in *J. Light. Technol.*, vol. 13, no. 7, pp. 1296-1302, Jul. 1995. 6

[35] X. Bao, Z. Zhou, and Y. Wang, «Review: distributed time-domain sensors based on Brillouin scattering and FWM enhanced SBS for temperature, strain and acoustic wave detection,» in *PhotoniX*, 2, 14 (2021). 6

[36] A. Minardo, R. Bernini, L. Amato and L. Zeni, «Bridge Monitoring Using Brillouin Fiber-Optic Sensors,» in *IEEE Sens. J*, vol. 12, no. 1, pp. 145-150, Jan. 2012. 6

[37] R. Moffat, J. Sotomayor, J. F. Beltrán, «Estimating tunnel wall displacements using a simple sensor based on a Brillouin optical time domain reflectometer apparatus,» in *International Journal of Rock Mechanics and Mining Sciences*, vol. 75, 2015, pp. 233-243, ISSN 1365-1609. 6

[38] J. Luo, Y. Hao, Q. Ye, Y. Hao, and L. Li, «Development of Optical Fiber Sensors Based on Brillouin Scattering and FBG for On-Line Monitoring in Overhead Transmission Lines,» in *J. Light. Technol.*, vol. 31, no. 10, pp. 1559-1565, May 15, 2013. 6

[39] A. Loayssa, and F. J. Lahoz, «Broad-band RF photonic phase shifter based on stimulated Brillouin scattering and single-sideband modulation,» in *IEEE Photonics Technol. Lett.*, vol. 18, no. 1, pp. 208-210, Jan. 1, 2006. 6

[40] B. Vidal, M. A. Piqueras, and J. Martí, «Tunable and reconfigurable photonic microwave filter based on stimulated Brillouin scattering,» in *Opt. Lett.*, 32, 23-25 (2007). 6, 26, 54

[41] B. Vidal, P.G. Huggard, B.N. Ellison, and N.J. Gomes, , «Optoelectronic generation of W-band millimetre-wave signals using Brillouin amplification,» in *Electron. Lett.*, vol. 46, no. 21, pp. 1449-1450, 14th October 2010. 6

[42] M. González Herráez, K. Y. Song, and L. Thévenaz, «Arbitrary-bandwidth Brillouin slow light in optical fibers,» in *Opt. Express 14*, 1395-1400 (2006). 6, 26, 28, 29

[43] A. Bergman, and M. Tur, «Brillouin Dynamic Gratings — A Practical Form of Brillouin Enhanced Four Wave Mixing in Waveguides: The First Decade and Beyond,» in *Sensors*, Sep. 2018, 18(9), 2863. 7

[44] J. Azaña, «Ultrafast analog all-optical signal processors based on fiber-grating devices,» in *IEEE Photonics J.*, vol. 2, no. 3, pp. 359-386, June 2010. 7

[45] B. J. Eggleton, C. G. Poulton, P. T. Rakich, et al., «Brillouin integrated photonics,» in *Nat. Photonics*, 13, 664–677 (2019). 7

[46] R. Pant, D. Marpaung, I. V. Kabakova, B. Morrison, C. G. Poulton, and B. J. Eggleton, «On-chip stimulated Brillouin Scattering for microwave signal processing and generation», in *Laser Photonics Rev.*, vol. 8, no. 5, p. 653-666, 2014. 7

[47] S. R. Mirnaziry, C. Wolff, M. J. Steel, B. J. Eggleton, and C. G. Poulton, «Stimulated Brillouin scattering in silicon/chalcogenide slot waveguides,» in *Opt. Express*, 24, 4786-4800 (2016). 7

[48] A. Choudhary, Y. Liu, B. Morrison, H. Vu, D. Y. Choi, P. Ma, S. Madden, D. Marpaung, and B. J. Eggleton, «High-resolution, on-chip RF photonic signal processor using Brillouin gain shaping and RF interference,» in *Sci. Rep.*, vol. 7, pp. 5932, 2017. 7, 25

[49] K. Ye, Y. Klaver, O. A. Jimenez Gordillo, R. Botter, O. Daulay, F. Morichetti, A. Melloni, and D. Marpaung, «Brillouin and Kerr nonlinearities of a low-index silicon oxynitride platform,» in *APL Photonics*, 8, 051302 (2023). 7

[50] F.Yang, F.Gyger, A. Godet, et al., «Large evanescently-induced Brillouin scattering at the surrounding of a nanofibre,» in *Nat. Commun.*, 13, 1432 (2022). 7

[51] M. Merklein, I. V. Kabakova, A. Zarifi, and B. J. Eggleton, «100 years of Brillouin scattering: Historical and future perspectives,» in *Appl. Phys. Rev.*, 9 (4), 0413061, December 2022. 7

[52] Z. Schmilovitch, N. Primerov, A. Zadok, A. Eyal, S. Chin, L. Thevenaz, and M. Tur, «Dual-pump push-pull polarization control using stimulated Brillouin scattering,» in *Opt. Exp.*, vol. 19, no. 27, pp. 25873, Dec. 2011. 7

[53] D. Samaniego, and B. Vidal, «Brillouin wavelength selective all-optical polarization conversion», in *Phot. Res.*, vol. 8, no. 4, pp. 440-447, Apr. 2020. 8, 9, 12, 40, 50

[54] P. Michel, et al., «Polarization-dependent theory of two-wave mixing in nonlinear media, and application to dynamical polarization control,» in *Phys. Rev. X*, p. 021039, vol. 10, no. 2, 2020. 10

[55] T. Horiguchi, N. Shibata, Y. Azuma, and M. Tateda, «Brillouin gain variation due to a polarization-state change of the pump or Stokes fields in standard single-mode fibers,» in *Opt. Lett.*, vol. 14, no. 6, p. 329-331, 1989. 8, 11, 13

[56] J. J. Martínez, A. Villafranca, C. D. Heras, M. I. Roche, J. M. Subias, J. Pelayo, E. Pellejer, P. Blasco, and J. I. Garcés, «In-band optical signal-to-noise ratio monitoring method based on high-resolution polarization analysis and induced differential group delay,» in *Appl. Opt. 49*, 6213-6216 (2010). 11

[57] D. Derickson in *Fiber Optic Test and Measurement*, 1st ed. Upper Saddle River, NJ, USA: Prentice Hall, 1998. 19, 50

[58] S. Chin, and L. Thévenaz, «Tunable photonic delay lines in optical fibers,» in *Laser & Photon. Review*, 6, no.6, pp. 724-738, Feb. 2012. 22, 25, 26, 28

[59] T. Schneider, R. Henker, K. U. Lauterbach, and M. Junker, «Comparison of delay enhancement mechanisms for SBS-based slow light systems,» in *Opt. Express*, vol. 15, no. 15, pp. 9606-9613, Jul. 2007. 24, 25

[60] Y. Okawachi, M. S. Bigelow, J. E. Sharping, Z. Zhu, A. Schweinsberg, D. J. Gauthier, R. W. Boyd, and A. L. Gaeta, «Tunable All-Optical Delays via Brillouin Slow Light in Optical Fiber,» in *Phys. Rev. Lett.*, 94, 153902, 2005. 25

[61] T. Tanemura, Y. Takushima, and K. Kikuchi, «Narrowband optical filter, with a variable transmission spectrum, using stimulated Brillouin scattering in optical fiber,» in *Opt. Lett.*, 27, 1552-1554 (2002). 26

[62] S. Hu, L. Li, X. Yi, and F. Teng, «Tunable dual-passband microwave photonic filter based on stimulated Brillouin scattering,» in *IEEE Photonics Technology Letters*, 29(3), 330-333,(2017). 26

[63] K. E. Peiponen, and J. J. Saarinen, «Generalized Kramers–Kronig relations in nonlinear optical- and THz-spectroscopy,» in *Rep. Prog. Phys.*, 72, 056401, 2009. 27, 63

[64] A. Zadok, A. Eyal, and M. Tur, «Extended delay of broadband signals in stimulated Brillouin scattering slow light using synthesized pump chirp,» in *Opt. Express*, 14, 8498-8505 (2006). 26

[65] K. Y. Song, and K. Hotate, «25 GHz bandwidth Brillouin slow light in optical fibers,» in *Opt. Lett.*, 32, 217-219 (2007). 26, 28

[66] B. Y.-K.Hu, «Kramers–Kronig in two lines,» in *Am. J. Phys.*, 57 (9): 821, 1989. 27, 63

[67] M. O. Van Deventer, and A. J. Boot, «Polarization properties of stimulated Brillouin scattering in single-mode fibers,» in *J. Light. Technol.*, vol. 12, no. 4, pp. 585–590, 1994. 30

[68] W. Wei, L. Yi, Y. Jaouën, and W. Hu, «Software-defined microwave photonic filter with high reconfigurable resolution,» in *Sci. Rep.*, 6, 35621 (2016). 31, 36

[69] A. Wiatrek, R. Henker, S. Preußler, and T. Schneider, «Comparative investigation of zero-broadening methods in Brillouin based slow-light systems,» in *IET Irish Signals and Systems Conference*, (ISSC 2009), 1-6, (2009). 40, 67, 68

[70] K. Bohnert, A. Frank, L. Yang, X. Gu, and G. M. Müller, «Polarimetric Fiber-Optic Current Sensor With Integrated-Optic Polarization Splitter,» in *J. Lightwave Technol.*, 37, 3672-3678 (2019). 43

[71] H. Kurokawa, H. Kawashima, H. Kasai, M. Kuroda, T. Yoshimura, and K. Asama, «An asymmetric optical splitter and its application to optical monitoring devices,» in *LEOS 2001, 14th Annual Meeting of the IEEE Lasers and Electro-Optics Society*, (Cat. No.01CH37242),vol. 1, pp. 232-233, San Diego, CA, USA, 2001. 43

[72] B. Mukherjee, «WDM optical communication networks: progress and challenges,» in *IEEE Journal on Selected Areas in Communications*, vol. 18, no. 10, pp. 1810-1824, Oct. 2000. 43

[73] H. Kobrinski, and K. W. Cheung, «Wavelength-tunable optical filters: applications and technologies,» in *IEEE Communications Magazine*, vol. 27, no. 10, pp. 53-63, Oct. 1989. 44

[74] N. R. Bernier, L.D. Tóth, A. Koottandavida, et al., «Nonreciprocal reconfigurable microwave optomechanical circuit,» in *Nat. Commun.*, 8, 604 (2017). 44

[75] W. Fu, F.-J. Shu, Y.-L.Zhang, C.-H. Dong, C.-L. Zou, and G.-C. Guo, «Integrated optical circulator by stimulated Brillouin scattering induced non-reciprocal phase shift,» in *Opt. Express*, 23, 25118-25127 (2015). 44

[76] L.Bi, J. Hu, P. Jiang, et al., «On-chip optical isolation in monolithically integrated non-reciprocal optical resonators,» Nature Photon 5, 758–762 (2011). 44

[77] Z. Shen, Y. L. Zhang, Y. Chen, et al., «Reconfigurable optomechanical circulator and directional amplifier,» in *Nat. Commun.*, 9, 1797 (2018). 44

[78] Y. Liu, A. Choudhary, D. Marpaung, and B. J. Eggleton, «Chip-Based Brillouin Processing for Phase Control of RF Signals,» in *IEEE Journal of Quantum Electronics*, vol. 54, no. 3, pp. 1-13, June 2018, Art no. 6300413. 44

[79] G. Bashan, ,H. H. Diamandi, Y. London, et al., «Forward stimulated Brillouin scattering and opto-mechanical non-reciprocity in standard polarization maintaining fibres,» in *Light Sci. Appl.*, 10, 119 (2021). 44

[80] Y. Antman, A. Clain, Y. London, and A. Zadok, «Optomechanical sensing of liquids outside standard fibers using forward stimulated Brillouin scattering,» in *Optica*, 3, 510-516 (2016). 44

[81] J. Yao, «Photonics to the Rescue: A Fresh Look at Microwave Photonic Filters,» in *IEEE Microwave Magazine*, vol. 16, no. 8, pp. 46-60, Sept. 2015. 46

[82] W. Zhang, and R. A. Minasian, «Switchable and tunable microwave photonic brillouin-based filter,» in *IEEE Photon. J.*, vol. 4, no. 5, pp. 1443–1455, Oct. 2012. 54

[83] D. Marpaung, B. Morrison, R. Pant, and B. J. Eggleton, «Frequency agile microwave photonic notch filter with anomalously-high stopband rejection,» in *Opt. Lett.*, vol. 38, no. 21, pp. 4300–4303, Nov. 2013. 54

[84] W. Wei, L. Yi, Y. Jaouën, and M. Morvan, «Brillouin rectangular optical filter with improved selectivity and noise performance,» in *IEEE Photon. Technol. Lett.*, vol. 27, no. 15, pp. 1593–1596, Aug. 2015. 54

[85] Y. Stern, K. Zhong, T. Schneider, R. Zhang, Y. Ben-Ezra, M. Tur, and A. Zadok, «Tunable sharp and highly selective microwave-photonic band-pass filters based on stimulated Brillouin scattering,» in *Photonics Res.*, vol. 2, no. 4, pp. B18–B25, Aug, 2014. 54

[86] D. Samaniego, and B. Vidal, «Photonic Microwave Filter With Steep Skirt Selectivity Based on Stimulated Brillouin Scattering,» in *IEEE Photon. J.*, Vol. 8, No. 6, pp. 1-7, Dec. 2016, Art no. 5502307. 53, 54

[87] C. Feng, S. Preussler, and T. Schneider, «Sharp tunable and additional noise-free optical filter based on Brillouin losses,» in *Photonics Res.*, vol. 6, no. 2, pp. 132–137, Feb. 2018. 54

[88] D. Samaniego, and B. Vidal, «Brillouin Microwave Filter with enhanced Skirt Selectivity using a Birefringent Fiber,» in *IEEE Photon. Technol. Lett.*, vol. 31, no. 6, pp. 431–434, Mar. 2019. 53, 54

[89] D. Marpaung, B. Morrison, M. Pagani, R. Pant, D. Y. Choi, B. Luther-Davies, S. J. Madden, and B. J. Eggleton, «Low-power, chip-based stimulated Brillouin scattering microwave photonic filter with ultrahigh selectivity,» in *Optica*, vol. 2, no. 2, pp. 76–83, Feb. 2015. 54

[90] A. Wise, M. Tur, and A. Zadok, «Sharp tunable optical filters based on the polarization attributes of stimulated Brillouin scattering,» in *Opt. Express*, vol. 19, no. 22, pp. 21945-21955, Oct. 2011. 53, 54

[91] P. Li, X. Zou, W. Pan, L. Yan, and S. Pan, «Tunable Photonic Radio-Frequency Filter with a Record High Out-of-Band Rejection,» in *IEEE Trans. Microw. Theory and Techn.*, vol. 65, no. 11, pp. 4502–4512, Nov. 2017. 53, 54

[92] B. Vidal, V. Polo, J. L. Corral, and J. Martí, «Photonic microwave filter with tuning and reconfiguration capabilities using optical switches and dispersive media,» in *Electron. Lett.*, vol. 39, no. 6, pp. 547-549, 20th March 2003. 53

[93] B. Vidal, T. Mengual, and J. Marti, «Photonic Microwave Filter with Single Bandpass Response based on Brillouin Processing and SSB-SC,» in *IEEE International Topical Meeting on Microwave Photonics (MWP2009)*, Valencia (Spain), 14-16 October 2009. 53

[94] B. Vidal, V. Polo, J. L. Corral, and J. Martí, «Harmonic suppressed photonic microwave filter,» in *J. Lightwave Technol.*,, vol. 21, no. 12, 3150-3154, December 2003. 53

[95] B. J. Eggleton, C. G. Poulton, P. T. Rakitch, M. J. Steel, and G. Bahl, «Brillouin integrated photonics,» in emphNat. Photonics, vol. 13, pp. 664-677, Oct. 2019. 53

[96] A. Choudhary, Y. Liu, D. Marpaung, and B. J. Eggleton, «On-Chip Brillouin Filtering of RF and Optical Signals,» in *IEEE J. Sel. Topics Quantum Electron.*, vol. 24, no. 6, no. 7600211, Nov./Dec. 2018. 53

[97] B. Vidal, «Photonic millimeter-wave frequency multiplication based on cascaded four-wave mixing and polarization pulling,» in *Opt. Lett.*, vol. 37, no. 24, pp. 5055–5057, Dec. 2012. 53

[98] T. Kurashima, T. Horiguchi, and M. Tateda, «Distributed-temperature sensing using stimulated Brillouin scattering in optical silica fibers,» in *Opt. Lett.*, 15, 1038-1040 (1990). 64

[99] Y. Aoki, K. Tajima, and I. Mito, «Input power limits of single-mode optical fibers due to stimulated Brillouin scattering in optical communication systems,» in *J. Light. Technol.*, vol. 6, no. 5, pp. 710-719, May 1988. 64

[100] M. Morant, T. Quinlan, S. Walker and R. Llorente, «Complete mitigation of Brillouin scattering effects in reflective passive optical networks using triple-format OFDM radio signals,» in *Optical Fiber Communication Conference and Exposition and the National Fiber Optic Engineers Conference*, Los Angeles, CA, USA, 2011, pp. 1-3. 64

[101] M. S. Kang, A. Brenn, and P. St.J. Russell, «All-Optical Control of Gigahertz Acoustic Resonances by Forward Stimulated Interpolarization Scattering in a Photonic Crystal Fiber,» in *Phys. Rev. Lett.*, 105, 269908, 2010. 65, 66

[102] Y. Antman, A. Clain, Y. London, and A. Zadok, «Optomechanical sensing of liquids outside standard fibers using forward stimulated Brillouin scattering,» in *Optica*, Vol. 3, Issue 5, pp. 510-516, 2016. 65

[103] G. Bashan, H. H. Diamandi, Y. London, E. Preter, and A. Zadok, «Optomechanical time-domain reflectometry,» in *Nat. Commun.*, 9, 2991, 2018. 65

[104] N. Primerov, and L. Thévenaz, «Generation and application of dynamic gratings in optical fibers using stimulated Brillouin scattering,» in *EPFL PhD Thesis*, 2013, Lausanne, EPFL. 66

[105] H. H. Diamandi, G. Bashan, Y. London, K. Sharma, K. Shemer, and A. Zadok «Interpolarization Forward Stimulated Brillouin Scattering in Standard Single-Mode Fibers,» in *Laser Photonics Rev.*, 16 (1) 2100337, Nov. 2021. 66

[106] A. Villafranca, J. A. Lázaro, Í. Salinas, and I.Garcés, «Stimulated Brillouin scattering gain profile characterization by interaction between two narrow-linewidth optical sources,» in *Opt. Express 13*, 7336-7341 (2005). 67

Publications

Scientific contributions derived from this Thesis

Journal publications:

- **G. Zoireff**, and B. Vidal, «Light-by-light polarization control using Stimulated Brillouin Scattering with retardance spectrum shaping,» in *Opt. Laser Technol.*, vol. 169, 110036, Feb. 2024.
- D. Samaniego, **G. Zoireff** and B. Vidal, «Brillouin-Induced Dynamic Arbitrary Birefringence,» in *Journ. of Light. Technol.*, vol. 39, no. 7, pp. 1961-1967, 1 April, 2021.
- **G. Zoireff**, D. Samaniego and B. Vidal, «Dynamic Filtering of Microwave Signals Through Brillouin-Based Polarization-Sensitive Balanced Detection,» in *IEEE J. Sel. Top. Quantum Electron.*, vol. 27, no. 2, pp. 1-6, Art no. 7500206, March-April 2021.

Other authors' contributions

Journal publications:

- **G. Zoireff**, P.A. Costanzo Caso, and L. A. Bulus Rossini, «On the performance of companding techniques for DMT optical links,» in *Opt. Commun.*, vol. 506, 127546, March 2022.
- **G. Zoireff**, P. A. Costanzo Caso, L. A. Bulus Rossini, and B. Vidal, «Transparent Multichannel Wireless Bridge for Optical Fiber Links based on a Two-Stage Upconversion,» in *Opt. Commun.*, vol. 5006, 127585, March 2022.

Conference proceedings:

- **G. Zoireff**, L. Morbidel, B. Vidal, L. A. Bulus Rossini, P. A. Costanzo Caso, «Radio-over-fiber optic link for millimeter wave signals,» in *107° Renión Argentina de Física (RAFA)*, Bariloche, Argentina, 27-30 sep. 2022.

- **G. Zoireff**, L. A. Bulus Rossini, J. Cogo, J. P. Pascual, P. A. Costanzo Caso, «Radiotelescopio Llama. Propuesta para generar y Distribuir señales de referencia para el Front-End de ondas milimétricas mediante tecnología fotónica,» in *107˚ Renión Argentina de Física (RAFA)*, Bariloche, Argentina, 27-30 sep. 2022.

Acknowledgment

Firstly, I would like to emphasize the support of my family and friends, who, from more than 10000 km away, made me feel closer to them. A special mention goes to my wife, Yanet, for standing by my side all the years that lasted this Ph.D. and still bears me every day. She always finds the right words to boost my mood when I feel homesick.

Secondly, I want to thank my supervisor, Prof. Borja Vidal. From the moment I arrived in Valencia, he gave me his trust and continuously encouraged me to keep going further. He has always been there whenever I needed him, correcting me when I made mistakes and giving his advice and experience to keep me on the right track. Besides all his knowledge and wisdom, he is such a nice person. I will be grateful to him for life.

Thirdly, my co-supervisors Laureano and Pablo played a significant role in this PhD. They contributed to the technical discussions and allowed me to move freely on every objective I pursued.

Finally, my friends from *la sala diáfana* were fundamental. I have never felt a cultural barrier between me and them, even though I come from a different country. On the contrary, since day one, they have shown goodwill and helped me with almost everything. They made me understand the "mechanics of the PhD" and the day-to-day of being a PhD student. Something that is not trivial, especially when you are starting. It is even more critical as time goes by because the PhD has plenty of ups and downs, and somehow, I felt relieved to know that (mostly) everyone is going through the same thing.

To summarize, during the three years spent at the NTC, I met wonderful people from whom I learned a lot. I am taking the best from them to become a better person.